Regulation of Mitochondria by Reversible Protein Phosphorylation

By

Joshua J. Carson

A dissertation submitted in partial fulfillment of

the requirements for the degree of:

Doctor of Philosophy

(Cellular and Molecular Biology)

at the

UNIVERSITY OF WISCONSIN – MADISON

2015

Date of final oral examination: 03/17/2015

The dissertation is approved by the following members of the Final Oral Committee:

Alan D. Attie, Professor, Biochemistry
Joshua J. Coon, Professor, Biomolecular Chemistry and Chemistry
John M. Denu, Professor, Biomolecular Chemistry
Thomas F.J. Martin, Professor, Biochemistry
David J. Pagliarini, Assistant Professor, Biochemistry

ACKNOWLEDGEMENTS

It has been my pleasure to work with many extraordinary people and scientists both before and during the course of my PhD.

I'd like to start at the very beginning with my friend Judit, who recommended that I apply to work in a lab off campus from our small liberal-arts university. I worked in the Tyler lab for a total of 7 years, 3 as an undergrad assistant and then for 4 years after I received my BS from the University of Denver. There, I learned the finer points of experimental design, molecular biology, and grant writing. The support I received from Jess gave me the freedom to work independently and the confidence to apply to a top-tier graduate school.

The decision to join Dave's lab was an easy one, his enthusiasm for science and his clear vision for the group drew me in from the very beginning. The Pagliarini Lab has grown significantly since that first semester when it was just five of us. Dave has guided the lab from 5 people to almost 20 with such a steady had that I'm amazed that he hasn't done this before! The lessons I have learned from Dave in hard work, setting goals, and navigating the right path to meet those goals are lessons that I won't soon forget and will serve me well throughout my career.

Jarred and Amelia, I share the privilege of being Dave's first graduate students with you, and it was great fun building the lab along with Kate, Nick and Grant that fist semester. Paul, we've been co-authors and baymates, I (almost) always enjoyed our conversations, and your help with writing grants and papers has been irreplaceable. Brendan, you were perhaps the only person in the lab that enjoyed puns as much as

Paul, and I've enjoyed talking through experiments with you. Natalie and Xiao, I'm glad to have worked on Ptc7 with you and to have struggled through yeast genetics together. I'm looking forward to a fantastic paper. Adam, you have a gift when it comes to cloning and the lab would fall apart without you. Mike, Holly, and Molly, I wish you well as you work through the marathon of grad school. To the Q-branch (Jon, Andrew, Danielle and Zach), you may have been across the hall, but you are the metaphorical center of the Pagliarini Lab!

I'd also like to thank my thesis committee, they've been a wonderful resource and I've looked forward to the advice that I've received at my yearly meetings. In fact, many of my committee members were also part of the many collaborations that Dave has organized. Professor Coon and his lab, especially Alex, have provided outstanding mass spectrometry tools and techniques. There are only a handful of labs in the world that have that level of MS prowess, and I've been fortunate to be able to collaborate with the Coon group. Professor Attie, with his fantastic mouse model and expertise in metabolic diseases, made my first paper a success. Professor Denu also provided encyclopedic knowledge of mitochondrial metabolism and taught me much about enzyme kinetics. I'd also like to thank the AHA for two years of funding.

I've made so many friends in Madison, both permanent residents and transient grad students, and I hope to nurture those friendships in the years to come. Nick, Tara, Chris, Lindsey, Matt, Dana, Josh, Jess, Cary, and Hillary, you have become some of my closest friends and I'm not sure I would have made it though grad school without you. Kristen, Bridget, Maria, and Mike I'm glad to have you as friends, and I'm looking forward to living with you in Madison in the coming years. I also would like to thank my

friends in Denver, Spencer and Tracy for being my oldest and closest friends, and Ben and Laura for the delicious meals and encouragement to continue on to grad school.

Finally, and most importantly, I'd like to thank my family. My parents have always supported my crazy fascination with science and encouraged me to continue with my studies. My siblings have rolled their eyes as I talked about mitochondria at the dinner table, but have also been supportive of my career goals and I love them. I recently acquired some new family members this last summer and I'm excited to also be a part of the Gaudio clan. To my wife Jennifer, I can scarcely find the words to convey the depths of my love and appreciation. I had never met you before I started grad school, but without your support, encouragement, and the occasional kick in the pants, I'm not sure I would have made it to my degree. We met at Les Chat in one of the most cliché ways possible, but I love our dogs, our house, and the life that we're building together and can't wait to grow with you in the future.

TABLE OF CONTENTS

LIST OF FIGURES

Chapter 2

Chapter 3

ABSTRACT

Regulation of Mitochondria by Reversible Protein Phosphorylation

by

Joshua John Carson

Under the supervision of Associate Professor David J. Pagliarini

At the University of Wisconsin – Madison

Mitochondria are dynamic organelles that must rapidly adapt to changing cellular metabolic and biosynthetic demands. Until recently, mitochondria have represented an underappreciated site of regulation by reversible phosphorylation. Furthermore, the pathogenic alterations that underlie metabolic disorders have increasingly represented one of the principal challenges in cell biology. Our work has focused on using quantitative proteomics and phosphoproteomics to identify dynamic phosphorylation sites and characterize the function of phosphorylation on mitochondrial enzymes. We began by charting the remodeling of the mouse liver mitochondrial proteome and phosphoproteome during both acute and chronic physiological transformations in more than 50 mice. Our analyses reveal that reversible phosphorylation is widespread in mitochondria, and is a key mechanism for regulating ketogenesis during the onset of obesity and type 2 diabetes. Specifically, we demonstrated that phosphorylation of a conserved serine on Hmgcs2 (S456) significantly enhances its catalytic activity in response to increased ketogenic demand. Additionally, we used activity based protein

profiling to identify kinases that are enriched in mitochondria, as well as kinases that are differentially enriched in the mitochondria of obese mice. We further report on the change in oxygen consumption rates in isolated mitochondria in response to treatment with calcium, and show that calcium uptake is also dependent on electron transport. We also show that phosphorylation sites in isolated mitochondria can be rapidly modulated by acute (10min) treatment with calcium as a stimulus. Finally, we performed multiplexed quantitative mass spectrometry to identify the targets of the mitochondrial phosphatase PTC7. Using yeast deletion strains, we identify over 50 putative phosphorylation sites that are unique to a deletion of PTC7. Furthermore, we demonstrate that phosphorylation of a conserved serine on Hem15, the final step in heme biosynthesis, decreases enzyme activity. Collectively, our work describes the plasticity of this organelle at high resolution and provides a framework for investigating the roles of proteome restructuring and reversible phosphorylation in mitochondrial adaptation.

CHAPTER 1: An Introduction to Mitochondrial Biology, Biochemistry, and Reversible Protein Phosphorylation

Introduction

Summary of the Thesis

Throughout the research that contributed to this dissertation, I have generated new insights into the regulation of mitochondria by reversible phosphorylation. I have used a multidisciplinary approach to show that phosphorylation is not only prevalent in the mitochondria, but also changes in response to varied physiological states. Through this work, I have also shown that kinases and phosphatases are the likely effectors of mitochondrial phosphorylation.

In Chapter 2, I present results from a published study that uses quantitative mass spectrometry to identify phosphorylation sites that change in abundance in response to changes in metabolic state. To do this we profiled mitochondrial phosphorylation sites from mice that differed in age, strain, or obesity-dependent diabetes. Furthermore, I show that one phosphorylation site can modulate enzyme activity of the protein HMGCS2 and lead to increased ketone body production in a tissue culture system.

In Chapter 3, I explore the proteins that are responsible for phosphorylation: kinases and phosphatases. Using an activity-based protein profiling technique, I show that there are different populations of kinases in the mitochondria of livers from lean and obese mice. I then show that calcium uptake in mitochondria can affect respiratory rates, and that acute treatment of isolated mitochondria with calcium can affect phosphorylation abundance. Next, I use a yeast model to profile the change in phosphorylation patterns upon deletion of a known mitochondrial phosphatase, and show that the phosphatase Ptc7 is important for iron homeostasis and the response to

oxidative stress. I also investigate the relevance of one phosphorylation site to regulate iron incorporation into heme by the enzyme Hem15. Finally, in Chapter 4, I discuss the overall findings from these studies and their larger relevance to the field of mitochondrial post-translational modifications.

Post-Translational Modifications

To adequately adapt to changes in the environment, signals must be conveyed throughout the cell to modulate protein transcription, expression, and activity. While the approximately 25,000 genes within the human genome encode the basis for cellular function, the complexity of the proteome dwarfs that of the genome with over 1 million protein isoforms within the cell (Stein, 2004). The intricacy of the proteome can be further refined by the addition of covalent modifications to specific amino acid side chains, which are commonly referred to as post-translational modifications (PTMs). A wide variety of PTMs exist within the cell including: acetylation, phosphorylation, ubiquitinylation, and methylation. These modifications perform a wide variety of roles such as regulating enzyme activity (Shimazu et al., 2010), and directing protein localization, interactions, and degradation (Deng et al., 2011; Rana et al., 2013). Because PTMs have such varied and profound roles regulating diverse cellular pathways, it is vital to more completely understand their molecular functions. To do this, we must be able to identify specific sites of modification and quantify those sites in relation to physiological conditions with the intention of using that information to obtain biochemical insights about the function of PTMs.

Phosphorylation

Reversible phosphorylation of a range of proteins, lipids and other molecules produce a variety of signaling cascades, and is widely considered to be the most prevalent form of PTM within a cell. Approximately one-third of proteins are estimated to have a phosphorylation event at some point during their life (Hubbard and Cohen, 1993). Phosphorylation can act as a molecular switch in signal transduction pathways by either the addition or removal of a phosphoryl group (PO_4). Phosphorylation is understood to have occurred when the gamma phosphate of ATP is transferred to a protein substrate. Protein kinases are the enzymes that perform this covalent modification by attaching a phosphoryl group to a free amino acid hydroxyl, while protein phosphatases perform the reverse reaction by removing the phosphoryl group and leaving behind a free hydroxyl group on the amino acid and a phosphate ion in solution. The most common form of phosphorylation is the addition of PO_4 to the hydroxyl residues of the amino acids: serine, threonine, and tyrosine. Furthermore, kinases themselves are often targets of phosphorylation and can be regulated by other kinases. One classic example of a kinase signaling cascade is the mitogen-activated protein kinase (MAPK) group, which are involved in a variety of essential cellular processes such as growth, differentiation, stress response, and apoptosis (Boutros et al., 2008; Pearson et al., 2001). In this cascade, cellular stimuli activate MAPKK kinases, which phosphorylate downstream MAPK kinases, and ultimately the MAP kinase. This signaling paradigm serves to amplify an extracellular signal and can mediate the broad range of biological responses available to a cell (Keshet and Seger, 2010). In addition, it is not uncommon for proteins to be phosphorylated at multiple sites. One classic

example is the pyruvate dehydrogenase complex (PDC), which converts pyruvate into acetyl-CoA in the mitochondrial matrix. The pyruvate dehydrogenase kinase phosphorylates the PDC at three specific residues which act in concert to inactivate the enzyme and deprive the TCA cycle of acetyl-CoA (Korotchkina, 2000; Yeaman et al., 1978). Reversible phosphorylation plays a vital role in nearly all aspects of cellular function; therefore it is perhaps not surprising that its dysfunction can cause a wide variety of cellular and organismal malfunctions.

While the functional significance of phosphorylation has been known for decades, recent advances in the capabilities of mass spectrometry (MS) has allowed for the identification and quantitation of numerous phosphorylation sites within every compartment of the cell (Grimsrud et al., 2010; Jensen, 2004). Interestingly, the mitochondria are intracellular organelles that, despite their importance and several classic examples, have had little investigation into the role that reversible phosphorylation can play in their regulation. Using advancements in phosphoproteomics, we now know that much of the mitochondrial proteome is widely phosphorylated (Boja et al., 2009; Cui et al., 2010; Deng et al., 2010; Grimsrud et al., 2012), yet the functional role for these phosphorylation sites are as yet largely undefined (Pagliarini and Dixon, 2006). Moving forward, if we hope to be able to target mitochondrial phosphorylation for therapeutic intervention, there must be a greater understanding of the dynamic nature of phosphorylation in the mitochondria, as well as the proteins that perform these modifications, kinases and phosphatases.

Protein Kinases

Protein kinases are the enzymes that catalyze the transfer of the gamma phosphate of ATP to a free hydroxyl group on serine, threonine, and tyrosine amino acids. While many molecules can be phosphorylated, such as lipids, carbohydrates, and other small molecules, these modifications are outside the scope of this thesis and will not be discussed here. The transfer of a phosphate from ATP to a proteinacious substrate can regulate virtually every major signal transduction network within a cell (Ubersax and Ferrell, 2007).

The human kinome contains over 500 genes and comprises approximately 2% of the genome, while the protein kinase family shares many specific catalytic domains (Hanks et al., 1988; Manning et al., 2002a). The superfamily of kinases contains 9 groups, 90 familes and 145 subfamiles with a wide variety of substrates and methods to promote substrate specificity (Manning et al., 2002b). Because of their broad involvement in a variety of cellular processes, it is not surprising that kinase dysfunction is involved in many diseases, and that kinases are an area of significant therapeutic interest (Karaman et al., 2008).

The most well characterized mitochondrial kinases are the pyruvate dehydrogenase kinase (PDHK) and the branched chain ketoacid dehydrogenase kinase (BCKDK) that reside in the matrix (Holness and Sugden, 2003; Wynn et al., 2004). These kinases are generally known to be physically associated with their respective complexes and are not believed to phosphorylate other substrates. Furthermore, recent proteomic surveys of the mitochondrial proteome have not identified any significant number of kinases (Mootha et al., 2003; Pagliarini et al., 2008). Therefore, it

seems likely that the hundreds of phosphorylation sites identified in the mitochondria must be the substrates of kinases that translocate to the mitochondria from other cellular compartments (Arciuch et al., 2009; O'Rourke et al., 2011).

Protein Phosphatases

While there are over 500 kinases in the human genome, the number of protein phosphatases is considerably smaller, only about 140 putative genes (Shi, 2009). Of these, the significant majority (over 100) are protein tyrosine phosphatases (PTPs) and about 30 are protein serine/threonine phosphatases (PSPs).

There are four groups and three classes of PTPs. The Class I PTPs are cysteine-based phosphatases, which contain both classic PTPs, and dual specific phosphatases. Class II PTPs are related to bacterial arsenate reductases while Class III contains the Cdc25 cell cycle regulators (Alonso et al., 2004). Likely because of their greater number, PTP specificity is often regulated at the substrate level, with a deep active site cleft allowing for the length of the tyrosine residue reach the bottom (Denu et al., 1996). The dual specificity phosphatases comprise the largest portion of the PTP superfamily with about 65 proteins. These phosphatases contain the ability to dephosphorylate proteinacious substrates as well as carbohydrates and lipids, hence giving them their name (Guan et al., 1991; Maehama and Dixon, 1998; Worby et al., 2006). The mechanism of this unique capability is due to a shallower active site cleft compared to classic PTPs, which allows the enzyme to accommodate a greater number of substrates. One dual specificity phosphatase (DUSP26) was discovered in the MitoCarta compendium of mitochondrial proteins, while two other dual specificity

proteins (DUSP18 and DUSP21) have also been shown to localize to the mitochondrial compartment (Pagliarini et al., 2008; Rardin et al., 2008).

While the mammalian phosphoproteome contains only approximately 2% phosphotyrosine, the remainder is either phosphothreonine (12%) or phosphoserine (86%) (Olsen et al., 2006). This leaves the vast majority of the thousands of phosphorylation sites to be removed by the relatively small number of PSPs. The ability of these phosphatases to achieve substrate specificity is accomplished by their wide variety of regulatory subunits (Shi, 2009). For instance, a family of four glycogen-targeting subunits that serve as a molecular scaffold and have distinct tissue expression patterns regulate protein phosphatase 1 (PP1) in response to insulin (Newgard et al., 2000).

There are three major families of PSPs, the phosphoprotein phosphatases (PPPs), the metal dependent protein phosphatases (PPMs) and the aspartate-based protein phosphatases (FCP/SCP). Lester Reed's group discovered one of the first phosphorylation events in the mitochondria in 1969 when they realized the E1 subunit of the pyruvate dehydrogenase complex was inhibited by phosphorylation (Linn et al., 1969). The phosphatase that relieves this inhibition is known as the pyruvate dehydrogenase phosphatase (PDP) and is a member of the PP2C sub-family of phosphatases which are part of the PPM family (Huang et al., 1998; Lawson et al., 1993). This phosphatase is localized to the mitochondrial matrix and is dependent on Mn^{2+}/Mg^{2+} for catalysis, which was the third type of metal dependent phosphatase to be classified. PDP has also been shown to be capable of dephosphorylating all three serines that are responsible for repression of the enzyme, thus de-repressing the

complex. In other compartments of the cell, Type 2C phosphatases have been shown to regulate cell survival, apoptosis, growth and the stress response (Tamura et al., 2006). A Type 2C phosphatase (PPTC7) has also been discovered in the mitochondria of murine cells on at least two different occasions (Pagliarini et al., 2008; Rhee et al., 2013), and it seems likely that this uncharacterized mitochondrial phosphatase may play a key role within the mitochondrial phosphoproteome.

Quantitative Mass Spectrometry to Study Phosphorylation

In the last decade, mass spectrometry (MS) has revolutionized the study of PTMs. Owing to advances in detection and computation, it is now possible to identify thousands of phosphorylation sites in a single experiment (Grimsrud et al., 2010; Merrill and Coon, 2013). Because MS is stochastic by nature, this makes it difficult to compare protein or phosphorylation abundance between either replicates or biological samples. Fortunately, the development of isobaric tags has solved this dilemma by allowing the relative comparison of peptides and phosphopeptides from different biological states in a single MS experiment. Isobaric tags add the same mass to each sample, and an equal amount of each sample is labeled with a separate tag. Commercially available systems (TMT, iTRAQ) have been designed with the ability to tag 6, 8, and 10 samples in one run (Ross, 2004; Thompson et al., 2003). Each tag contains both a balance and reporter region, and because the sum of each region is the same for all tags, peptides that have been labeled co-elute and appear as a single peak during the first phase of tandem MS (MS1). Upon fractionation for sequencing in the second phase (MS2) the reporter region is dissociated from the peptide. Finally,

the intensities of the reporter region can be used to determine the relative abundance of each peptide in the original sample.

Peptides with phosphorylation will be a relatively small proportion of the total proteome in an average biological sample. Therefore, to be able to detect phosphorylation, phosphopeptides must first be enriched within a sample. In a general isobaric experiment, samples are homogenized, denatured, and enzymatically digested with a protease, commonly trypsin and/or LysC. Each sample is labeled with a unique isobaric tag, and all the samples are mixed together. To enrich for phosphorylation, samples are passed through an immobilized metal affinity chromatography (IMAC) column or, more recently, magnetic IMAC beads (Andersson and Porath, 1986). After this process, samples are fractionated and subjected to nano-liquid chromatography followed by MS/MS (Tandem nLC-MS/MS).

In a conventional shotgun proteomics approach, peptide intensities and mass-to-charge ratios (m/z) are recorded in an initial scan, commonly referred to as MS1. Next, the m/z values for peaks with high intensity are selected for sequencing by MS2. In MS2 the peptide is fragmented and sequenced based on the m/z of the resulting peptide. In an ideal experiment, the fragmentation technique will create a series of fragment ions that differ in mass by one amino acid. This way, not only can the primary sequence of the peptide be assessed, but the specific position of the phosphorylated residue can also be determined (Grimsrud et al., 2010). Finally, a comparison of the unphosphorylated peptides to the phosphorylated peptides can allow for a determination of the relative phosphorylation occupancy, which is a change in the modification normalized to the change in protein levels.

There are also other MS based quantification techniques available, including SILAC and NeuCode (Hebert et al., 2013b; Ong et al., 2002). In the SILAC method, cells are grown in non-radioactive heavy isotopes of essential amino acids. SILAC can improve upon isobaric tags by removing the technical variability of digesting samples before mixing and by performing quantitation during the MS1 scan. This solves the problem of peptide precursors being co-isolated for MS2 where it becomes impossible to differentiate which precursor released an amount of each reporter tag (Wenger et al., 2011). Unfortunately, only three samples can be included in a single run, which limits the ability for multiplexing. NeuCode overcomes this multiplexing limit by using high mass resolution MS to exploit the mass defect in stable isotopes. The isotopes are also sufficiently similar in mass to appear as a single peak in a low mass resolution run, also solving the peptide precursor problem mentioned above. In the end though, while both SILAC and NeuCode offer significant advantages to isobaric tagging, they both currently require situations where it is possible to grow either cells or an organism in isotopically labeled amino acids, which greatly increases the cost.

It is important to note that the above methods provide only relative abundance measurements of phosphorylation, not absolute stoichiometry. It is impossible to know if a two-fold change in phosphorylation represents a change from 50% to 100%, from 20% to 40% or from 1% to 2%. This is important to consider, especially when attempting to determine the biological function of a novel phosphorylation site. If a phosphorylation event activates a protein, it is possible that a small absolute increase in phosphorylation could have a meaningful biological outcome. But if a phosphorylation site inhibits a protein, the change could be 4-fold (1%-4%), and still

have 96% of a protein be in the activated state. This would be unlikely to have a significant biological effect. It is possible to use absolute quantification analysis (AQUA) to determine the stoichiometry of a sample (Gerber et al., 2003). Unfortunately, this method is much more time intensive and low-throughput, and is only practical for studying small subsets of phosphorylation sites.

Mitochondria

Approximately two billion years ago, a primordial eukaryotic cell engulfed an energy producing aerobic protobacterium (Lane, 2005), thus beginning the process of evolution toward modern eukaryotic cells with their energy producing organelles, mitochondria. These 10 million billion mitochondria found in the human body produce over 90% of cellular ATP through the process of oxidative phosphorylation (OXPHOS). While mitochondria have changed drastically over the course of evolution, they still retain several unique characteristics, including their unmistakable double-membrane architecture, and their own genome (Friedman and Nunnari, 2014). A singe mammalian cell can contain hundreds of copies of mitochondrial DNA (mtDNA), which is a circular 16.6 kilobase molecule encoding 13 essential subunits of the electron transport chain (ETC), two ribosomal RNAs, and 22 tRNAs necessary for translation of the mitochondrial proteins (Wallace, 2013). The remainder of the approximately 1300-mitochondrial proteins are encoded from the nuclear genome, which is regulated independently of the mitochondrial genome (Pagliarini et al., 2008). This dual-genome paradigm is exceedingly rare amongst eukaryotic organelles, and must be regulated dynamically in order to adapt to the changing metabolic needs of the cell.

The previous notion of mitochondria as small, independent, kidney bean-shaped factories has given way to the realization that not only do mitochondria have different tissue specificities throughout the body, but that they are a vast network that fuses, divides, and direct many essential cellular tasks (McBride et al., 2006; Nunnari and Suomalainen, 2012). Even the number of mitochondria can be vastly different in diverse cell types and organisms. There are approximately 1200 mitochondria in the average rat cell, while the giant amoeba *Chaos chaos* can have as many as 500 thousand mitochondria (Deng et al., 2002). Far more than simple energy generation, we now know that mitochondria are a central hub for many biosynthetic, catabolic, and metabolic pathways. Mitochondria play a role in the synthesis of lipids (Eaton, 2002), the maintenance of redox status, regulation of calcium levels (Rutter and Rizzuto, 2000), the production of reactive oxygen species (ROS), and the initiation of apoptosis (Green and Reed, 1998).

All mitochondria are contained with a double membrane structure that is separated by the inner membrane space (IMS). The outer membrane is semi-permeable, and allows for the movement of small molecules of less than 10 kDa across the membrane. In contrast, the inner membrane is relatively impermeable which allows for the buildup of a membrane potential that mitochondria use to generate ATP through OXPHOS. Pyruvate and fatty acids generate acetyl-CoA, which is the first molecule in the TCA cycle, which catalyzes the formation of NADH and $FADH_2$ as reducing equivalents. The four members of the electron transport chain (ETC) then oxidize NADH and $FADH_2$ to generate the electrochemical gradient used to create ATP by the ATP synthase complex. One byproduct of this system is that when excess electrons

exist, they can be combined with molecular oxygen to produce superoxide (Chance et al., 1979), a reactive oxygen species (ROS). Metabolic control is extremely important, and in response to excessive amounts of ROS, mitochondria can initiate apoptosis by opening the permeability transition pore (Wallace, 2012). Mitochondrial dysfunction is linked to over 200 human diseases, including inborn errors of metabolism (Calvo and Mootha, 2010), type 2 diabets mellitus (Szendroedi et al., 2011), neurodegenerative diseases (Lin and Beal, 2006), cancer (Wallace, 2012), and mitochondrial function is also linked to the aging process (Mammucari and Rizzuto, 2010; Raffaello and Rizzuto, 2010).

Reversible Phosphorylation in Mitochondria and Relevance to Human Health

While interest in mitochondria began to wane after the mechanism of OXPHOS was elucidated by Peter Mitchell in the late 1960's, the importance of mitochondria has seen a resurgence in the last 10 years as mitochondrial dysfunction is increasingly linked to disease states (Pagliarini and Rutter, 2013; Vafai and Mootha, 2012). Advances in research tools have also contributed to this resurgence, with quantitative mass spectrometry, systems biology, and powerful new microscopy techniques all providing distinct insights into the nature of mitochondrial biology. Indeed, we now know of over 150 distinct mitochondrial syndromes (Thorburn, 2004; Vafai and Mootha, 2012), with OXPHOS disorders being the most prevalent, but the specific genetic cause for many of these disorders is still unknown (Skladal et al., 2003). Efforts have been made to uncover the genetic basis for many of these diseases including next-gen sequencing (Chakravarti et al., 2013), metabolic profiling (Newgard, 2012), and

mapping the mitochondrial proteome (Hung et al., 2014; Pagliarini et al., 2008; Rhee et al., 2013). Unfortunately there are no known cures, and little therapeutic intervention available for the vast majority of genetically inherited mitochondrial disorders.

In addition to primary genetic disorders, as mentioned above, there are a host of other common diseases that have been connected to mitochondrial dysfunction such as metabolic syndrome, heart failure (HF), and various cancers. Specific examples include the glutamine-dependent reductive carboxylation seen in certain cancer cells (Mullen et al., 2013), the aberrant mitochondrial beta-oxidation in many tissues of patients with insulin resistance and T2DM (Muoio and Neufer, 2012), and the shift in substrate utilization from fatty acids towards glucose oxidation in late stage HF (O'Rourke et al., 2011). Furthermore, mitochondrial dysfunction is also prevalent in obesity-related cardiac dysfunction (Sack, 2009) – although debate still continues over whether this is a cause or an effect of the disease (Chattopadhyay et al., 2011). If we hope to understand the progression of these diseases and to develop new treatments, we must understand more about the regulation of mitochondrial function.

Regulation of mitochondria by PTMs has been known for several decades, since phosphorylation was shown to regulate the PDC. More recently, advances in mass spectrometry have resulted in the discovery of hundreds of mitochondrial proteins that contain PTMs including malonylation (Park et al., 2013; Rardin et al., 2013), acetylation (Hebert et al., 2013a; Still et al., 2013; Wang et al., 2010), glutarylation (Tan et al., 2014), and phosphorylation (Grimsrud et al., 2012; Lee et al., 2007). The apparent pervasiveness of mitochondrial PTMs and the demonstration of their functionality has led us to hypothesize that mismanagement of these modifications is an important

underlying feature of mitochondrial pathophysiology.

Of particular interest is phosphorylation, where a large, negatively charged phosphoryl group can alter protein function by affecting protein interactions or by altering enzymatic activity. The major mediators of phosphorylation are the protein kinases and phosphatases. While there are several phosphatases that have been identified in the mitochondria, the number of kinases known to either reside or localize to this organelle is much smaller. Many classic cytosolic kinases such as Akt, PKC and PKA have been reported to affect phosphorylation within mitochondria as well as on the mitochondrial surface (Horbinski and Chu, 2005). A-kinase anchoring proteins (AKAPs) are known to localize to the outer mitochondrial membrane (Carlucci et al., 2008), and an adenylyl cyclase and phosphodiesterase system has recently been described in the mitochondrial matrix (Acin-Perez et al., 2011; 2009). Using advanced quantitative techniques, we now know that hundreds of phosphorylation sites exist in the mitochondria, and that they are dynamic in response to different physiological conditions.

Mitochondrial dysfunction has also become increasingly linked to obesity, T2DM, metabolic syndrome and the various maladies that are associated with these diseases. Because regulation of proteins often involves PTMs, it is likely that the differences in phosphorylation seen in lean and obese mice can contribute to the etiology of disease progression. While the profiling of PTMs in mitochondria has become progressively more common, much is still not understood about how these transitory chemical marks serve to regulate protein function, or about the enzymes that add and remove them. Many areas in the field of mitochondrial PTMs remain unidentified and unexplored. By

using an integrated approach to test hypotheses, including mass spectrometry, systems biology, and biochemistry, new discoveries can be made that will further reveal the role of mitochondria in health and disease.

References

Acin-Perez, R., Russwurm, M., Günnewig, K., Gertz, M., Zoidl, G., Ramos, L., Buck, J., Levin, L.R., Rassow, J., Manfredi, G., et al. (2011). A phosphodiesterase 2A isoform localized to mitochondria regulates respiration. Journal of Biological Chemistry *286*, 30423–30432.

Acin-Perez, R., Salazar, E., Kamenetsky, M., Buck, J., Levin, L.R., and Manfredi, G. (2009). Cyclic AMP Produced inside Mitochondria Regulates Oxidative Phosphorylation. Cell Metabolism *9*, 265–276.

Alonso, A., Sasin, J., Bottini, N., Friedberg, I., Friedberg, I., Osterman, A., Godzik, A., Hunter, T., Dixon, J., and Mustelin, T. (2004). Protein tyrosine phosphatases in the human genome. Cell *117*, 699–711.

Andersson, L., and Porath, J. (1986). Isolation of phosphoproteins by immobilized metal (Fe3+) affinity chromatography. Analytical Biochemistry *154*, 250–254.

Arciuch, V.G.A., Alippe, Y., Carreras, M.C., and Poderoso, J.J. (2009). Mitochondrial kinases in cell signaling: Facts and perspectives. Advanced Drug Delivery Reviews *61*, 1234–1249.

Boja, E.S., Phillips, D., French, S.A., Harris, R.A., and Balaban, R.S. (2009). Quantitative Mitochondrial Phosphoproteomics Using iTRAQ on an LTQ-Orbitrap with High Energy Collision Dissociation. J. Proteome Res. *8*, 4665–4675.

Boutros, T., Chevet, E., and Metrakos, P. (2008). Mitogen-activated protein (MAP) kinase/MAP kinase phosphatase regulation: roles in cell growth, death, and cancer. Pharmacol. Rev. *60*, 261–310.

Calvo, S.E., and Mootha, V.K. (2010). The mitochondrial proteome and human disease. Annu Rev Genomics Hum Genet *11*, 25–44.

Carlucci, A., Lignitto, L., and Feliciello, A. (2008). Control of mitochondria dynamics and oxidative metabolism by cAMP, AKAPs and the proteasome. Trends in Cell Biology *18*, 604–613.

Chakravarti, A., Clark, A.G., and Mootha, V.K. (2013). Distilling pathophysiology from complex disease genetics. Cell *155*, 21–26.

Chance, B., Sies, H., and Boveris, A. (1979). Hydroperoxide metabolism in mammalian organs. Physiological Reviews *59*, 527–605.

Chattopadhyay, M., GuhaThakurta, I., Behera, P., Ranjan, K.R., Khanna, M., Mukhopadhyay, S., and Chakrabarti, S. (2011). Mitochondrial bioenergetics is not impaired in nonobese subjects with type 2 diabetes mellitus. Metabolism 1–9.

Cui, Z., Hou, J., Chen, X., Li, J., Xie, Z., Xue, P., Cai, T., Wu, P., Xu, T., and Yang, F. (2010). The profile of mitochondrial proteins and their phosphorylation signaling network in INS-1 beta cells. J. Proteome Res. *9*, 2898–2908.

Deng, N., Zhang, J., Zong, C., Wang, Y., Lu, H., Yang, P., Wang, W., Young, G.W., Wang, Y., Korge, P., et al. (2011). Phosphoproteome analysis reveals regulatory sites in major pathways of cardiac mitochondria. Molecular & Cellular Proteomics *10*, M110.000117–M110.000117.

Deng, W.-J., Nie, S., Dai, J., Wu, J.-R., and Zeng, R. (2010). Proteome, phosphoproteome, and hydroxyproteome of liver mitochondria in diabetic rats at early pathogenic stages. Molecular & Cellular Proteomics *9*, 100–116.

Deng, Y., Kohlwein, S.D., and Mannella, C.A. (2002). Fasting induces cyanide-resistant respiration and oxidative stress in the amoeba Chaos carolinensis: implications for the cubic structural transition in mitochondrial membranes. Protoplasma *219*, 160–167.

Denu, J.M., Stuckey, J.A., Saper, M.A., and Dixon, J.E. (1996). Form and function in protein dephosphorylation. Cell *87*, 361–364.

Eaton, S. (2002). Control of mitochondrial beta-oxidation flux. Prog. Lipid Res. *41*, 197–239.

Friedman, J.R., and Nunnari, J. (2014). Mitochondrial form and function. Nature *505*, 335–343.

Gerber, S.A., Rush, J., Stemman, O., Kirschner, M.W., and Gygi, S.P. (2003). Absolute quantification of proteins and phosphoproteins from cell lysates by tandem MS. Proc. Natl. Acad. Sci. U.S.a. *100*, 6940–6945.

Green, D.R., and Reed, J.C. (1998). Mitochondria and apoptosis. Science *281*, 1309–1312.

Grimsrud, P.A., Carson, J.J., Hebert, A.S., Hubler, S.L., Niemi, N.M., Bailey, D.J., Jochem, A., Stapleton, D.S., Keller, M.P., Westphall, M.S., et al. (2012). A quantitative map of the liver mitochondrial phosphoproteome reveals posttranslational control of ketogenesis. Cell Metabolism *16*, 672–683.

Grimsrud, P.A., Swaney, D.L., Wenger, C.D., Beauchene, N.A., and Coon, J.J. (2010). Phosphoproteomics for the Masses. ACS Chem. Biol. *5*, 105–119.

Guan, K.L., Broyles, S.S., and Dixon, J.E. (1991). A Tyr/Ser protein phosphatase encoded by vaccinia virus. Nature *350*, 359–362.

Hanks, S.K., Quinn, A.M., and Hunter, T. (1988). The protein kinase family: conserved features and deduced phylogeny of the catalytic domains. Science *241*, 42–52.

Hebert, A.S., Dittenhafer-Reed, K.E., Yu, W., Bailey, D.J., Selen, E.S., Boersma, M.D., Carson, J.J., Tonelli, M., Balloon, A.J., Higbee, A.J., et al. (2013a). Calorie Restriction and SIRT3 Trigger Global Reprogramming of the Mitochondrial Protein Acetylome. Mol. Cell *49*, 186–199.

Hebert, A.S., Merrill, A.E., Bailey, D.J., Still, A.J., Westphall, M.S., Strieter, E.R., Pagliarini, D.J., and Coon, J.J. (2013b). Neutron-encoded mass signatures for multiplexed proteome quantification. Nat Meth 1–5.

Holness, M.J., and Sugden, M.C. (2003). Regulation of pyruvate dehydrogenase complex activity by reversible phosphorylation. Biochem. Soc. Trans. *31*, 1143–1151.

Horbinski, C., and Chu, C.T. (2005). Kinase signaling cascades in the mitochondrion: a matter of life or death. Free Radical Biology and Medicine *38*, 2–11.

Huang, B., Gudi, R., Wu, P., Harris, R.A., and Hamilton, J. (1998). Isoenzymes of pyruvate dehydrogenase phosphatase DNA-derived amino acid sequences, expression, and regulation. Journal of Biological ….

Hubbard, M.J., and Cohen, P. (1993). On target with a new mechanism for the regulation of protein phosphorylation. Trends in Biochemical Sciences *18*, 172–177.

Hung, V., Zou, P., Rhee, H.-W., Udeshi, N.D., Cracan, V., Svinkina, T., Carr, S.A., Mootha, V.K., and Ting, A.Y. (2014). Proteomic mapping of the human mitochondrial intermembrane space in live cells via ratiometric APEX tagging. Mol. Cell *55*, 332–341.

Jensen, O.N. (2004). Modification-specific proteomics: characterization of post-translational modifications by mass spectrometry. Curr Opin Chem Biol *8*, 33–41.

Karaman, M.W., Herrgard, S., Treiber, D.K., Gallant, P., Atteridge, C.E., Campbell, B.T., Chan, K.W., Ciceri, P., Davis, M.I., Edeen, P.T., et al. (2008). A quantitative analysis of kinase inhibitor selectivity. Nature Biotechnology *26*, 127–132.

Keshet, Y., and Seger, R. (2010). The MAP kinase signaling cascades: a system of hundreds of components regulates a diverse array of physiological functions. Methods in Molecular Biology *661*, 3–38.

Korotchkina, L.G. (2000). Probing the Mechanism of Inactivation of Human Pyruvate Dehydrogenase by Phosphorylation of Three Sites. Journal of Biological Chemistry *276*, 5731–5738.

Lane, N. (2005). Power, Sex, Suicide: Mitochondria and the meaning of life (Oxford University Press).

Lawson, J.E., Niu, X.D., Browning, K.S., Trong, H.L., Yan, J., and Reed, L.J. (1993). Molecular cloning and expression of the catalytic subunit of bovine pyruvate dehydrogenase phosphatase and sequence similarity with protein phosphatase 2C. Biochemistry *32*, 8987–8993.

Lee, J., Xu, Y., Chen, Y., Sprung, R., Kim, S.C., Xie, S., and Zhao, Y. (2007). Mitochondrial phosphoproteome revealed by an improved IMAC method and MS/MS/MS. Mol. Cell Proteomics *6*, 669–676.

Lin, M.T., and Beal, M.F. (2006). Mitochondrial dysfunction and oxidative stress in neurodegenerative diseases. Nature *443*, 787–795.

Linn, T.C., Pettit, F.H., and Reed, L.J. (1969). Alpha-keto acid dehydrogenase complexes. X. Regulation of the activity of the pyruvate dehydrogenase complex from beef kidney mitochondria by phosphorylation and dephosphorylation. Proc. Natl. Acad. Sci. U.S.a. *62*, 234–241.

Maehama, T., and Dixon, J.E. (1998). The tumor suppressor, PTEN/MMAC1, dephosphorylates the lipid second messenger, phosphatidylinositol 3,4,5-trisphosphate. The Journal of Biological Chemistry *273*, 13375–13378.

Mammucari, C., and Rizzuto, R. (2010). Signaling pathways in mitochondrial dysfunction and aging. Mechanisms of Ageing and Development *131*, 536–543.

Manning, G., Whyte, D.B., Martinez, R., Hunter, T., and Sudarsanam, S. (2002a). The protein kinase complement of the human genome. Science *298*, 1912–1934.

Manning, G., Plowman, G.D., Hunter, T., and Sudarsanam, S. (2002b). Evolution of protein kinase signaling from yeast to man. Trends in Biochemical Sciences *27*, 514–520.

McBride, H.M., Neuspiel, M., and Wasiak, S. (2006). Mitochondria: More Than Just a Powerhouse. Current Biology *16*, R551–R560.

Merrill, A.E., and Coon, J.J. (2013). Quantifying proteomes and their post-translational modifications by stable isotope label-based mass spectrometry. Curr Opin Chem Biol *17*, 779–786.

Mootha, V.K., Bunkenborg, J., Olsen, J.V., Hjerrild, M., Wisniewski, J.R., Stahl, E., Bolouri, M.S., Ray, H.N., Sihag, S., Kamal, M., et al. (2003). Integrated analysis of protein composition, tissue diversity, and gene regulation in mouse mitochondria. Cell *115*, 629–640.

Mullen, A.R., Wheaton, W.W., Jin, E.S., Chen, P.-H., Sullivan, L.B., Cheng, T., Yang, Y., Linehan, W.M., Chandel, N.S., and DeBerardinis, R.J. (2013). Reductive carboxylation supports growth in tumour cells with defective mitochondria. Nature *481*, 385–388.

Muoio, D.M., and Neufer, P.D. (2012). Lipid-Induced Mitochondrial Stress and Insulin Action in Muscle. Cell Metabolism *15*, 595–605.

Newgard, C.B., Brady, M.J., O'Doherty, R.M., and Saltiel, A.R. (2000). Organizing glucose disposal: emerging roles of the glycogen targeting subunits of protein phosphatase-1. Diabetes *49*, 1967–1977.

Newgard, C.B. (2012). Interplay between lipids and branched-chain amino acids in development of insulin resistance. Cell Metabolism *15*, 606–614.

Nunnari, J., and Suomalainen, A. (2012). Mitochondria: in sickness and in health. Cell *148*, 1145–1159.

Olsen, J.V., Blagoev, B., Gnad, F., Macek, B., Kumar, C., Mortensen, P., and Mann, M. (2006). Global, In Vivo, and Site-Specific Phosphorylation Dynamics in Signaling Networks. Cell *127*, 635–648.

Ong, S.-E., Blagoev, B., Kratchmarova, I., Kristensen, D.B., Steen, H., Pandey, A., and Mann, M. (2002). Stable isotope labeling by amino acids in cell culture, SILAC, as a simple and accurate approach to expression proteomics. Mol. Cell Proteomics *1*, 376–386.

O'Rourke, B., Van Eyk, J.E., and Foster, D.B. (2011). Mitochondrial protein phosphorylation as a regulatory modality: implications for mitochondrial dysfunction in heart failure. Congestive Heart Failure (Greenwich, Conn.) *17*, 269–282.

Pagliarini, D.J., and Dixon, J.E. (2006). Mitochondrial modulation: reversible phosphorylation takes center stage? Trends in Biochemical Sciences *31*, 26–34.

Pagliarini, D.J., and Rutter, J. (2013). Hallmarks of a new era in mitochondrial biochemistry. Genes & Development *27*, 2615–2627.

Pagliarini, D.J., Calvo, S.E., Chang, B., Sheth, S.A., Vafai, S.B., Ong, S.-E., Walford, G.A., Sugiana, C., Boneh, A., and Chen, W.K. (2008). A Mitochondrial Protein Compendium Elucidates Complex I Disease Biology. *134*, 112–123.

Park, J., Chen, Y., Tishkoff, D.X., Peng, C., Tan, M., Dai, L., Xie, Z., Zhang, Y., Zwaans, B.M.M., Skinner, M.E., et al. (2013). SIRT5-Mediated Lysine Desuccinylation Impacts Diverse Metabolic Pathways. Mol. Cell *50*, 919–930.

Pearson, G., Robinson, F., Beers Gibson, T., Xu, B.E., Karandikar, M., Berman, K., and Cobb, M.H. (2001). Mitogen-activated protein (MAP) kinase pathways: regulation and physiological functions. Endocrine Reviews *22*, 153–183.

Raffaello, A., and Rizzuto, R. (2010). Mitochondrial longevity pathways. BBA - Molecular Cell Research 1–9.

Rana, A., Rera, M., and Walker, D.W. (2013). Parkin overexpression during aging reduces proteotoxicity, alters mitochondrial dynamics, and extends lifespan. Proceedings of the National Academy of Sciences.

Rardin, M.J., He, W., Nishida, Y., Newman, J.C., Carrico, C., Danielson, S.R., Guo, A., Gut, P., Sahu, A.K., Li, B., et al. (2013). SIRT5 Regulates the Mitochondrial Lysine Succinylome and Metabolic Networks. Cell Metabolism *18*, 920–933.

Rardin, M.J., Wiley, S.E., Murphy, A.N., Pagliarini, D.J., and Dixon, J.E. (2008). Dual specificity phosphatases 18 and 21 target to opposing sides of the mitochondrial inner membrane. The Journal of Biological Chemistry *283*, 15440–15450.

Rhee, H.-W., Zou, P., Udeshi, N.D., Martell, J.D., Mootha, V.K., Carr, S.A., and Ting, A.Y. (2013). Proteomic mapping of mitochondria in living cells via spatially restricted enzymatic tagging. Science *339*, 1328–1331.

Ross, P.L. (2004). Multiplexed Protein Quantitation in Saccharomyces cerevisiae Using Amine-reactive Isobaric Tagging Reagents. Molecular & Cellular Proteomics *3*, 1154–1169.

Rutter, G.A., and Rizzuto, R. (2000). Regulation of mitochondrial metabolism by ER Ca2+ release: an intimate connection. Trends in Biochemical Sciences *25*, 215–221.

Sack, M.N. (2009). Type 2 diabetes, mitochondrial biology and the heart. Journal of Molecular and Cellular Cardiology *46*, 842–849.

Shi, Y. (2009). Serine/threonine phosphatases: mechanism through structure. Cell *139*, 468–484.

Shimazu, T., Hirschey, M.D., Hua, L., Dittenhafer-Reed, K.E., Schwer, B., Lombard, D.B., Li, Y., Bunkenborg, J., Alt, F.W., Denu, J.M., et al. (2010). SIRT3 Deacetylates Mitochondrial 3-Hydroxy-3-Methylglutaryl CoA Synthase 2 and Regulates Ketone Body Production. Cell Metabolism *12*, 654–661.

Skladal, D., Halliday, J., and Thorburn, D.R. (2003). Minimum birth prevalence of mitochondrial respiratory chain disorders in children. Brain *126*, 1905–1912.

Stein, L.D. (2004). Human genome: end of the beginning. Nature *431*, 915–916.

Still, A.J., Floyd, B., Hebert, A.S., Bingman, C.A., Carson, J.J., Gunderson, D.R., Dolan, B., Grimsrud, P.A., Dittenhafer-Reed, K.E., Stapleton, D.S., et al. (2013). Quantification of mitochondrial acetylation dynamics highlights prominent sites of metabolic regulation. Journal of Biological Chemistry.

Szendroedi, J., Phielix, E., and Roden, M. (2011). The role of mitochondria in insulin resistance and type 2 diabetes mellitus. Nature Reviews Endocrinology.

Tamura, S., Toriumi, S., Saito, J.-I., Awano, K., Kudo, T.-A., and Kobayashi, T. (2006). PP2C family members play key roles in regulation of cell survival and apoptosis. Cancer Sci. *97*, 563–567.

Tan, M., Peng, C., Anderson, K.A., Chhoy, P., Xie, Z., Dai, L., Park, J., Chen, Y., Huang, H., Zhang, Y., et al. (2014). Lysine Glutarylation Is a ProteinPosttranslational Modification Regulated by SIRT5. Cell Metabolism *19*, 605–617.

Thompson, A., Schäfer, J., Kuhn, K., Kienle, S., Schwarz, J., Schmidt, G., Neumann, T., Johnstone, R., Mohammed, A.K.A., and Hamon, C. (2003). Tandem Mass Tags: A Novel Quantification Strategy for Comparative Analysis of Complex Protein Mixtures by MS/MS. Anal. Chem. *75*, 1895–1904.

Thorburn, D.R. (2004). Mitochondrial disorders: prevalence, myths and advances. J Inherit Metab Dis *27*, 349–362.

Ubersax, J.A., and Ferrell, J.E. (2007). Mechanisms of specificity in protein phosphorylation. Nat Rev Mol Cell Biol *8*, 530–541.

Vafai, S.B., and Mootha, V.K. (2012). Mitochondrial disorders as windows into an ancient organelle. Nature *491*, 374–383.

Wallace, D.C. (2012). Mitochondria and cancer. Nat. Rev. Cancer *12*, 685–698.

Wallace, D.C. (2013). A mitochondrial bioenergetic etiology of disease. J. Clin. Invest. *123*, 1405–1412.

Wang, Q., Zhang, Y., Yang, C., Xiong, H., Lin, Y., Yao, J., Li, H., Xie, L., Zhao, W., Yao, Y., et al. (2010). Acetylation of Metabolic Enzymes Coordinates Carbon Source Utilization and Metabolic Flux. Science *327*, 1004–1007.

Wenger, C.D., Lee, M.V., Hebert, A.S., McAlister, G.C., Phanstiel, D.H., Westphall, M.S., and Coon, J.J. (2011). Gas-phase purification enables accurate, multiplexed proteome quantification with isobaric tagging. Nat Meth *8*, 933–935.

Worby, C.A., Gentry, M.S., and Dixon, J.E. (2006). Laforin, a dual specificity phosphatase that dephosphorylates complex carbohydrates. The Journal of Biological Chemistry *281*, 30412–30418.

Wynn, R.M., Kato, M., Machius, M., Chuang, J.L., Li, J., Tomchick, D.R., and Chuang, D.T. (2004). Molecular Mechanism for Regulation of the Human Mitochondrial Branched-Chain α-Ketoacid Dehydrogenase Complex by Phosphorylation. Structure *12*, 2185–2196.

Yeaman, S.J., Hutcheson, E.T., Roche, T.E., Pettit, F.H., Brown, J.R., Reed, L.J., Watson, D.C., and Dixon, G.H. (1978). Sites of phosphorylation on pyruvate dehydrogenase from bovine kidney and heart. Biochemistry *17*, 2364–2370.

CHAPTER 2:

A Quantitative Map of the Liver Mitochondrial Phosphoproteome Reveals Posttranslational Control of Ketogenesis

This chapter was published in the following journal article:

Grimsrud PA*, Carson JJ*, Hebert AS, Hubler SL, Niemi NM, Bailey DJ, Jochem A, Stapleton DS, Keller MP, Westphall MS, Yandell BS, Attie AD, Coon JJ, and Pagliarini DJ. (2012) A quantitative map of the liver mitochondrial phosphoproteome reveals post-translational control of ketogenesis. Cell Metabolism 16, 672-683.

*Grimsrud and Carson contributed equally to this work.

Summary

Mitochondria are dynamic organelles that play a central role in a diverse array of metabolic processes. Elucidating mitochondrial adaptations to changing metabolic demands and the pathogenic alterations that underlie metabolic disorders represent principal challenges in cell biology. Here, we performed multiplexed quantitative mass spectrometry-based proteomics to chart the remodeling of the mouse liver mitochondrial proteome and phosphoproteome during both acute and chronic physiological transformations. Our analyses reveal that reversible phosphorylation is widespread in mitochondria, and is a key mechanism for regulating ketogenesis during the onset of obesity and type 2 diabetes. Specifically, we have demonstrated that phosphorylation of a conserved serine on Hmgcs2 significantly enhances its catalytic activity in response to increased ketogenic demand. Collectively, our work describes the plasticity of this organelle at high resolution and provides a framework for investigating the roles of proteome restructuring and reversible phosphorylation in mitochondrial adaptation.

Introduction

Mitochondria are centers of metabolism and signaling whose function is essential to nearly all eukaryotic cells (Nunnari and Suomalainen, 2012). Mitochondrial dysfunction is associated with a spectrum of rare inborn errors of metabolism, and with an increasing number of common human diseases including Parkinson's, Alzheimer's, various cancers, metabolic syndrome, and type 2 diabetes (T2D) (Nunnari and Suomalainen, 2012; Szendroedi et al., 2012; Wallace, 2005). Recent large-scale efforts have helped to define the mammalian mitochondrial proteome and to reveal its variability across a range of tissues (Forner et al., 2006; Foster et al., 2006; Johnson et al., 2007; Pagliarini et al., 2008). Collectively, this work has advanced our understanding of basic mitochondrial biology and has catalyzed the discovery of multiple gene mutations underlying mitochondrial diseases (Calvo and Mootha, 2010). Nonetheless, important steps remain for achieving a systems-level understanding of this organelle and its contribution to disease pathophysiology. Among these are elucidating how this proteome is altered in conditions involving mitochondrial dysfunction and more comprehensively assessing the role of post-transcriptional and post-translational mechanisms in regulating mitochondrial protein activities.

Mounting evidence suggests that mitochondrial adaptation relies on a range of reversible post-translational modifications (PTMs). Already, focused efforts have linked the importance of these modifications to apoptosis, oxidative phosphorylation, the hypoxia response, and mitochondrial biogenesis (O'Rourke et al., 2011; Pagliarini and Dixon, 2006), and large-scale studies have revealed that much of the mitochondrial proteome possesses phosphorylated (Boja et al., 2009; Deng et al., 2010; Zhao et al.,

2011) or acetylated (Choudhary et al., 2009; Kim et al., 2006; Zhao et al., 2010) residues. Nevertheless, our understanding of specific protein and PTM alterations that affect this organelle's function across defined biological conditions remains in its infancy. This is principally due to the fact that large-scale investigations of mitochondrial PTMs often fail either to identify specific sites of modification or to produce quantitative data on how these sites change in abundance across contrasting biological states, making it difficult to spotlight bona fide regulatory sites from amongst a background of stable or adventitious modifications (Cui et al., 2010; Deng et al., 2011; Gnad et al., 2010; Hopper et al., 2006; Lee et al., 2007; Reinders et al., 2007).

Here, we performed deep, multiplexed quantitative proteomics and site-specific phosphoproteomics of mouse liver mitochondria across a series of contrasting biological states (Figure 1A, 4A). First, we analyzed both lean (wild type) and obese (leptin deficient) mice at two different ages (4 weeks or 10 weeks), each from two common strains (C57BL/6J (B6) and BTBR). These analyses were primarily motivated by the suspected contribution of mitochondrial dysfunction to premature aging (Wojtovich et al., 2012), the onset of obesity and obesity-linked insulin resistance (Lowell and Shulman, 2005; Szendroedi et al., 2012), and by the sharp contrast in T2D susceptibility between these two strains (Stoehr et al., 2000). To achieve extensive coverage of proteins and phosphoproteins, and to quantify their fold-change values between conditions, we conducted five independent 8-way comparisons (40 mice total) using high resolution and high mass accuracy mass spectrometry (MS) with isobaric tagging (Lee et al., 2011; Phanstiel et al., 2011; Ross et al., 2004; Thompson et al., 2003). Using this same approach, we further analyzed the rapid mitochondrial

phosphoprotein changes that occur in wild type B6 mice during acute fasting and refeeding. Collectively, we identified 637 phosphosites — including more than 100 not previously reported — on 251 mitochondrial proteins, and revealed that a large proportion of these sites are dynamic and reversible during these acute and chronic transformations.

We leveraged this quantitative dataset to reveal that phosphorylation is an important mechanism for regulating ketone body production. We have demonstrated that Hmgcs2, which catalyzes the first committed step of ketogenesis in the mitochondrion (Reed et al., 1975), is phosphorylated on 10 separate residues. Phosphorylation of five of these sites change dynamically across our biological conditions ($q<0.1$), and at least one — phosphorylation of serine 456 — significantly enhances enzyme activity. We have further shown that phosphorylation of this site occurs in response to increased ketogenic demand both in cell culture and in our mouse models, whose serum β-hydroxybutyrate increase with obesity and the onset of T2D. Our protein and phosphorylation compendium, termed MitoMod, is freely available at mitomod.biochem.wisc.edu.

Results and Discussion

Comparative Proteomic Analyses of Mouse Liver Mitochondria

The goal of our initial proteomic analyses was to establish a comprehensive and quantitative map of mitochondrial protein abundances and site-specific protein phosphorylation levels across the contrasting biological conditions of age, mouse strain, and obesity status. To do so, we performed these analyses in two phases. In the univariate phase, we analyzed liver mitochondria from four lean (wild type) and four obese (leptin-/-, ob/ob) 10 week-old B6 mice (Figure 1A). In addition to elucidating the mitochondrial alterations that accompany the onset of obesity, this initial phase enabled us to assess the breadth and depth at which our analysis platform could capture the mitochondrial proteome and phosphoproteome. In the multivariate phase, we analyzed 40 mice differing by three variables: age, strain, and obesity (Figure 1A). These animals included lean (wild type) and obese (ob/ob) mice from both diabetes-susceptible (BTBR) and diabetes-resistant (B6) strains, each as either adolescents (4 weeks of age) or adults (10 weeks of age). To profile all forty mice, we conducted five sets of biological replicates. This phase enabled us to identify mitochondrial alterations that correlate with a series of biological states.

For each phase, we purified mitochondria only to the extent required to achieve near comprehensive coverage of the liver MitoCarta protein list. MitoCarta is a tissue-specific compendium of mitochondrial proteins that was complied using in-depth mass spectrometry-based proteomic analyses of highly purified mitochondria, machine learning, and GFP microscopy (Pagliarini et al., 2008). Here, simple mitochondrial enrichments were sufficient to achieve the desired coverage, allowing us to minimize

the sample-to-sample variation introduced by extensive purification procedures, and to maximize coverage of other co-purifying organelles. Our univariate phase identified 3,447 unique proteins and 3,895 unique phosphoisoforms (site-specific phosphorylation patterns) from just over 1 million MS/MS scans. These include 693 of the 700 liver mitochondrial proteins noted above (Pagliarini et al., 2008), and 449 mitochondrial phosphoisoforms. When the protein measurements were subjected to unsupervised hierarchical clustering, the mice grouped as expected according to their metabolic status (lean or obese), demonstrating our ability to accurately profile unique proteome signatures for contrasting metabolic states (Figure 1B). After correcting for multiple hypotheses, statistically significant differences ($q<0.1$) in abundance were observed for 1,014 proteins (325 mitochondrial, Figures 1H and S1B) and 720 phosphoisoforms (102 mitochondrial, Figure 1H and S1D).

Our univariate measurements revealed extensive and reproducible remodeling of the liver mitochondrial proteome and phosphoproteome with obesity (Figure 1B-D, S1B-D). For example, pathway analysis of mitochondrial protein abundance alterations (Figures S1C) showed coordinate induction of fatty acid oxidation (Figure 1C) and oxidative phosphosphorylation (OxPhos) (Figure 1G) proteins, with repression of reactive oxygen species (ROS) detoxification enzymes (Figure S1C), consistent with known obesity-induced liver alterations (Buchner et al., 2011; Deng et al., 2010; Lan et al., 2003; Lazarin Mde et al., 2011; Takamura et al., 2008). Mitochondrial phosphorylation changes were prominent in a range of central metabolic pathways (see mitomod.biochem.wisc.edu and Tables S1A-E). For example, the three most statistically significant changes ($q<0.002$) in phosphorylation of MitoCarta proteins in

the univariate phase were found on enzymes involved in ketogenesis (Hmgcs2), lipogenesis (Gpam), and retinol metabolism (Dhrs4). These observations motivate mechanistic follow-up studies, as each of these pathways is key for proper liver function and is linked to hepatic changes caused by obesity (Berry et al., 2011; Kuhajda et al., 2011; Laffel, 1999). Although we focus on mitochondrial-specific changes, our data also reveal many significant alterations in protein and phosphorylation from the endoplasmic reticulum (ER) and peroxisomes — organelles with obesity-induced responses interconnected with mitochondrial dysfunction (Hotamisligil, 2010; Noland et al., 2007) (Tables S1A-E). The wealth of site-specific protein phosphorylation measurements (and corresponding protein abundance levels) in our large-scale dataset can help to generate new hypotheses regarding the role of post-translational regulation of metabolic enzymes during the development of obesity and obesity-linked insulin resistance.

Given the efficacy of our univariate phase at quantifying a wide range of obesity-induced mitochondrial proteome/phosphoproteome alterations (Figures 1B-D, S1B-D), we proceeded to analyze 40 additional mice in our multivariate phase (Figure 1A). The experimental design of this phase enables us to identify proteomic and phosphoproteomic aspects that change as a function of specific variables including age, obesity status, mouse strain, and combinations thereof (see Figure S1A for a description of all comparisons). Here, we identified 3,684 unique proteins, including 98% of the liver mitochondrial proteins previously identified by MS in the MitoCarta study (Pagliarini et al., 2008). Of the 5,948 unique phosphoisoforms identified, 508 are on mitochondrial proteins. Across all conditions assessed in these two analyses, we

have identified statistical significant changes ($q<0.1$) in 268 of these mitochondrial phosphoisoforms (on 136 proteins), as well as abundance alterations for 534 mitochondrial proteins (mitomod.biochem.wisc.edu). Importantly, our analyses of a large number of biological replicates across two separate experiments demonstrate that our measurements are both accurate and reproducible (Figures 1B-E, Figure S1B-G).

When we performed unsupervised hierarchical clustering of the MitoCarta-specific protein abundance measurements for all eight conditions assessed, the mice grouped primarily by strain. Interestingly, the B6 mice displayed secondary grouping based on obesity status, while secondary groupings for BTBR mice were separated by diabetes status (Figure 1F). Pathway analysis of our data reveals that the diabetic 10 week-old BTBR mice, opposite their B6 counterparts, have repressed expression of glycolytic and TCA cycle enzymes (Figure S1H), congruent with the decreased glucose utilization and increased channeling of acetyl CoA into ketogenesis seen in fasting hyperglycemia (Berry et al., 1983; Lan et al., 2003). Similarly, while OxPhos proteins are induced with obesity in B6 mice, they are decreased in obese hyperglycemic BTBR mice (Figure 1G), perhaps partially explaining discrepancies in the reported effect of obesity on liver mitochondrial respiration in different mouse models (Buchner et al., 2011; Holmstrom et al., 2012; Raffaella et al., 2008). Collectively, these analyses begin to capture the global plasticity of the mitochondrial proteome, and highlight individual proteins and pathways in this organelle that are key to cellular metabolic adaptation to multiple physiological states (Figure 1H).

A Quantitative Map of Mitochondrial Phosphoproteome Dynamics

Our analyses advance the notion that reversible phosphorylation is a key mechanism for regulating mitochondrial protein function. Our work expands the number of known mouse liver mitochondrial phosphosites by 123, while capturing 77% of those reported previously (Huttlin et al., 2010; Lee et al., 2007; Monetti et al., 2011; Villen et al., 2007). These phosphorylation events are pervasive within this organelle: at least one protein from each of the major mitochondrial metabolic pathways we investigated was phosphorylated, including those highlighted in Figure 2. Importantly, we are able to detect phosphorylation even on proteins of low expression (Figure S2), suggesting that we are approaching a comprehensive assessment of this modification in mitochondria.

Our analyses help to discern which proteins might be particularly important targets of phosphorylation. First, by organizing the mitochondrial proteome into pathways and complexes, it is clear that certain proteins have a disproportionately high number of phosphorylation sites, even when the corresponding proteins are each detected at comparable levels. Such proteins include Atp5a1 of OxPhos (Figure 2A) and Hmgcs2 of the ketogenesis pathway (Figure 2B), which each have at least three-fold more phosphorylation sites than other members of their respective pathways. Second, by comparing our data with a recent muscle phosphoproteomic study (Zhao et al., 2011), we find a high degree of overlap in phosphorylation targets for certain pathways (e.g. 15 of our 27 phosphorylated OxPhos subunits, Figure 2A), suggesting that a common set of proteins are subject to phosphorylation in different tissues. Third, and most importantly, because our approach quantifies phosphorylation sites across a

range of conditions, we can identify those sites that change dynamically. We find that a large proportion (41%) of mitochondrial phosphorylation sites significantly and reproducibly change between at least one of our comparison groups ($q<0.1$). As illustrated in Figure 2A, residues on 14 of the 27 phosphorylated OxPhos subunits noted above are subject to dynamic phosphorylation ($q<0.1$), and thus represent potential regulatory sites (red dots in Figure 2A).

The design of our multivariate study enables us to associate specific protein and phosphorylation changes with particular physiological transitions. Of the 235 mitochondrial phosphosites whose abundances significantly change in any of the comparisons in our multivariate dataset ($q<0.1$), 134 demonstrate associations with age, mouse strain, or onset of obesity, independent of other factors (Figure 3A, Table S1C). For example, phosphorylation of serine 162 on the mitochondrial ribosomal subunit Lactb increases specifically in an age-dependent manner in both strains, regardless of their obesity status (Figure 3B). It is tempting to speculate that the decreased phosphorylation of Lactb on S162 in 10 week-old mice could contribute to the increased susceptibility to obesity and insulin resistance seen in mice that overexpress this protein (Bains et al., 2004; Chen et al., 2008). Likewise, the phosphorylation levels of serine 55 on Acadl and threonine 46 on Slc25a5 were significantly altered in strain- and obesity-centric manners, respectively (Figure 3B). Acadl is an acyl-CoA dehydrogenase that catalyzes the first step in mitochondrial beta-oxidation of long straight-chain fatty acids (Lea et al., 2000). We hypothesize that the increase in phosphorylation on s55 in BTBR mice promotes enhanced lipid oxidation, consistent with BTBR animals having resistance to the development of fatty liver in

obesity (Lan et al., 2003). Likewise, the obesity-induced decrease in phosphorylation of Slc25a5 (Ant2), the mitochondrial ATP/ADP translocase, could contribute to the alterations of liver mitochondrial respiratory efficiency found in mice with obesity-induced insulin resistance (Buchner et al., 2011; Harper et al., 2008). Collectively, these examples of condition-specific changes in mitochondrial phosphorylation reveal how our data can be leveraged to generate hypotheses about how a given site affects protein function and to elucidate important mitochondrial processes that are altered in defined physiological states.

Acute Mitochondrial Phosphorylation Changes During Fasting/Refeeding

Our multivariate analyses described above provide a map of the liver mitochondrial phosphoproteome, and describe how individual phosphosites are altered during gradual, long-term physiological changes. Next, to ensure that many of the phosphorylation events we detect represent bona fide reversible sites of modification, and to further refine our hypotheses about the function of individual phosphosites, we measured changes in the mitochondrial phosphoproteome during an acute fasting/refeeding experiment. Here, eight lean (wild type) B6 mice were fasted overnight (16 hrs), after which half of the animals were allowed to feed ad libitum for two hours (Figure 4A). Serum metabolite analyses revealed the expected refeeding responses: insulin and glucose levels were elevated and β-hydroxybutyrate levels were diminished in refed versus fasted animals (Figure 4B).

Refeeding caused rapid changes to 88 MitoCarta phosphoisoforms (58 decreasing and 30 increasing at $q<0.1$), with generally small or nonexistent underlying

changes to protein levels (Figure 4D). The average magnitude of change for significantly altered MitoCarta phosphosites ($q<0.1$) was significantly greater than that of MitoCarta protein abundance changes (53% vs. 12%, respectively, $p<0.01$). Notably, these included the expected decreases in phosphorylation of pyruvate dehydrogenase E1α S232, S292 and S300 (Caterson et al., 1987) and branched chain ketoacid dehydrogenase E1 S338 (Lu et al., 2009) (Figure 4C). Likewise, expected changes to non-mitochondrial proteins were observed, including increased phosphorylation of glycogen synthase kinase 3 alpha S21 (Fang et al., 2000) and decreased phosphorylation of inositol 1,4,5-triphosphate receptor 1 S1588 (Wang et al., 2012), confirming the reliability of our experimental design (Figure 4C). We also observe dynamic phosphorylation on mitochondrial proteins from a wide range of pathways and processes, including oxidative phosphorylation (Atp5a1, Atp5j, Ndufv3, Cox4i1), the TCA cycle (Idh3g), fatty acid oxidation (Acaa1b, Acadvl, Hadha, Ehhadh), the urea cycle (Glud1, Slc25a13, Otc, Cps1), and hormone metabolism (Comt). These dynamic phosphosphorylation events could contribute to changes in the activities of these enzymes or flux through their corresponding pathways that have been implicated in fasting/starvation responses (Capeau, 2008; Griffiths et al., 1995; Ismahan and Parvez, 1978; Verweij et al., 2012). Moreover, we observe reciprocal regulation of S694 (decreasing) and S687 (increasing) on Gpam, the mitochondrial outer membrane enzyme that catalyzes the rate-limiting step in glycerolipid biosynthesis. Gpam phosphorylation (particularly S694) also showed significant differences with obesity in our univariate study and between strains in our multivariate study, which may contribute to the differences in susceptibility to obesity-induced hepatic steatosis that

we have previously reported in these mice (Lan et al., 2003), and to the profound changes in glycerolipid production known to occur during aging (Collison et al., 2005; Houtkooper et al., 2011). Last, these data suggest that mitochondrial pathways such as heme biosynthesis (Alas1), synthesis of mitochondrial-specific fatty acids (Mcat), and protein translation (Rg9mtd1, Mrpl1, Mrpl45, Mrps36) are subject to rapid, post-translational regulation in response to refeeding (Figure 4D). Collectively, this analysis demonstrates that mitochondrial phosphorylation is indeed reversible and responsive to acute metabolic perturbations

Kinase Activities Predicted via Phosphopeptide Data

Our observation that dynamic phosphorylation is widespread among mitochondrial proteins motivated us to investigate which kinases might be performing these modifications. To do so, we employed two phosphosite analyses. First, we directly searched our data for phosphorylation found on known kinase motifs, as defined in the Phosida database (Gnad et al., 2011). This analysis suggested that a wide variety of kinases might be active in this organelle: 13 different kinases were each associated with at least 20 MitoCarta phosphosites (Figure 5A). A caveat to this analysis, however, is that it does not take into account the frequency at which each motif appears in the proteome at the primary sequence level (regardless of phosphorylation status). A second caveat is that this analysis is biased toward established kinase motifs. Given these shortcomings, we also analyzed our data using the Motif-X algorithm (Schwartz and Gygi, 2005), which identifies amino acid residues overrepresented at specific positions around phosphorylation sites relative to all

phosphorylatable residues (taking into account the rate of motif occurrence). Motif-X analysis revealed four such amino acid sequences around MitoCarta phosphosites, including those that loosely match to the CK2 (sxxE) and PKA (Rxxs) consensus sites (Figure 5B). Together, these analyses suggest that PKA and CK2 are among the active kinases in mitochondria, consistent with recent phospho-motif analysis of muscle mitochondrial proteins (Zhao et al., 2011), and with reports of PKA phosphorylating complex IV subunits (Acin-Perez et al., 2011; Acin-Perez et al., 2009). Furthermore, across our entire multivariate dataset (mitochondrial and non-mitochondrial proteins), phosphorylation levels on proteins with putative PKA and CK2 motifs increase in an age- and obesity-dependent manner ($p<0.05$), suggesting that these kinases may be responsible for some of the increased mitochondrial phosphorylation seen during these transitions (Figure 5C; see Figure S3 and Tables S1A-E for all kinase activity predictions).

Phosphorylation of serine 456 on Hmgcs2 promotes ketogenesis

The combination of our quantitative proteomics data and kinase activity predictions enabled us to predict which phosphorylation events might regulate specific mitochondrial proteins. Among the most highly phosphorylated proteins in our study was Hmgcs2, the enzyme that catalyzes the rate-limiting step in ketogenesis. We identified 10 phosphorylated residues on Hmgcs2 (Figure 2B), and phosphorylation abundance on five of these sites exhibited significant changes in at least one comparison ($q<0.1$). Two of these sites, S433 and S456, are conserved in the human ortholog (HMGCS2) and had phosphorylation patterns that changed between our

strains, which have differing susceptibility to T2D (Stoehr et al., 2000). This led us to hypothesize that phosphorylation of these sites might regulate enzyme activity and contribute to the elevated ketone body levels we observe in obese diabetic BTBR mice (Figure 6A). Due to a primary sequence difference between B6 and BTBR mice near the S433 phosphorylation site (Figure S4A), we were unable to directly measure the relative abundance of this site between strains using the iTRAQ system. However, spectral counts suggest that this site is only prominent in B6 animals (Figure S4A), where it exhibits a significant obesity-induced increase in 10 week-old mice ($q<0.03$ in both univariate and multivariate studies). Alternately, S456 exhibits an obesity-induced increase in both strains, with a more pronounced increase in BTBR mice (Figures 6B,C). As highlighted in Figure 6D, S456 on Hmgcs2 falls within consensus motifs for both protein kinase A (PKA) and caseine kinase 2 (CK2) — two of the kinases predicted to be active in our mitochondrial survey (Figures 5, S3) and that have previously been associated with mitochondrial regulation (Acin-Perez et al., 2011; Acin-Perez et al., 2009; Rao et al., 2011; Schmidt et al., 2011; Zhao et al., 2011).

To evaluate the effect of these dynamic phosphorylation events on Hmgcs2 enzymatic activity, we performed biochemical assays on a series of human HMGCS2 variants. We mutated each phosphorylated residue to an acidic residue (aspartic acid or glutamic acid) to mimic phosphorylation (S433D, S456D/E) or to a non-phosphorylatable residue (alanine or methionine) to mimic dephosphorylation (S433A, S456A/M). We immunoprecipitated these Flag-tagged variants, along with wild type and catalytically inactive (C166A) HMGCS2, from HEK293 cells, and tested the activity of each variant in an in vitro activity assay (Skaff and Miziorko, 2010). As seen in Figure

6E, the phosphomimetics for serine 456 each resulted in an approximate 50% increase in enzyme activity over wild type and the S456A variant. A third variant (S456M), which approximates the steric change of the phosphomimetics without conferring a negative charge, also had no increase in enzyme activity (Figure 6E). The S433 phosphomimetic, however, had no increase in activity (Figure 6F, S4B), suggesting that phosphorylation on this site has a role distinct from directly modifying Hmgcs2 enzymatic activity. This change in S456 mutants was consistent across multiple substrate concentrations (Figure 6F) and amounts of protein (Figure S4C).

Given the motifs present on S456 (Figure 6D), we tested the ability of recombinant PKA to activate enzyme activity by incubating it with wild type HMGCS2 and each of the above S456 variants before repeating the activity assays. As seen in Figure 7A, only wild type HMGCS2, which possesses a phosphorylatable serine 456, had its activity increased by PKA. MS analysis of the PKA-treated HMGCS2 verified that serine 456 was indeed phosphorylated by this treatment (Figure 7B), and that the untreated enzyme had no detectible phosphorylation on this site. CK2 increased WT HMGCS2 activity to an even greater extent (Figure 7A) than PKA, with this effect likewise abrogated by mutation of S456. Interestingly, this result is consistent with the human ortholog of HMGCS2 (Figure 7B) having a slightly weaker PKA consensus site around S456 than the mouse ortholog (Figure 6B), while maintaining a strong CK2 consensus sequence.

We next sought to determine if S456 phosphorylation is important for the activation of HMGCS2 in response to increased ketogenic demand. To do so, we immunoprecipitated WT and mutant HMGCS2 from HEK293 cells cultured in either

standard or ketogenic media, which increases ketone body production (Figure 7C) (Sengupta et al., 2010). WT HMGCS2 was approximately 2-fold more active when purified from cells grown in ketogenic media ($p<0.001$) (Figure 7D). This effect was ablated with mutation of S456 (Figure 7D), with neither the S456A or S456D mutants showing a change in activity between media conditions (note S456D activity was still greater than S456A activity, consistent with Figures 6E-F). Disruption of either the PKA (453A) or CK2 (458A) consensus sites also abrogated HMGCS2 activity in ketogenic media (Figure 7X), although variants missing proline 457 or other surrounding residues behaved similarly to wild type (Figure S7X). Moreover, WT HMGCS2 purified from 293 cells grown in ketogenic media could not be further activated by in vitro phosphorylation with CK2, suggesting maximal phosphorylation occupancy of S456 in ketogenic conditions (Figure 7E).

As a final test of the importance of S456 phosphorylation on the activation of HMGCS2, we measured ketone body production from HEK 293 cells expressing HMGCS2 variants. In standard media, 293 cells produce miniscule amounts of β-hydroxybutyrate (β-HB), in large part due to the nearly complete absence of HMGCS2 expression (Figure S7X). However, expression of exogenous HMGCS2 results in significant β-HB production, which is further activated by ketogenic media (Figure S7C) (Sengupta et al., 2010). Here, we expressed wild type, 456A or 456D HMGCS2 in 293 cells under both standard and ketogenic conditions and measured β-HB production after 72 hours. Consistent with our in vitro activity results (Figure 7D), mutation of S456 significantly attenuated the fold-change increase in ketone body production following a switch to ketogenic media (Figure 7F). Also consistently, cells harboring the 456D

mutant had a greater ketogenic output than those with the 456A mutant. Interestingly, cells expressing wild type HMGCS2 had the greatest total β-HB production. This suggests that, in vivo, mutation of this site might affect other properties of HMGCS2, such as proper mitochondrial localization, interactions with other proteins, or its modification by other known PTMs (e.g., acetylation, succinylation, or palmitoylation)(Kostiuk et al., 2008; Quant et al., 1990; Shimazu et al., 2010). Nonetheless, the combination of our mass spectrometry analyses, in vitro enzyme activity measurements, and cellular β-HB assays strongly support a role for HMGCS2 S456 phosphorylation in enhancing ketogenic output.

Conclusions

We have established a quantitative proteomic compendium that charts dynamic changes in mitochondria and mitochondria-associated organelles across a series of contrasting biological states. This resource, termed MitoMod (mitomod.wisc.edu), captures both protein and phosphoprotein alterations, and is further leveraged by our previous matched microarray data from the same tissue samples (Keller et al., 2008). These measurements enable the interrogation of post-transcriptional and post-translational mechanisms important for mitochondrial adaptation. Additionally, our quantitative data highlights mitochondrial alterations that track with distinct mouse strains and with varying biological states, including the transition from adolescence to adulthood, the onset of obesity, or the development of T2D, and the response to acute fasting/refeeding.

Whereas the importance of phosphorylation has been appreciated for a handful of mitochondrial proteins for decades (Pagliarini and Dixon, 2006), more recent work enabled by advancements in phosphoproteomics technologies (Grimsrud et al., 2010b) have suggested a more pervasive role for this PTM (Boja et al., 2009; Deng et al., 2010; Gnad et al., 2010; Hopper et al., 2006; Lee et al., 2007; O'Rourke et al., 2011; Zhao et al., 2011). Here, our analyses across a range of physiological conditions with extensive biological replication using state-of-the-art quantitative proteomic strategies support this notion, as we have revealed that a large percentage of mitochondrial proteins possess bona fide dynamic phosphosites. We identified Hmgcs2, the enzyme that catalyzes the rate-limiting step in ketogenesis, as a key target for reversible phosphorylation. We have shown that phosphorylation of this enzyme on a conserved

serine significantly enhances its enzymatic activity. Furthermore, we have demonstrated that this phosphorylation event occurs in response to an increased demand for ketone body production, and is a likely contributor to the enhanced serum ketone body levels we observe in obese and diabetic mice. To the best of our knowledge, this is the first demonstration of a role for phosphorylation in regulating ketogenesis, an essential pathway for maintaining organismal metabolic homeostasis, especially when glucose levels are limiting. Together, our large-scale analyses and focused biochemistry results suggest that many, if not most, mitochondrial metabolic pathways may be subject to fine-tuning by reversible phosphorylation.

While our work provides a thorough assessment of mitochondrial phosphorylation, much remains to be learned about the nature and importance of this modification in regulating mitochondrial activities. Most notably, although our motif analyses have aided in identifying potential kinases responsible for our observed phosphorylation, definitive demonstration of kinases residing within — or translocating to — mitochondria has largely remained elusive (O'Rourke et al., 2011; Pagliarini and Dixon, 2006). As such, with few exceptions, we do not yet understand when, where, and how mitochondrial proteins are phosphorylated. Second, as PTMs are typically involved in rapid modulation of protein function, it will be important to continue to profile how the mitochondrial phosphosites we have identified change in response to other acute stresses, such as hypoxia, temperature change, inflammatory cytokines, elevated reactive oxygen species levels, and various dietary changes. Moving forward, we aim to address these outstanding issues, as well as to explore the interrelationship of phosphorylation with other prominent PTMs, including acetylation, methylation, and

glycosylation. In doing so, we aim to elucidate the signaling networks that act to manipulate mitochondrial function, and to identify specific signaling molecules that can be targeted therapeutically to help remedy mitochondrial dysfunction in metabolic disease.

Acknowledgements

We thank Jonathan Stefely for help with Acetyl CoA synthesis, Alan Higbee and Xiao Guo for targeted MS analysis of HMGCS2 phosphorylation, Eric Verdin (UCSF) for generously donating HMGCS2 constructs, and John Denu and Kristin Dittenhafer for advice on the HMGCS2 activity assay. We also thank Danielle Swaney for advice on MS methodology and Douglas Phanstiel, Craig Wenger, and Nambirajan Rangarajan for informatics assistance. This work was supported by a Searle Scholars Award and by NIH grants RC1DK086410 (to D.J.P.), R01GM080148 (to J.J. Coon), R01DK058037 and R01DK66369 (to A.D.A.), and F32DK091049 (to P.A.G.) and AHA grant 12PRE839 (to J.J. Carson). Alan Attie is a member of Pfizer's CVMED scientific advisory committee, and Josh Coon is a consultant for Thermo Fisher Scientific.

Experimental Procedures

Animal models

Breeding, sacrificing, and tissue harvesting of mice from our in-house colonies at the University of Wisconsin Biochemistry Department was described previously, for both the univariate (Zhao et al., 2009) and multivariate (Keller et al., 2008) phases of this study. Briefly, all mice were male, bred and housed in an environmentally controlled facility on a 12-h light/dark cycle (6 am–6 pm, respectively). Mice were provided free access to water at all times and to a standard rodent chow (Purina no. 5008) ab libitum, except during a fasting period (8 am–noon) in order to obtain plasma at 4 or 10 weeks of age, after which they were sacrificed by decapitation. Liver tissue was dissected, flash frozen with liquid N2, and stored at -80°C until use. For a final study, lean (wild type) B6 mice were fasted overnight (16 hrs), after which half of the animals were allowed to feed ad libitum for two hours prior to sacrifice. For the fasting/refeeding study, fresh liver tissue was used. All procedures were approved by the University of Wisconsin Animal Care and Use Committee. Serum ketone bodies were determined using an Autokit Total Ketone Bodies assay (Wako).

Proteomics sample preparation

Tissue sections from each liver were used for mitochondrial enrichment, using previous methods modified for phosphoproteomics by the addition of phosphatase inhibitors (Pagliarini et al., 2008), as well mRNA profiling as described (Keller et al., 2008). Pelleted proteins (0.5 mg/sample) were digested using previous methods (Grimsrud et al., 2010a), with slight modifications such as the sequential use of LysC

and trypsin to ensure robust digestion of all samples. Peptides for each preparation were labeled with a unique 8-plex iTRAQ reagent and the samples were mixed in batches of eight. Peptides were separated by strong cation exchange chromatography (SCX), and after aliquots were removed for unmodified peptide quantitation, immobilized metal affinity chromatography (IMAC) was performed on each fraction to enrich for phosphopeptides as described (Phanstiel et al., 2011).

Large-scale tandem MS data collection and analysis

Nano-LC-MS/MS analysis was performed on an ETD-enabled LTQ Orbitrap Velos (Thermo Fisher Scientific). All fractions were subjected to data-dependent analysis using instrument methods developed previously for improved quantitation accuracy with isobaric tags, relying on either post-acquisition filtering (Phanstiel et al., 2011) or real-time filtering (Wenger et al., 2011a) of precursors, for the univariate and multivariate phases of our study, respectively. At least two runs using all HCD (Olsen et al., 2007) fragmentation were performed for each sample. An additional run using back-to-back ETD (Syka et al., 2004) and HCD on each precursor was performed on each phosphopeptide fraction. For the fed/fasted study, peptide and phosphopeptide fractions were subjected to two runs: one run used all HCD fragmentation (applying post-acquisition filtering of precursors) and one run used HCD fragmentation along with our recently developed QuantMode method, which applies precursor filtering during data collection through gas phase purification of peptides prior to dissociation (Wenger et al., 2011a). Tandem MS data was searched with OMSAA (Geer et al., 2004) against a concatenated target-decoy UniProt database consisting of mouse proteins

(Elias and Gygi, 2007). Our custom software COMPASS (Wenger et al., 2011b) was then utilized to filter the resulting peptide identifications to 1% FDR, normalize iTRAQ reporter ion intensities for all peptide spectral matches (PSMs) across each replicate separately, group peptides from all replicates to common parsimonious protein groups at 1% FDR, localize phosphorylation sites to specific residues at 95% probability, and sum the reporter ion intensities of all PSMs for all unique proteins and protein phosphorylation sites identified in individual replicates.

Proteomics statistical analysis

Microsoft Access and Excel were utilized for statistical analysis of protein and site-specific phosphorylation measurements. We evaluated the significance of a given protein, phosphoisoform, or normalized phosphoisoform change by computing p-values, assuming a log-normal distribution for measurement error. A total of 39 such comparisons were made for each measurement; three of these comparisons were Age, Strain, and Obesity. Each comparison was made without adjustment for other factors or comparisons. We corrected for multiple hypothesis testing by computing a false discovery rate (FDR, q-value) where we assumed two populations (changing and unchanging) and that the unchanging population had p-values which are uniformly distributed from 0 to 1 (Figures S2A). FDR (q-values) were calculated separately for each measurement type (e.g. Protein). For more details on significance testing, see Supplemental Experimental Procedures. All protein and phosphoprotein measurements, as well as motif and kinase activity predictions are listed in Tables S1A-E (see Figure S1 for descriptions of all comparisons).

MitoMod database development

All of the proteomic/phosphoproteomic data generated from this study were utilized to develop an interactive website, called MitoMod, that is freely available at mitomod.biochem.wisc.edu. Here, users can browse the data or search for information on specific proteins of interest in a gene-centric (gene symbol) or protein-centric (UniProt Accession) fashion. For each measurement, users can select comparisons of interest between the physiological conditions assessed to reveal relevant graphs, quantitative values, and statistical analysis. The entire analyzed dataset, as well as the raw MS data (Thermo .raw files) and a table of all our iTRAQ tag-mouse pairings can also be downloaded for independent analysis.

Biochemical assessment of HMGCS2 regulation

HEK293 cells were cultured in DMEM supplemented with 10% FBS and antibiotics (50 μg/ml Penicillin and 50 units/ml Streptomycin). All expression constructs were derived from pcDNA3.1 (Invitrogen) as described previously (Shimazu et al., 2010). Site-directed mutagenesis to create HMGCS2 variants was performed using standard PCR-based cloning techniques and all constructs were verified by DNA sequencing. Transfections were performed at ~70% confluence and cells were lysed and protein subjected to immunoblotting with HRP-conjugated anti-Flag antibody to assess expression. For ketogenic media (KM) experiments (Sengupta et al., 2010), cells were grown in KM (DMEM without the addition of FBS, and supplemented with 2mM sodium octanoate) from 24-72 hours after transfection, samples of media were reserved at each time point, and ketone bodies were measured. Flag-tagged HMGCS2 was

purified and its activity assessed as described previously (Shimazu et al., 2010; Skaff and Miziorko, 2010). See Supplemental Experimental Procedures for further details.

References

Acin-Perez, R., Gatti, D.L., Bai, Y., and Manfredi, G. (2011). Protein phosphorylation and prevention of cytochrome oxidase inhibition by ATP: coupled mechanisms of energy metabolism regulation. Cell metabolism 13, 712-719.

Acin-Perez, R., Salazar, E., Kamenetsky, M., Buck, J., Levin, L.R., and Manfredi, G. (2009). Cyclic AMP produced inside mitochondria regulates oxidative phosphorylation. Cell metabolism 9, 265-276.

Bains, R.K., Wells, S.E., Flavell, D.M., Fairhall, K.M., Strom, M., Le Tissier, P., and Robinson, I.C.A.F. (2004). Visceral obesity without insulin resistance in late-onset obesity rats. Endocrinology 145, 2666-2679.

Berry, D.C., Jin, H., Majumdar, A., and Noy, N. (2011). Signaling by vitamin A and retinol-binding protein regulates gene expression to inhibit insulin responses. Proc Natl Acad Sci U S A 108, 4340-4345.

Berry, M.N., Clark, D.G., Grivell, A.R., and Wallace, P.G. (1983). The calorigenic nature of hepatic ketogenesis: an explanation for the stimulation of respiration induced by fatty acid substrates. Eur J Biochem 131, 205-214.

Boja, E.S., Phillips, D., French, S.A., Harris, R.A., and Balaban, R.S. (2009). Quantitative Mitochondrial Phosphoproteomics Using iTRAQ on an LTQ-Orbitrap with High Energy Collision Dissociation. J Proteome Res 8, 4665-4675.

Buchner, D.A., Yazbek, S.N., Solinas, P., Burrage, L.C., Morgan, M.G., Hoppel, C.L., and Nadeau, J.H. (2011). Increased mitochondrial oxidative phosphorylation in the liver is associated with obesity and insulin resistance. Obesity (Silver Spring) 19, 917-924.

Calvo, S.E., and Mootha, V.K. (2010). The mitochondrial proteome and human disease. Annu Rev Genomics Hum Genet 11, 25-44.
Capeau, J. (2008). Insulin resistance and steatosis in humans. Diabetes Metab 34, 649-657.

Caterson, I.D., Astbury, L.D., Williams, P.F., Vanner, M.A., Cooney, G.J., and Turtle, J.R. (1987). The activity of the pyruvate dehydrogenase complex in heart and liver from mice during the development of obesity and insulin resistance. The Biochemical journal 243, 549-553.

Chen, Y.Q., Zhu, J., Lum, P.Y., Yang, X., Pinto, S., MacNeil, D.J., Zhang, C.S., Lamb, J., Edwards, S., Sieberts, S.K., et al. (2008). Variations in DNA elucidate molecular networks that cause disease. Nature 452, 429-435.

Choudhary, C., Kumar, C., Gnad, F., Nielsen, M.L., Rehman, M., Walther, T.C., Olsen, J.V., and Mann, M. (2009). Lysine acetylation targets protein complexes and co-regulates major cellular functions. Science 325, 834-840.

Collison, L.W., Kannan, L., Onorato, T.M., Knudsen, J., Haldar, D., and Jolly, C.A. (2005). Aging reduces glycerol-3-phosphate acyltransferase activity in activated rat splenic T-lymphocytes. Biochim Biophys Acta 1687, 164-172.

Cui, Z., Hou, J., Chen, X., Li, J., Xie, Z., Xue, P., Cai, T., Wu, P., Xu, T., and Yang, F. (2010). The profile of mitochondrial proteins and their phosphorylation signaling network in INS-1 beta cells. J Proteome Res 9, 2898-2908.

Deng, N., Zhang, J., Zong, C., Wang, Y., Lu, H., Yang, P., Wang, W., Young, G.W., Korge, P., Lotz, C., et al. (2011). Phosphoproteome analysis reveals regulatory sites in major pathways of cardiac mitochondria. Mol Cell Proteomics 10, M110 000117.

Deng, W.J., Nie, S., Dai, J., Wu, J.R., and Zeng, R. (2010). Proteome, Phosphoproteome, and Hydroxyproteome of Liver Mitochondria in Diabetic Rats at Early Pathogenic Stages. Molecular & Cellular Proteomics 9, 100-116.

Elias, J.E., and Gygi, S.P. (2007). Target-decoy search strategy for increased confidence in large-scale protein identifications by mass spectrometry. Nat Methods 4, 207-214.

Fang, X., Yu, S.X., Lu, Y., Bast, R.C., Jr., Woodgett, J.R., and Mills, G.B. (2000). Phosphorylation and inactivation of glycogen synthase kinase 3 by protein kinase A. Proc Natl Acad Sci U S A 97, 11960-11965.

Forner, F., Foster, L.J., Campanaro, S., Valle, G., and Mann, M. (2006). Quantitative proteomic comparison of rat mitochondria from muscle, heart, and liver. Mol Cell Proteomics 5, 608-619.

Foster, L.J., de Hoog, C.L., Zhang, Y., Xie, X., Mootha, V.K., and Mann, M. (2006). A mammalian organelle map by protein correlation profiling. Cell 125, 187-199.

Geer, L.Y., Markey, S.P., Kowalak, J.A., Wagner, L., Xu, M., Maynard, D.M., Yang, X., Shi, W., and Bryant, S.H. (2004). Open mass spectrometry search algorithm. J Proteome Res 3, 958-964.

Gnad, F., Forner, F., Zielinska, D.F., Birney, E., Gunawardena, J., and Mann, M. (2010). Evolutionary constraints of phosphorylation in eukaryotes, prokaryotes, and mitochondria. Mol Cell Proteomics 9, 2642-2653.

Gnad, F., Gunawardena, J., and Mann, M. (2011). PHOSIDA 2011: the posttranslational modification database. Nucleic Acids Res 39, D253-260.

Griffiths, M.A., Baker, D.H., Yu, X.X., Novakofski, J., Oscai, L., and Ji, L.L. (1995). Effects of acute exercise on hepatic lipogenic enzymes in fasted and refed rats. J Appl Physiol 79, 879-885.

Grimsrud, P.A., den Os, D., Wenger, C.D., Swaney, D.L., Schwartz, D., Sussman, M.R., Ane, J.M., and Coon, J.J. (2010a). Large-Scale Phosphoprotein Analysis in Medicago truncatula Roots Provides Insight into in Vivo Kinase Activity in Legumes. Plant Physiol 152, 19-28.

Grimsrud, P.A., Swaney, D.L., Wenger, C.D., Beauchene, N.A., and Coon, J.J. (2010b). Phosphoproteomics for the masses. ACS Chem Biol 5, 105-119.

Harper, M.E., Green, K., and Brand, M.D. (2008). The efficiency of cellular energy transduction and its implications for obesity. Annu Rev Nutr 28, 13-33.

Holmstrom, M.H., Iglesias-Gutierrez, E., Zierath, J.R., and Garcia-Roves, P.M. (2012). Tissue-specific control of mitochondrial respiration in obesity-related insulin resistance and diabetes. Am J Physiol Endocrinol Metab 302, E731-739.

Hopper, R.K., Carroll, S., Aponte, A.M., Johnson, D.T., French, S., Shen, R.F., Witzmann, F.A., Harris, R.A., and Balaban, R.S. (2006). Mitochondrial matrix phosphoproteome: effect of extra mitochondrial calcium. Biochemistry 45, 2524-2536.

Hotamisligil, G.S. (2010). Endoplasmic reticulum stress and the inflammatory basis of metabolic disease. Cell 140, 900-917.

Houtkooper, R.H., Argmann, C., Houten, S.M., Canto, C., Jeninga, E.H., Andreux, P.A., Thomas, C., Doenlen, R., Schoonjans, K., and Auwerx, J. (2011). The metabolic footprint of aging in mice. Sci Rep 1, 134.

Huttlin, E.L., Jedrychowski, M.P., Elias, J.E., Goswami, T., Rad, R., Beausoleil, S.A., Villen, J., Haas, W., Sowa, M.E., and Gygi, S.P. (2010). A tissue-specific atlas of mouse protein phosphorylation and expression. Cell 143, 1174-1189.

Ismahan, G., and Parvez, S. (1978). Effect of starvation and pattern of feeding upon activities of enzymes catechol-O-methyltransferase and monoamine oxidase in heart and liver of developing rats. J Nutr 108, 585-594.

Johnson, D.T., Harris, R.A., French, S., Blair, P.V., You, J., Bemis, K.G., Wang, M., and Balaban, R.S. (2007). Tissue heterogeneity of the mammalian mitochondrial proteome. Am J Physiol Cell Physiol 292, C689-697.

Keller, M.P., Choi, Y., Wang, P., Davis, D.B., Rabaglia, M.E., Oler, A.T., Stapleton, D.S., Argmann, C., Schueler, K.L., Edwards, S., et al. (2008). A gene expression network model of type 2 diabetes links cell cycle regulation in islets with diabetes susceptibility. Genome Res 18, 706-716.

Kim, S.C., Sprung, R., Chen, Y., Xu, Y., Ball, H., Pei, J., Cheng, T., Kho, Y., Xiao, H., Xiao, L., et al. (2006). Substrate and functional diversity of lysine acetylation revealed by a proteomics survey. Mol Cell 23, 607-618.

Kostiuk, M.A., Corvi, M.M., Keller, B.O., Plummer, G., Prescher, J.A., Hangauer, M.J., Bertozzi, C.R., Rajaiah, G., Falck, J.R., and Berthiaume, L.G. (2008). Identification of palmitoylated mitochondrial proteins using a bio-orthogonal azido-palmitate analogue. Faseb J 22, 721-732.

Kuhajda, F.P., Aja, S., Tu, Y., Han, W.F., Medghalchi, S.M., El Meskini, R., Landree, L.E., Peterson, J.M., Daniels, K., Wong, K., et al. (2011). Pharmacological glycerol-3-phosphate acyltransferase inhibition decreases food intake and adiposity and increases insulin sensitivity in diet-induced obesity. Am J Physiol Regul Integr Comp Physiol 301, R116-130.

Laffel, L. (1999). Ketone bodies: a review of physiology, pathophysiology and application of monitoring to diabetes. Diabetes Metab Res Rev 15, 412-426.

Lan, H., Rabaglia, M.E., Stoehr, J.P., Nadler, S.T., Schueler, K.L., Zou, F., Yandell, B.S., and Attie, A.D. (2003). Gene expression profiles of nondiabetic and diabetic obese mice suggest a role of hepatic lipogenic capacity in diabetes susceptibility. Diabetes 52, 688-700.

Lazarin Mde, O., Ishii-Iwamoto, E.L., Yamamoto, N.S., Constantin, R.P., Garcia, R.F., da Costa, C.E., Vitoriano Ade, S., de Oliveira, M.C., and Salgueiro-Pagadigorria, C.L. (2011). Liver mitochondrial function and redox status in an experimental model of non-alcoholic fatty liver disease induced by monosodium L-glutamate in rats. Exp Mol Pathol 91, 687-694.

Lea, W., Abbas, A.S., Sprecher, H., Vockley, J., and Schulz, H. (2000). Long-chain acyl-CoA dehydrogenase is a key enzyme in the mitochondrial beta-oxidation of unsaturated fatty acids. Biochim Biophys Acta 1485, 121-128.

Lee, J., Xu, Y., Chen, Y., Sprung, R., Kim, S.C., Xie, S., and Zhao, Y. (2007). Mitochondrial phosphoproteome revealed by an improved IMAC method and MS/MS/MS. Mol Cell Proteomics 6, 669-676.

Lee, M.V., Topper, S.E., Hubler, S.L., Hose, J., Wenger, C.D., Coon, J.J., and Gasch, A.P. (2011). A dynamic model of proteome changes reveals new roles for transcript alteration in yeast. Mol Syst Biol 7, 514.

Lowell, B.B., and Shulman, G.I. (2005). Mitochondrial dysfunction and type 2 diabetes. Science 307, 384-387.

Lu, G., Sun, H., She, P., Youn, J.Y., Warburton, S., Ping, P., Vondriska, T.M., Cai, H., Lynch, C.J., and Wang, Y. (2009). Protein phosphatase 2Cm is a critical regulator of branched-chain amino acid catabolism in mice and cultured cells. The Journal of clinical investigation 119, 1678-1687.

Monetti, M., Nagaraj, N., Sharma, K., and Mann, M. (2011). Large-scale phosphosite quantification in tissues by a spike-in SILAC method. Nat Methods 8, 655-658.

Noland, R.C., Woodlief, T.L., Whitfield, B.R., Manning, S.M., Evans, J.R., Dudek, R.W., Lust, R.M., and Cortright, R.N. (2007). Peroxisomal-mitochondrial oxidation in a rodent model of obesity-associated insulin resistance. Am J Physiol Endocrinol Metab 293, E986-E1001.

Nunnari, J., and Suomalainen, A. (2012). Mitochondria: in sickness and in health. Cell 148, 1145-1159.

O'Rourke, B., Van Eyk, J.E., and Foster, D.B. (2011). Mitochondrial protein phosphorylation as a regulatory modality: implications for mitochondrial dysfunction in heart failure. Congestive Heart Failure 17, 269-282.

Olsen, J.V., Macek, B., Lange, O., Makarov, A., Horning, S., and Mann, M. (2007). Higher-energy C-trap dissociation for peptide modification analysis. Nat Methods 4, 709-712.

Pagliarini, D.J., Calvo, S.E., Chang, B., Sheth, S.A., Vafai, S.B., Ong, S.E., Walford, G.A., Sugiana, C., Boneh, A., Chen, W.K., et al. (2008). A mitochondrial protein compendium elucidates complex I disease biology. Cell 134, 112-123.

Pagliarini, D.J., and Dixon, J.E. (2006). Mitochondrial modulation: reversible phosphorylation takes center stage? Trends Biochem Sci 31, 26-34.

Phanstiel, D.H., Brumbaugh, J., Wenger, C.D., Tian, S., Probasco, M.D., Bailey, D.J., Swaney, D., Tervo, M., Bolin, J.M., Ruotti, V., et al. (2011). Proteomic and phosphoproteomic comparison of human ES and iPS cells. In Press.

Quant, P.A., Tubbs, P.K., and Brand, M.D. (1990). Glucagon activates mitochondrial 3-hydroxy-3-methylglutaryl-CoA synthase in vivo by decreasing the extent of succinylation of the enzyme. Eur J Biochem 187, 169-174.

Raffaella, C., Francesca, B., Italia, F., Marina, P., Giovanna, L., and Susanna, I. (2008). Alterations in hepatic mitochondrial compartment in a model of obesity and insulin resistance. Obesity (Silver Spring) 16, 958-964.

Rao, S., Gerbeth, C., Harbauer, A., Mikropoulou, D., Meisinger, C., and Schmidt, O. (2011). Signaling at the gate: phosphorylation of the mitochondrial protein import machinery. Cell Cycle 10, 2083-2090.

Reed, W.D., Clinkenbeard, D., and Lane, M.D. (1975). Molecular and catalytic properties of mitochondrial (ketogenic) 3-hydroxy-3-methylglutaryl coenzyme A synthase of liver. J Biol Chem 250, 3117-3123.

Reinders, J., Wagner, K., Zahedi, R.P., Stojanovski, D., Eyrich, B., van der Laan, M., Rehling, P., Sickmann, A., Pfanner, N., and Meisinger, C. (2007). Profiling phosphoproteins of yeast mitochondria reveals a role of phosphorylation in assembly of the ATP synthase. Mol Cell Proteomics 6, 1896-1906.

Ross, P.L., Huang, Y.N., Marchese, J.N., Williamson, B., Parker, K., Hattan, S., Khainovski, N., Pillai, S., Dey, S., Daniels, S., et al. (2004). Multiplexed protein quantitation in Saccharomyces cerevisiae using amine-reactive isobaric tagging reagents. Mol Cell Proteomics 3, 1154-1169.

Schmidt, O., Harbauer, A.B., Rao, S., Eyrich, B., Zahedi, R.P., Stojanovski, D., Schonfisch, B., Guiard, B., Sickmann, A., Pfanner, N., et al. (2011). Regulation of mitochondrial protein import by cytosolic kinases. Cell 144, 227-239.

Schwartz, D., and Gygi, S.P. (2005). An iterative statistical approach to the identification of protein phosphorylation motifs from large-scale data sets. Nat Biotechnol 23, 1391-1398.

Sengupta, S., Peterson, T.R., Laplante, M., Oh, S., and Sabatini, D.M. (2010). mTORC1 controls fasting-induced ketogenesis and its modulation by ageing. Nature 468, 1100-1104.

Shimazu, T., Hirschey, M.D., Hua, L., Dittenhafer-Reed, K.E., Schwer, B., Lombard, D.B., Li, Y., Bunkenborg, J., Alt, F.W., Denu, J.M., et al. (2010). SIRT3 deacetylates mitochondrial 3-hydroxy-3-methylglutaryl CoA synthase 2 and regulates ketone body production. Cell metabolism 12, 654-661.

Skaff, D.A., and Miziorko, H.M. (2010). A visible wavelength spectrophotometric assay suitable for high-throughput screening of 3-hydroxy-3-methylglutaryl-CoA synthase. Anal Biochem 396, 96-102.

Stoehr, J.P., Nadler, S.T., Schueler, K.L., Rabaglia, M.E., Yandell, B.S., Metz, S.A., and Attie, A.D. (2000). Genetic obesity unmasks nonlinear interactions between murine type 2 diabetes susceptibility loci. Diabetes 49, 1946-1954.

Syka, J.E., Coon, J.J., Schroeder, M.J., Shabanowitz, J., and Hunt, D.F. (2004). Peptide and protein sequence analysis by electron transfer dissociation mass spectrometry. Proc Natl Acad Sci U S A 101, 9528-9533.

Szendroedi, J., Phielix, E., and Roden, M. (2012). The role of mitochondria in insulin resistance and type 2 diabetes mellitus. Nat Rev Endocrinol 8, 92-103.

Takamura, T., Misu, H., Matsuzawa-Nagata, N., Sakurai, M., Ota, T., Shimizu, A., Kurita, S., Takeshita, Y., Ando, H., Honda, M., et al. (2008). Obesity upregulates genes involved in oxidative phosphorylation in livers of diabetic patients. Obesity (Silver Spring) 16, 2601-2609.

Thompson, A., Schafer, J., Kuhn, K., Kienle, S., Schwarz, J., Schmidt, G., Neumann, T., Johnstone, R., Mohammed, A.K., and Hamon, C. (2003). Tandem mass tags: a novel quantification strategy for comparative analysis of complex protein mixtures by MS/MS. Anal Chem 75, 1895-1904.

Verweij, M., Sluiter, W., van den Engel, S., Jansen, E., Ijzermans, J.N., and de Bruin, R.W. (2012). Altered mitochondrial functioning induced by preoperative fasting may underlie protection against renal ischemia/reperfusion injury. J Cell Biochem.

Villen, J., Beausoleil, S.A., Gerber, S.A., and Gygi, S.P. (2007). Large-scale phosphorylation analysis of mouse liver. Proc Natl Acad Sci U S A 104, 1488-1493.

Wallace, D.C. (2005). A mitochondrial paradigm of metabolic and degenerative diseases, aging, and cancer: a dawn for evolutionary medicine. Annu Rev Genet 39, 359-407.

Wang, Y., Li, G., Goode, J., Paz, J.C., Ouyang, K., Screaton, R., Fischer, W.H., Chen, J., Tabas, I., and Montminy, M. (2012). Inositol-1,4,5-trisphosphate receptor regulates hepatic gluconeogenesis in fasting and diabetes. Nature 485, 128-132.

Wenger, C.D., Lee, M.V., Hebert, A.S., McAlister, G.C., Phanstiel, D.H., Westphall, M.S., and Coon, J.J. (2011a). Gas-phase purification enables accurate, multiplexed proteome quantification with isobaric tagging. Nat Methods 8, 933-935.

Wenger, C.D., Phanstiel, D.H., Lee, M.V., Bailey, D.J., and Coon, J.J. (2011b). COMPASS: a suite of pre- and post-search proteomics software tools for OMSSA. Proteomics 11, 1064-1074.

Wojtovich, A.P., Nadtochiy, S.M., Brookes, P.S., and Nehrke, K. (2012). Ischemic preconditioning: the role of mitochondria and aging. Exp Gerontol 47, 1-7.

Zhao, E., Keller, M.P., Rabaglia, M.E., Oler, A.T., Stapleton, D.S., Schueler, K.L., Neto, E.C., Moon, J.Y., Wang, P., Wang, I.M., et al. (2009). Obesity and genetics regulate microRNAs in islets, liver, and adipose of diabetic mice. Mamm Genome 20, 476-485.

Zhao, S., Xu, W., Jiang, W., Yu, W., Lin, Y., Zhang, T., Yao, J., Zhou, L., Zeng, Y., Li, H., et al. (2010). Regulation of cellular metabolism by protein lysine acetylation. Science 327, 1000-1004.

Zhao, X., Leon, I.R., Bak, S., Mogensen, M., Wrzesinski, K., Hojlund, K., and Jensen, O.N. (2011). Phosphoproteome analysis of functional mitochondria isolated from resting human muscle reveals extensive phosphorylation of inner membrane protein complexes and enzymes. Mol Cell Proteomics 10, M110 000299.

Tables and Figures

Figure 1: Large-scale measurement of liver mitochondrial protein abundance and phosphorylation in mouse models of obesity and type 2 diabetes.

A) We performed our initial analyses in two phases as depicted on the left: a univariate (obesity) experiment of B6 mice at 10 weeks of age (8 mice, 2 conditions), and a multi-variable experiment (40 mice, all 8 conditions depicted). Our proteomics workflow is illustrated on the right: Livers were dissected, enriched for mitochondria, and used for high resolution quantitative proteomic/phosphoproteomic analyses with 8-plex iTRAQ. The iTRAQ reporter ions observed during tandem MS provide relative quantification of the identified proteins and phosphorylation sites. B) Unsupervised hierarchical clustering of 4 lean (L) and 4 obese (O) mice based on all measureable proteins from the univariate experiment. Values are mean protein abundance, relative to the average of all eight mice, on a log2 scale from <-1 to >1 (values ranged from -3.2 to 1.8). C) Abundance of individual fatty acid oxidation proteins in lean (light grey) and obese (dark grey) mice from the univariate experiment. Values are in the same units as in panel B, error bars indicate SD, and asterisks indicate a statistically significant difference between lean and obese mice ($q<0.1$). D) Volcano plot of fold phosphorylation change (normalized to protein abundance change) vs. -log (p value) for each normalized phosphosite measurement for mitochondrial (red) and non-mitochondrial (grey) proteins from the univariate experiment. E) Abundance fold-change (obese/lean) for all proteins with significant obesity-dependent alterations ($q<0.1$) in B6 mice at 10 weeks, with the multivariate experiment on the x-axis and the univariate experiment on the y-axis. The percent of measurements in discordance

between the two studies (light grey dots) is indicated. F) Unsupervised hierarchical clustering of each condition from the multivariate experiment based on mitochondrial proteins quantified in all five replicates. Values are mean protein abundance for each condition, relative to all eight conditions, on a log2 scale from <-1 to >1 (values ranged from -1.14 to 1.07). G) Abundance fold changes for individual oxidative phosphorylation proteins (each represented by a circle, separated to Oxphos complex) measured in the univariate experiment (obese/lean values are shown in light grey) and the multivariate experiment (obese 10-week B6 mice relative to all other animals shown in black, obese 10-week BTBR mice relative to all others animals shown in red). H) Numbers indicate all protein and phosphorylation identifications (IDs) at 1% FDR, quantified with iTRAQ reporter ions in at least one comparison (Quant), and significantly changing between any condition that was measured (Δ) at $q<0.1$ for both the univariate and multivariate experiments. Results are shown for both mitochondrial proteins (MitoCarta) and all proteins identified (Total). See also Figure S1.

Figure 1:

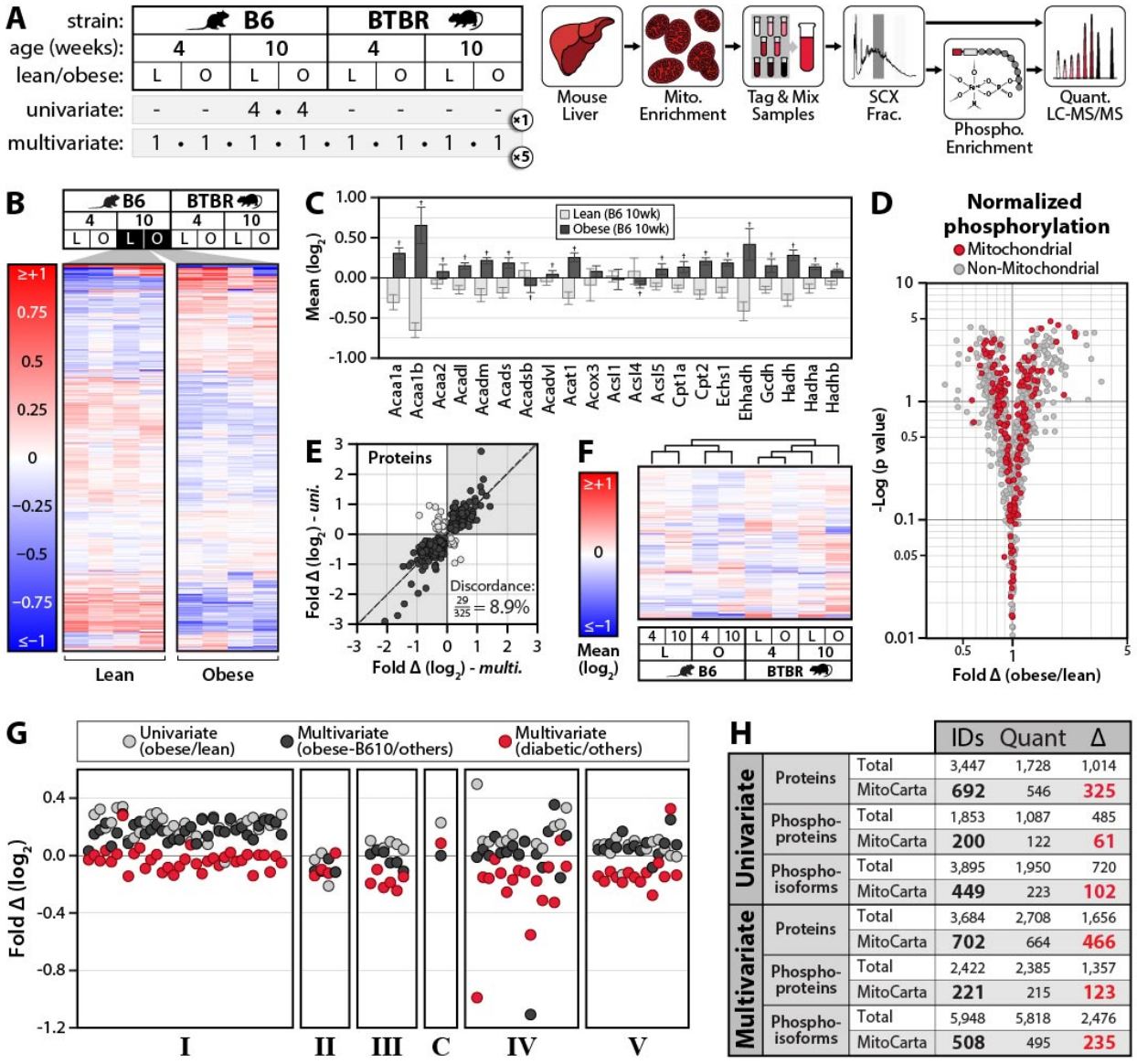

H

			IDs	Quant	Δ
Univariate	Proteins	Total	3,447	1,728	1,014
		MitoCarta	**692**	546	**325**
	Phospho-proteins	Total	1,853	1,087	485
		MitoCarta	**200**	122	**61**
	Phospho-isoforms	Total	3,895	1,950	720
		MitoCarta	**449**	223	**102**
Multivariate	Proteins	Total	3,684	2,708	1,656
		MitoCarta	**702**	664	**466**
	Phospho-proteins	Total	2,422	2,385	1,357
		MitoCarta	**221**	215	**123**
	Phospho-isoforms	Total	5,948	5,818	2,476
		MitoCarta	**508**	495	**235**

Figure 2: Phosphorylation assessment across the mitochondrial proteome.

A-D) Identification of phosphorylation sites within key mitochondrial pathways: A) oxidative phosphorylation (OxPhos) B) ketone body production C) the TCA cycle D) fatty acid oxidation. Phosphorylation sites exhibiting significant changes ($q<0.1$) are in red; sites that are not changing significantly are in grey; and sites identified, but not quantified are represented as white circles. See also Figure S3.

Figure 2:

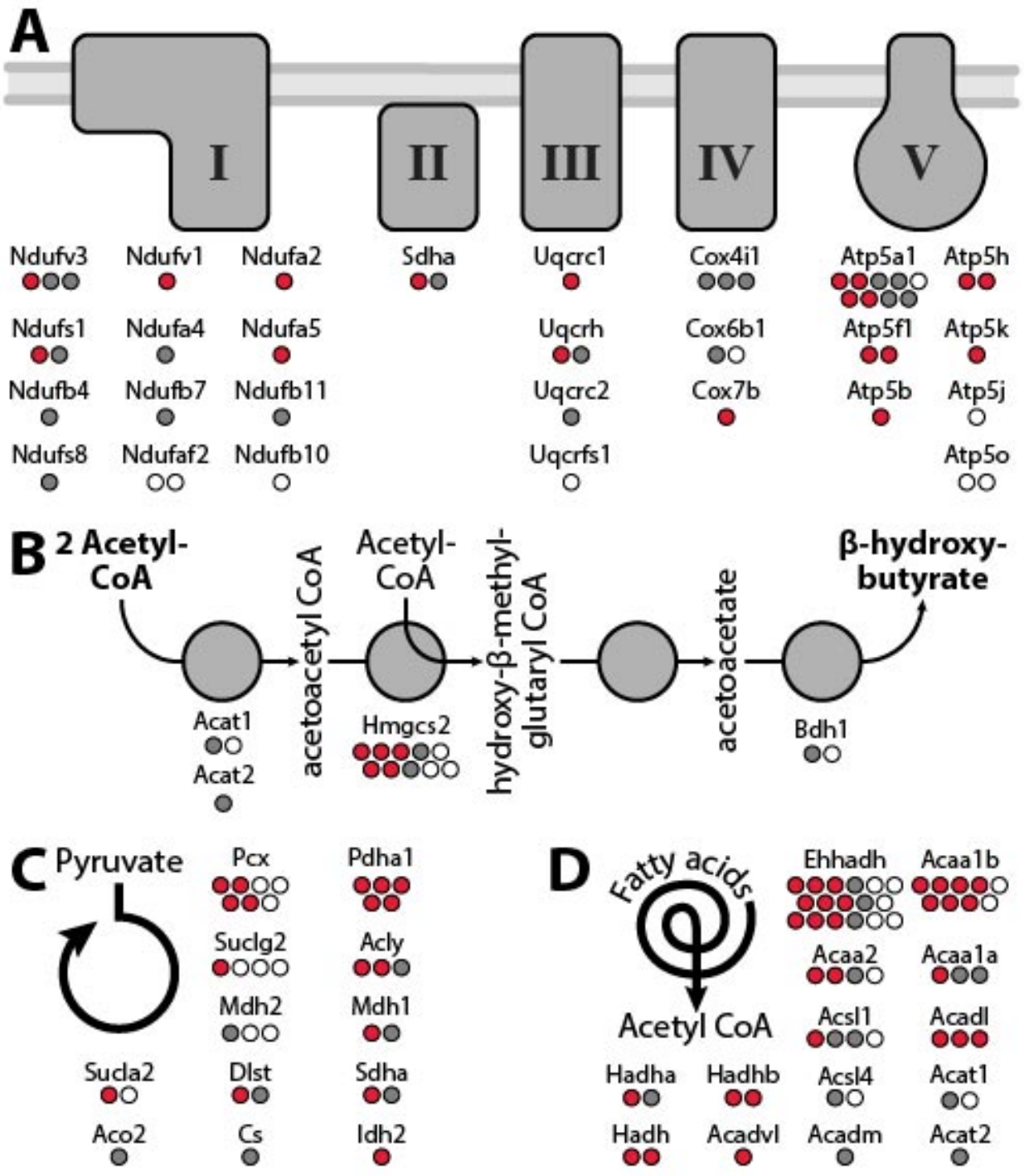
A
I
II
III
IV
V
Ndufv3
Ndufv1
Ndufa2
Sdha
Uqcrc1
Cox4i1
Atp5a1
Atp5h
Ndufs1
Ndufa4
Ndufa5
Uqcrh
Cox6b1
Atp5f1
Atp5k
Ndufb4
Ndufb7
Ndufb11
Uqcrc2
Cox7b
Atp5b
Atp5j
Ndufs8
Ndufaf2
Ndufb10
Uqcrfs1
Atp5o
B
2 Acetyl-CoA
acetoacetyl CoA
Acetyl-CoA
hydroxy-β-methyl-glutaryl CoA
acetoacetate
β-hydroxy-butyrate
Acat1
Acat2
Hmgcs2
Bdh1
C
Pyruvate
Pcx
Pdha1
Suclg2
Acly
Mdh2
Mdh1
Sucla2
Dlst
Sdha
Aco2
Cs
Idh2
D
Fatty acids
Acetyl CoA
Ehhadh
Acaa1b
Acaa2
Acaa1a
Acsl1
Acadl
Hadha
Hadhb
Acsl4
Acat1
Hadh
Acadvl
Acadm
Acat2

Figure 3: Multivariate proteomic dataset utilized to identify changes in mitochondrial protein phosphorylation amongst specific physiological conditions.

A) Heat map showing unsupervised hierarchical clustering of all quantified mitochondrial phosphoisoforms across each single-variable comparison; strain (S), age (A) and obesity (O). Values are fold changes between all mice differing by the indicated variable, on a log2 scale from <-1 to >1 (actual values ranged from -2.7 to 2.2). B) The top shows 8-plex iTRAQ-based quantification of phosphorylation of Acadl serine 55, Lactb serine 162, and Slc25a5 threonine 46 is shown for each condition (with error bars representing SD from all 5 replicates quantified) relative to the average of all eight conditions. The bottom shows the same data analyzed with relative abundance reflecting the fold-change between all 40 mice of the multivariate experiment separated by one variable at a time (eg., strain analysis represents all 20 B6 mice vs. all 20 BTBR mice). The colored bars correspond to the comparisons with the average of the datapoints highlighted in black on the top panel as the numerator and the white datapoints as the denominator. Asterisk indicates statistical significance at $q<0.1$. See also Figure S2.

Figure 3:

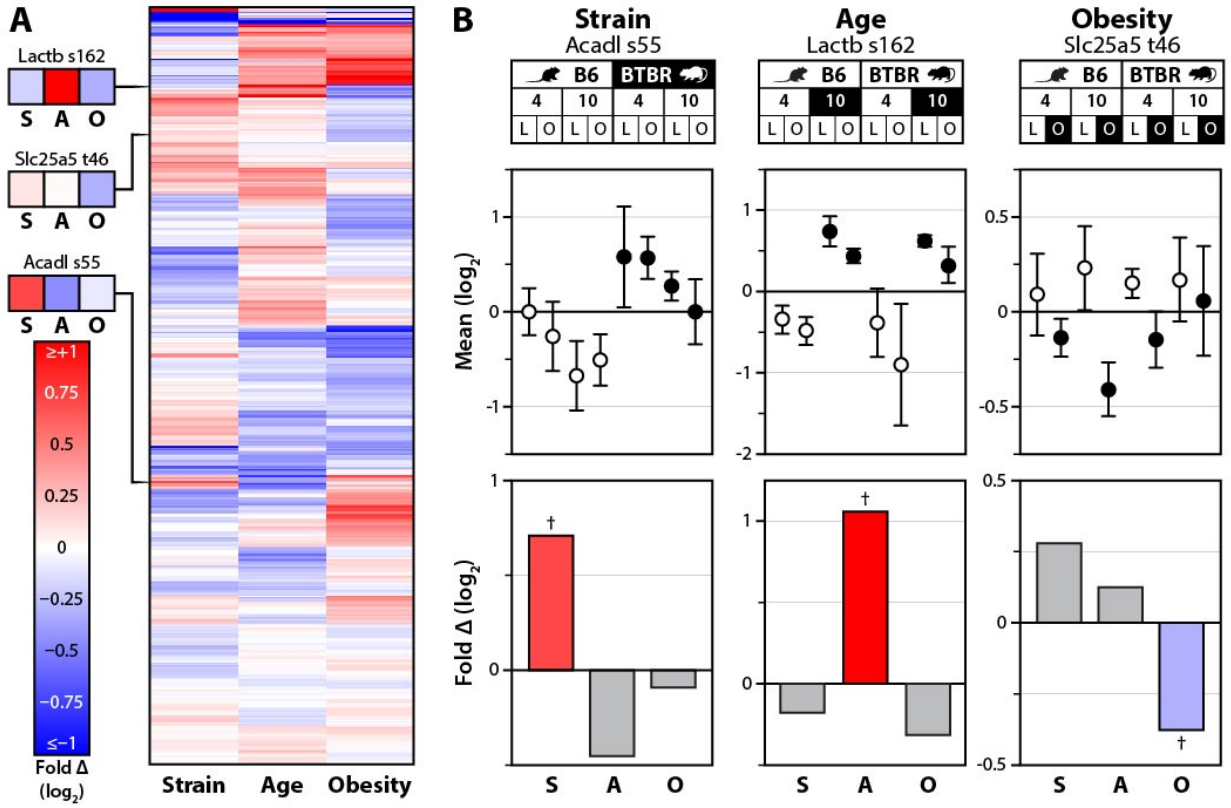
A
Lactb s162
S A O
Slc25a5 t46
S A O
Acadl s55
S A O
≥+1
0.75
0.5
0.25
0
−0.25
−0.5
−0.75
≤−1
Fold Δ (log2)
Strain
Age
Obesity
B
Strain
Acadl s55
Age
Lactb s162
Obesity
Slc25a5 t46
B6
BTBR
4
10
L O
Mean (log2)
Fold Δ (log2)
†
S
A
O

Figure 4: Acute phosphorylation changes across the mitochondrial proteome upon fasting and re-feeding.

A) Eight lean (wild type) B6 mice were fasted overnight (16 hrs), after which half of the animals were allowed to feed ad libitum for two hours. Liver mitochondria were subjected to the same large-scale 8-plex proteomic/phosphoproteomics workflow as described in Figure 1. B) Glucose, insulin, and beta-hydroxybuturate were measured from serum samples taken immediately after sacrifice. C) Quantification of phosphorylation changes on previously characterized regulatory phosphosites are expressed as fold change on a log2 scale (refed/fasted). Asterisks indicate statistical significance ($q<0.1$). D) All mitochondrial proteins (MitoCarta) identified are ranked on the x-axis by protein abundance fold change (and then by alphabetical order of their representative gene symbol). Each protein measurement is represented by a single black dot. Relative quantitation for all quantified mitochondrial phosphoisoforms (each represented by a single red dot) are plotted at the same position on the x-axis as is their corresponding protein abundance measurement. Selected phosphosites of note are indicated. The few phosphosites for which the corresponding protein was not quantified were assigned a protein fold change of “0” for graphical purposes, putting them towards the middle of the ranking.

Figure 4:

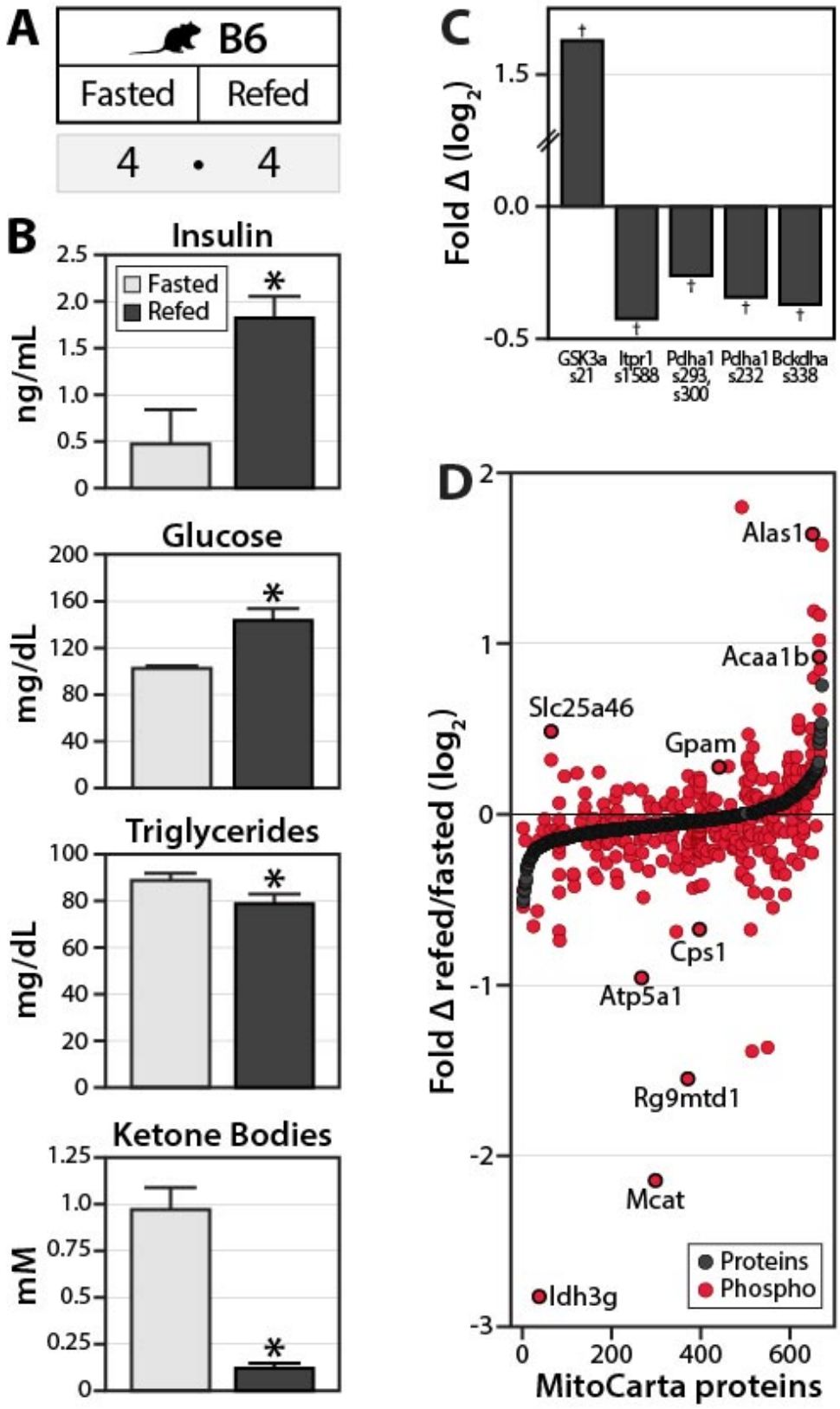
A
B6
Fasted
Refed
4 • 4
B
Insulin
ng/mL
Fasted
Refed
Glucose
mg/dL
Triglycerides
mg/dL
Ketone Bodies
mM
C
Fold Δ (log2)
GSK3a s21
Itpr1 s1588
Pdha1 s293, s300
Pdha1 s232
Bckdha s338
D
Fold Δ refed/fasted (log2)
MitoCarta proteins
Alas1
Acaa1b
Slc25a46
Gpam
Cps1
Atp5a1
Rg9mtd1
Mcat
Idh3g
Proteins
Phospho

Figure 5: Protein phosphorylation measurements reveal potential kinase-substrate relationships.

A) Selected kinases and known substrate consensus sequences from the Phosida database are indicated, with X indicating any amino acid and red lower-case letters indicating the phosphorylated residues. The number of MS/MS-identified mitochondrial phosphorylation sites and phosphoproteins (MitoCarta) that satisfy the consensus sequence requirements for each kinase are listed. B) Motif-X logo indicating amino acid sequence motifs overrepresented around phosphorylation sites identified specifically on MitoCarta proteins. The red letters at position "0" indicate the phosphorylated residue and the probability of an amino acids being present within 17 residues to each side are represented by the height of the respective single-letter symbol. Residues that are "fixed" in the motif (or are always present) span the entire height of the logo and are shown in black (non-fixed residues are in grey). C) Relative changes in kinase activity were predicted by averaging phosphosite quantitation for all substrates (mitochondrial and non-mitochondrial) phosphorylated on PKA (left) or CK2 (right) consensus sites. Values are expressed as fold change on a log2 scale between 10 week and 4 week mice (10 week/4 week) in both the lean (light grey bars) and obese (black bars) conditions (asterisk indicates statistical significance at $P<0.05$). See also Figure S4.

Figure 5:

A

Protein kinase	Sequence preference	MitoCarta phospho-sites	MitoCarta phospho-proteins
CK1	S-X-X-s/t S/T-X-X-X-s	184	111
CAMK2	R-X-X-s/t R-X-X-s/t-V	126	97
GSK3	s-X-X-X-S	111	75
PKA	R-X-s/t R-R/K-X-s/t K-R-X-X-s/t	101	75
CK2	s/t-X-X-E	93	76
CHK1	M/I/L/V-X-R/K-X-X-s/t	45	41
NEK6	L-X-X-s/t	43	37
ERK/MAPK	P-X-s/t-P V-X-s/t-P P-E-s/t-P	35	34
PKD	L/V/I-X-R/K-X-X-s/t	39	36
CDK1	s/t-P-X-K/R s/t-P-K/R	34	30
PLK1	E/D-X-s/t-F/L/I/Y/W/V/M	33	27
PKB/AKT	R-R/S/T-X-s/t-X-S/T R-X-R-X-X-s/t	29	27
CDK2	s/t-P-X-K/R	20	20

B

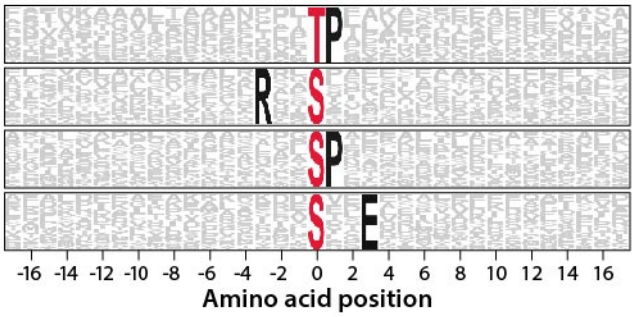

C

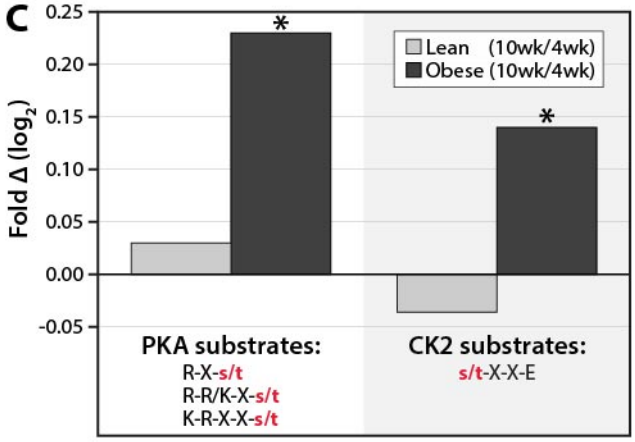

Figure 6: Identification of serine 456 on Hmgcs2 as a candidate regulatory PTM.

A) β-hydroxybutyrate levels were measured in serum from lean and obese B6 and BTBR mice at 10 weeks of age. Bars indicate SEM, and asterisks (*) indicate significance at $p<0.01$. B) Single scan MS2 spectrum and manual validation identifying phosphorylation of serine 456 (S456) on mouse Hmgcs2. The inset shows iTRAQ reporter ions providing relative quantitation of S456 phosphorylation in lean (L) and obese (O) mice from the univerate study. C) Relative phosphorylation levels on Hmgcs2 S456 in the multivariate experiment. Datapoints indicate fold change on a log2 scale, relative to the average of all eight conditions, with error bars indicating the SD of all replicates quantified. Note, conditions highlighted in black are the same as those assessed in panel A. D) Schematic of Hmgcs2 primary sequence highlighting identified phosphorylated residues, including the PKA and CK2 consensus site at S456. E) Activity of flag-tagged wild type (WT), S456D, S456E, S456A, S456M, 433A, 433D, 343T, and C166A (catalytically dead) HMGCS2 and GFP control, at a single substrate concentration (1000 μM Ac-CoA). Activity is expressed as a percent of WT and error bars indicate SD of triplicate analyses. F) Enzyme activity kinetic curve at multiple substrate concentrations for flag-tagged wild type (WT), S456A, S456D, and C166A (catalytically dead) HMGCS2. Error bars indicate SD. Kinetic parameters for selected Hmgcs2 variants are shown at the right. See also Figure S5

Figure 6:

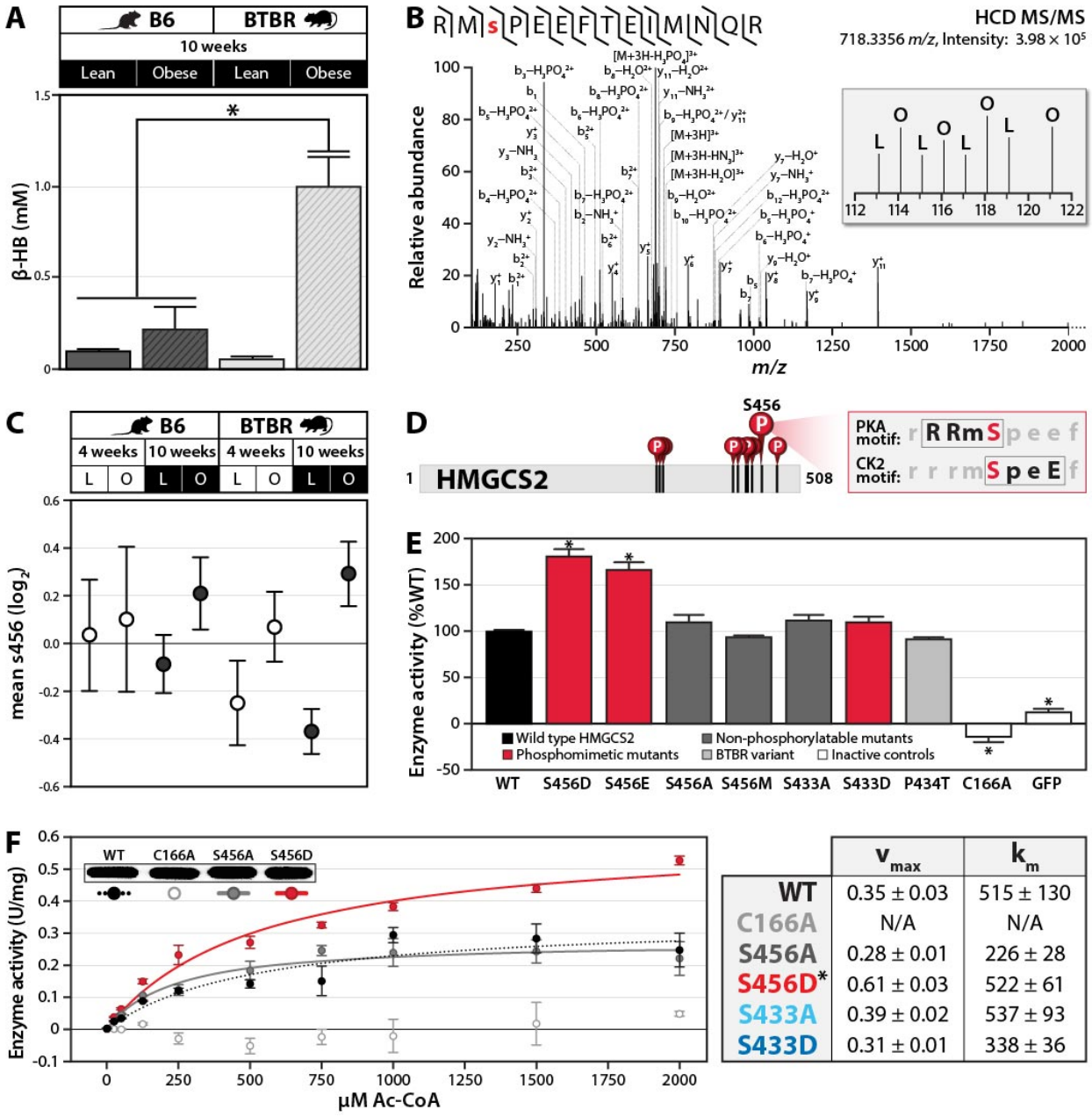

	v_{max}	k_m
WT	0.35 ± 0.03	515 ± 130
C166A	N/A	N/A
S456A	0.28 ± 0.01	226 ± 28
S456D*	0.61 ± 0.03	522 ± 61
S433A	0.39 ± 0.02	537 ± 93
S433D	0.31 ± 0.01	338 ± 36

Figure 7: Phosphorylation of serine 456 on Hmgcs2 increases enzyme activity and is induced during ketogenesis.

A) Percent increase in Hmgcs2 activity after the addition of either PKA (left) or CK2 (right), error bars indicate SEM. B) Mass spectrum (average of 25 MS2 scans) identifying phosphorylation of S456 on human HMGCS2 after the in vitro kinase reaction with PKA seen in panel A. C) β-hydroxybutyrate levels were measured in culture medium from HEK293 cells transfected with WT or C166A Hmgcs2, and subsequently cultured for 72 hours in either standard or ketogenic media. Bars indicate SD and asterisks (*) indicate significance at $p<0.001$. D) Hmgcs2 enzyme activity at a single substrate concentration (1000 μM Ac-CoA) after immuoprecipitation from HEK293 cells in either standard or ketogenic media for 72 hours. Values are normalized to WT in standard media, error bars indicate SEM and asterisks (*) indicate significance at $p<0.001$. E) Enzyme activity kinetic curve at multiple substrate concentrations for flag-tagged WT HMGCS2 immuoprecitiated from HEK293 cells cultured for 72 hours in either standard or ketogenic media, and subsequently subjected to in vitro phosphorylation with CK2. Error bars indicate SD. Kinetic parameters are shown in the inset. F) Activity assay of HMGCS2 kinase recognition site mutants. G) β-hydroxybutyrate levels in HEK293 cells transfected with S456A or S456D mutant HMGCS2 over a timecourse of culturing in ketogeic media. See also Figure S5.

Figure 7:

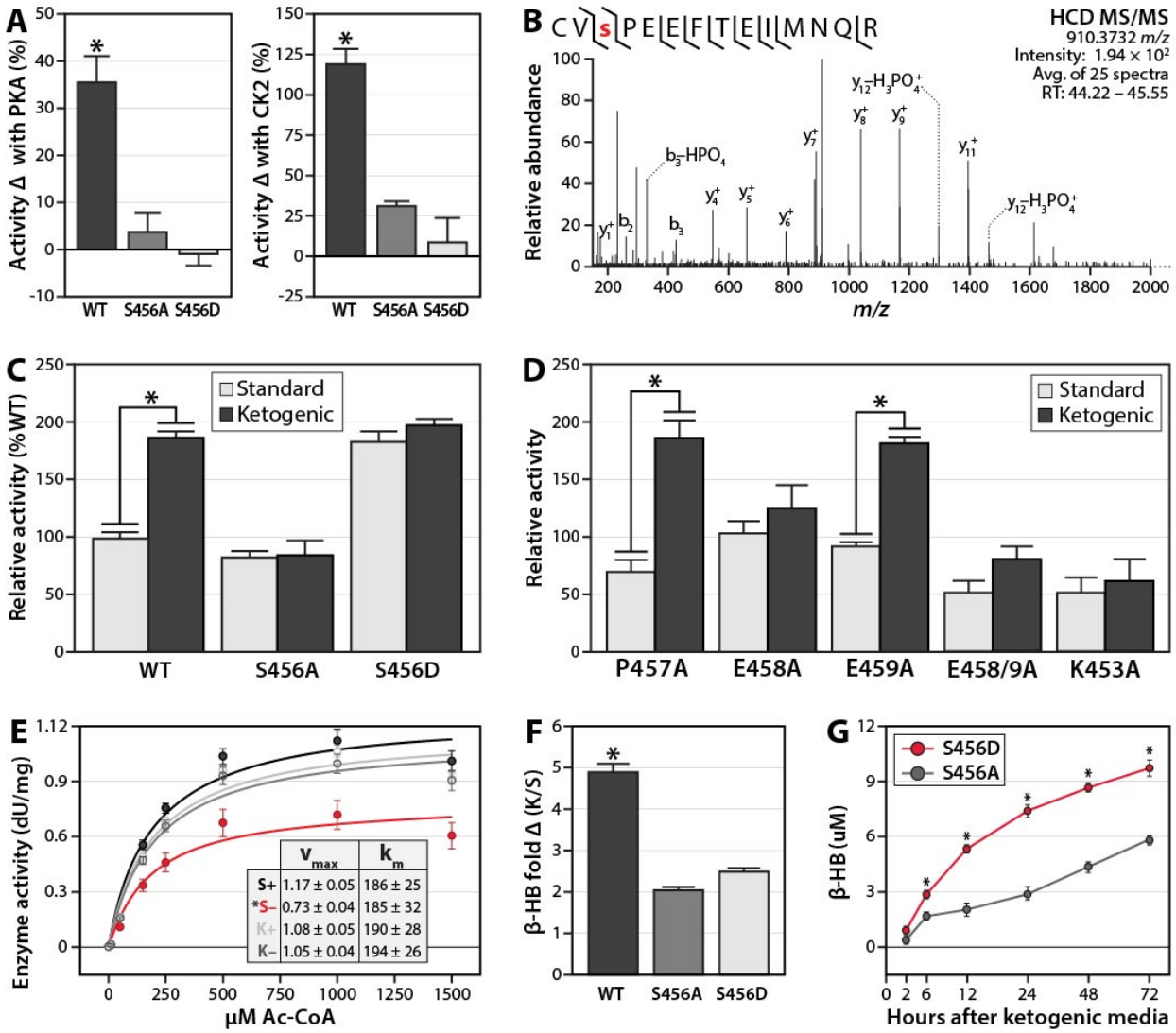
A
Activity Δ with PKA (%)
WT S456A S456D
Activity Δ with CK2 (%)
WT S456A S456D
B
C V s P E E F T E I M N Q R
HCD MS/MS
910.3732 m/z
Intensity: 1.94 × 10²
Avg. of 25 spectra
RT: 44.22 – 45.55
Relative abundance
m/z
C
Relative activity (%WT)
Standard
Ketogenic
WT S456A S456D
D
Relative activity
Standard
Ketogenic
P457A E458A E459A E458/9A K453A
E
Enzyme activity (dU/mg)
μM Ac-CoA
Vmax Km
S+ 1.17 ± 0.05 186 ± 25
*S– 0.73 ± 0.04 185 ± 32
K+ 1.08 ± 0.05 190 ± 28
K– 1.05 ± 0.04 194 ± 26
F
β-HB fold Δ (K/S)
WT S456A S456D
G
S456D
S456A
β-HB (uM)
Hours after ketogenic media

Supplemental Experimental Procedures

Chemicals and Supplies

8-plex iTRAQ Reagents were purchased from Applied Biosystems (Carlsbad, CA). Protease (Complete mini EDTA-free) and phosphatase (PhosSTOP) inhibitor cocktail tablets were purchased from Roche (Mannheim, Germany). The BCA Protein Assay Kit was purchased from Pierce Biotechnology (Rockford, IL). Trypsin Gold, Protein Kinase A, and Caseine Kinase 2, were purchased from Promega (Madison, WI). Lysyl Endopeptidase (LysC) and Autokit Total Ketone Bodies were purchased from Wako Chemicals (Richmond, VA). Sep-Pak tC18 and C18 cartridges were purchased from Waters (Milford, MA). A Poly SULFOETHYL A column (200 x 9.4 mm, 5 mm, 200 Å) was purchased from PolyLC (Columbia, MD). Ni-NTA Magnetic Agarose Beads and Single-Tube Magnet were purchased from Qiagen (Valencia, CA). C18 resin (5 μm pore size) was purchased from Alltech (Deerfield, IL). Inline MicroFilters and MicroTight column unions, fittings, and sleeves were purchased from Upchurch Scientific (Oak Harbor, WA). Fused-silica capillary tubing was purchased from Polymicro Technologies (Phoenix, AZ). LITHISIL lithium silicate was purchased from PQ Corporation (Valley Forge, PA). Formic acid and trifluoroacetic acid ampoules were purchased from Thermo Scientific (Rockford, IL). Gibco Dulbecco's Modified Eagle Medium (DMEM), Fetal Bovine Serum (FBS), Phosphate Buffered Saline (PBS), Trypsin-EDTA, and Penicillin-Streptomycin were purchased from Life Technologies (Carlsbad, CA). Anti-FLAG M2 beads and FLAG peptide were purchased from Sigma. Mouse monoclonal anti-FLAG (HRP-linked) and anti-β-actin antibodies were purchased from sigma and anti-mouse IgG secondary antibody (HRP-linked) was purchased from Cell Signaling.

All other chemicals were purchased from Sigma-Aldrich (St. Louis, MO).

Mitochondrial Enrichment

Crude mitochondrial enrichment was performed using previously described methods (Pagliarini et al., 2008), modified for phosphoproteomics, with all steps carried out at 4°C. Frozen (-80°C) liver sections (~150 mg wet tissue weight) were placed into a Potter-Elvehjem glass/Teflon homogenizer along with 8 mL of MSHE Buffer (220 mM Mannitol, 70mM sucrose, 5mM HEPES, pH 7.41mM EGTA, 1x protease inhibitor tablet, and 1x phosphatase inhibitor tablet) supplemented with 0.5% BSA. The tissue was homogenized with 4 homogenizer strokes at 1000 rpm, and the resulting homogenate was decanted into a new tube. The homogenizer was rinsed with an additional 2 mL MSHE (supplemented with 0.5% BSA), which was added to the homogenate. The sample was centrifuged at 800 x g for 10 min in a bench-top conical centrifuge. The small amount of lipid that formed at the top of supernatant was carefully aspirated. The supernatant, containing the mitochondria, was gently drawn off with a pipet-aid and transferred to an ultra-clear 12 mL centrifuge tube. The samples were centrifuged at 8000 x g for 10 min, and the resulting supernatant and any loose material was aspirated and discarded, leaving a dark brown pellet with a light brown halo around the center. An additional 1mL of MSHE Buffer (supplemented with 0.5% BSA) was added to the pellet, which was disrupted by washing it from the side of the tube until homogenous using as few pipetting strokes as possible. Crude mitochondria were transferred to a 1.5 mL microfuge tube and centrifuged at 8,000 x g for 10 min in bench-top centrifuge. The supernatant was aspirated and discarded. The pellet was re-

suspended in MSHE (without BSA) and centrifuged at 8,000 x g for 10 min in bench-top centrifuge. The supernatant was aspirated and discarded, and the mitochondrial pellet was flash frozen in liquid N2 and stored at -80°C until ready for use.

Protein Digestion and iTRAQ Labeling of Peptides

Proteins were digested using modifications to previously described methods (Grimsrud et al., 2010). Crude mitochondrial pellets were re-suspended in 350 µl Resuspension Buffer (8M urea, 40 mM Tris, pH 8.0, 30 mM NaCl, 1mM Na orthovanadate, 6 mM Na pyrophosphate, 2 mM MgCl2, 1 mM CaCl2, 1X protease inhibitor tablet, 1x phosphatase inhibitor tablet). Following mild heating at 37°C for 1 hour with intermittent incubation in a sonicating water bath in three 10 minute intervals, protein concentration was determined using the BCA assay. After DTT was added to a final concentration of 2 mM, the samples were vortexed and incubated at 37°C for 30 minutes to reduce disulfides. Samples were cooled to room temperature, iodoacetimide was added to a final concentration of 7 mM, and the samples were vortexed and incubated at room temperature in the dark for 30 minutes to alkylate cysteines. Additional DTT was added to a final concentration of 7 mM to quench the unreacted iodoacetimide. For each sample, 500 µg of protein was aliquoted to a new tube and enough Resuspension Buffer was added to bring the samples up to equal volumes. After addition of 5 µg LysC to each sample, the samples were vortexed and incubated at 37°C for 4 hours. After the urea concentration was subsequently diluted to 1.5M by the addition of 50 mM Tris, pH 8.0, 1mM CaCl2, 5µg trypsin was added, and the samples were vortexed and incubated overnight at 37°C. Enough 10% TFA

was added (final concentration ~1%) to acidify the sample, and the peptides were desalted by solid phase extraction (SPE) using 50 mg tC18 Sep-Pak cartridges (Waters). Samples were dried in a speed vac, and labeled with 8-plex iTRAQ reagents. For all replicates, each sample was reconstituted in 20 µl dissolution buffer and 14 µl water, and mixed with the contents of one vial of a unique 8-plex iTRAQ reagents (tags 113 through 119, and 121), which had been previously dissolved in 50 µl isopropanol (see mitomod.biochem.wisc.edu for all iTRAQ tag-mouse pairings). The samples were incubated for 1 hour at room temperature, vortexing briefly every 15 minutes. For each replicate, 2µl of all eight samples was removed, combined, and subjected to a small-scale (no peptide pre-fractionation or phosphopeptide enrichment) LC-MS/MS test—utilizing beam-type collisional activation dissociation in the ion injection pathway (iHCD) of a modified linear ion trap (LTQ, Thermo Scientific) mass spectrometer (McAlister et al., 2011)—to test for complete iTRAQ labeling and equal sample mixing. The individual iTRAQ-labeled peptide samples were stored at -80°C until further use.

Peptide Fractionation and Phosphopeptide Enrichment

After confirming complete iTRAQ labeling, peptide samples were mixed in equal ratios (adjusting for any deviation from 1:1:1:1:1:1:1:1 in the small scale test mixture assessment described above) for each replicate separately, dried in a speed vac, and subjected to strong cation exchange (SCX) chromatography as described previously (Swaney et al., 2009), with slight modifications. Samples were re-suspended in 400 µl SCX Buffer A (5 mM KH2PO4, 30% acetonitrile, pH 2.65) and enough diluted phosphoric acid was added (~40 µl) to bring the pH below 3. Samples were injected on

a polysulfoethylaspartamide column (9.4 x 200 mm; PolyLC) and a surveyor LC quaternary pump (Thermo Scientific) was operated at a flow rate of 3.0 ml/min. Typically, 6 SCX fractions were collected over 36 minutes using the following gradient: 0-1 min, 100% SCX Buffer A; 0-2.5 min, 0-10% SCX Buffer B (5 mM KH2PO4, 30% acetonitrile, 350 mM KCl, pH 2.65); 2.5-17.5 min, 10-60% SCX Buffer B, 17.5-20.5 min, 60-100% Buffer B. Buffer B was held at 100% for 3.5 minutes. The column was washed for 4 min with SCX Buffer C (50 mM KH2PO4, 500 mM KCl, pH 7.5) followed by 2.5 min with water, prior to re-equilibration with SCX Buffer A. For one technical replicate of the univariate study (Figure 1A), however, 16 fractions were collected over a longer gradient, as used previously for whole cell analysis (Swaney et al., 2009). After it was determined that decreasing the number of fractions and shortening the gradient for a second technical replicate of the univariate study did not decrease the number of MitoCarta protein identifications, 6 SCX fractions and the above gradient were utilized for all of the biological replicates for the multivariate and fasting/refeeding studies. Fractions were frozen at -80°C, lyophilized, desalted by SPE, and dried in a speed vac.

Each desalted SCX fraction was re-suspended in 1 ml 80% acetonitrile/0.1% TFA. For each sample, 5% (50 µl) was removed, dried in a speed vac, and saved at -80°C for quantification of non-phosphopeptides. The remaining 95% (950 µl) of each fraction was subjected to immobilized metal affinity chromatography (IMAC) with magnetic beads (Qiagen) to enrich for phosphopeptides, as described previously (Phanstiel et al., 2011). Following three washes with water, the beads were incubated in 40 mM EDTA, pH 8.0 for 30 minutes while shaking, and subsequently washed with water again three times. The beads were then incubated with 100 mM FeCl3 for 30 minutes while

shaking, and were washed once with a 1:1:1 solution of acetonitrile/methanol, 0.1% acetic acid and three times with 80% acetonitrile/0.1% TFA. Samples were added to the beads and were incubated for 30 minutes while shaking, and subsequently washed four times with 1 ml 80% acetonitrile/0.1% TFA and eluted for 1 minute by vortexing in 100 µl of 1:1 acetonitrile:0.7% NH4OH in water. Eluted phosphopeptides were acidified immediately with 5% formic acid and dried in a speed vac.

Nano-LC-MS/MS

High mass accuracy tandem MS was utilized for isobaric tag-based quantitative proteomics using our previously described methods (Lee et al., 2011; Phanstiel et al., 2011), with slight modifications. All samples were reconstituted in 20ul 0.2% formic acid. Precolumns (75 µm inner diameter x 5 cm) and analytical columns (50 µm inner diameter x 15 cm) were made in-house with C18 particles (Alltech), as described previously (Ficarro et al., 2009). For each Nano-LC-MS/MS run, a nanoACQUITY UPLC system (Waters Corporation) was used to load 4.5 µl of sample onto a precolumn for concentrating and desalting for 10 min at a flow rate of 1 µl per minute. Peptides were subsequently separated over an analytical column at a flow rate of 300 nL/min using gradients of varied amounts of LC Buffer A (0.2% formic acid) and LC Buffer B (100% acetonitrile, 0.2% formic acid). Phosphopeptide fractions were separated over the following gradient: 0-1 minute, hold at 1% acetonitrile; 1-115 minutes, 1–30% acetonitrile; 115-120 minutes, 30-80% acetonitrile; 120-125 minutes, isocratic elution at 80%. For non-phosphopeptide fractions, the following gradient was used: 0-1 minutes, 1–5% acetonitrile; 1-160 minutes, 5-25% acetonitrile; 160-180 minutes, 25-

35% acetonitrile; 180-185 minutes, isocratic elution at 80% acetonitrile.

Eluted peptides were subjected to electrospray ionization (Fenn et al., 1989) and online infusion into an ETD-enabled LTQ Velos Orbitrap mass spectrometer (Thermo Fisher Scientific). MS1 survey scans of peptide cations were performed in the orbitrap at 30,000 or 60,000 resolution, precursors were selected for fragmentation using a 3.0 Th isolation window, and orbitrap MS/MS interrogation was performed at 7,500 resolution. At least two runs were performed for each sample where the top ten most abundant ions of charge state 2 or greater from each MS1 scan were selected for fragmentation with HCD (45 normalized collision energy). An additional run using back-to-back ETD (35 normalized collision energy, 70 ms activation time) and HCD on the top five most abundant precursors of charge state 3 or greater was performed on each phosphopeptide fraction. Dynamic exclusion was enabled for 60 s, with a max exclusion list of 500 with an exclusion width of 0.55 Th below and 2.55 Th above the selected average mass. MS/MS was always performed in the LTQ. Tune methods had AGC target settings of 1x106 for FTMS1, 5x104 for FTMSN, and 4x105 for ETD reagent ions, and max inject times of 200 ms for FTMS1, 200 ms for FT MSN, and 100ms for ETD. For all runs from the multivariate study, real-time precursor purity filtering (RTF) was performed on the fly during precursor selection by modification of the instrument control method as described previously (Wenger et al., 2011a). Using RTF, precursors were only selected for fragmentation if they had interfering ions present below a threshold of 0.25 times the precursor's intensity within an m/z window of 3.6 Th. For the univariate study, post-acquisition filtering (PAF) was applied to remove quantitation for MS2 spectra with this same level of interference (0.25) observed in their

corresponding MS1 spectrum, as described previously (Phanstiel et al., 2011). For the fasting/refeeding study, peptide and phosphopeptide fractions from each of 6 SCX fractions were subjected to two runs: one run used all HCD fragmentation (35 normalized collision energy) (applying PAF as described above, dynamic exclusion of 10 ppm around selected isotopes, MS1 AGC of 1x105, and max inject time of 100 ms) and one run used HCD fragmentation (40 normalized collision energy) along with our recently developed instrument control method, QuantMode, which increases quantitative accuracy and dynamic range for isobaric-labeled samples through gas phase purification of peptides prior to dissociation (Wenger et al., 2011a). SF6 reagent ions were used to perform the proton transfer reaction required to purify precursors. MS2 AGC and max inject times were set to 2x106 and 200 ms respectively.

Sequence Identification and Protein/Phosphoprotein Quantitation

The Coon OMSSA Proteomics Software Suite (COMPASS) was utilized to analyze tandem MS spectra as described previously (Wenger et al., 2011b). Merged .dta text files consisting of MS2 peak lists were extracted from Thermo .raw files were generated using the COMPASS module DTA Generator. Remaining precursors were removed from all spectra and ETD preprocessing was performed for ETD spectra, which increases database search identifications (Good et al., 2009). The Open Mass Spectrometry Search Algorithm (OMSSA) (Geer et al., 2004) was used to search peak lists against a concatenated target-decoy database (Elias and Gygi, 2007) consisting of mouse proteins are their nonsense reverse complements. The Mus musculus complete proteome set, consisting of reviewed (UniProtKB/Swiss-Prot) and unreviewed

(UniProtKB/TrEMBL) protein sequences from UniProt (www.uniprot.org/taxonomy/10090) was utilized as the target protein database, which contained 48,070 entries at the time of download (8/3/11). The decoy entries for concatenated target-decoy database were prepared with Database Maker by reversing the protein sequences for all UniProt entries. All database searches included a precursor mass tolerance setting of ±4.5 Da and monoisotopic mass tolerance of ±0.01 Da for fragment ions, and allowed for up to 3 missed cleavages with trypsin. Fixed modifications included carbamidomethylation of cysteines and 8-plex iTRAQ (as a user modification) on the N-terminus and lysines. Standard variable modifications included oxidation of methionines and 8-plex iTRAQ on tryosines. For phosphopeptide runs specifically, additional variable modifications included phosphorylation with neutral loss on serine and threonine residues and intact phosphorylation on tyrosine residues for HCD spectra, and intact phosphorylation on serine, threonine, and tyrosine for ETD spectra. For each replicate, identifications from non-phosphopeptide and phosphopeptide runs were separately filtered to an estimated 1% false discovery rate (FDR) at the unique peptide level with FDR Optimizer. The COMPASS module TagQuant was utilized to assign quantitative values to all peptide spectral matches (PSMs) using iTRAQ reporter ion intensities, apply isotope purity corrections, and normalize quantitation for all PSMs across each replicate individually (with data from corresponding phosphopeptide runs and non-phosphopeptide runs normalized together) as a loading control. Protein Hoarder was used to group peptides (from all replicates together) to parsimonious protein groups at 1% FDR at the unique protein level (using only peptides unique to each protein group for protein-level scoring), and

sum the reporter ion intensities of all PSMs (with interference below 0.25, as described above) for a given unique protein within each replicate individually. Phosphopeptides and peptides shared between protein groups were excluded from protein quantitation calculations. Phosphinator was utilized to localize phosphoryl groups to specific residues at 95% probability (Ascore = 13) (Beausoleil et al., 2006)for all phosphopeptides identified at 1% peptide level FDR and sum reporter ion intensities of all localized phosphopeptides identifying a given phosphoisoform (pattern of co-detected localized phosphorylation sites) within each replicate individually (Phanstiel et al., 2011).

Statistical Comparisons of Proteomic Measurements

We converted the .csv files from Protein Hoarder and Phosphinator to a tab-delimited format and reduced the protein descriptions to UniProt protein names. An in-house program written in Microsoft Access, called COMPASS Reader, processed the data in an automated fashion. The processing is stored in Access tables and then converted to Excel workbooks for ease of use. COMPASS Reader utilized the following workflow:

1) Import– Import to normalized database structure. All data is imported into a set of tables. This transformation includes, for example, the separation of data values (measurements) from metadata (e.g. names of proteins).

2) Value Transformation– Truncated Log Transform. Individual values are converted into a form that approximates a normal distribution overall. In our case we needed to discard all measurements less than 212 and take the log (base 2) of the

remaining measurements.

3) Value Normalization– Removal of Block Effect. For each measurement-replicate we compute the average across all measured samples and reduce the condition-measurement-replicate by the mean. Note that this step is only relevant for display of the measurements for all eight physiological conditions; the various comparisons between sets of conditions automatically remove this block effect.

4) Reduce technical replicates– Average measurements from the same mouse. This reduces the two technical replicates of the univariate experiment to a single collection of 8 mice, but has no effect on the multivariate experiment.

5) Score Protein Significance– t-test. For each measurement-comparison (see below for list of comparisons), compute a p-value for the null hypothesis that the In-Group has the same (normal) distribution as the Out-Group. We assume the same variance for this test.

6) Multiple Hypothesis Testing– FDR Calculation. For each measurement_type-comparison we count the number of measurement comparisons that have a p-value greater than 0.5. We use this as an estimate of half of the True Negative cases (TN) (i.e. measurements that do not change between the two groups of the comparison). We assume that the p-values of unchanging measurement-comparisons are uniformly distributed between 0 and 1 (Figure S1E); this means that the expected number of false positives with p-values less than x is equal to x times TN. Thus, we can count the number of estimated positives (Pos(x)) who have p-values less than x. This gives us an estimate of the FDR as: FDR(x) = x * TN / Pos(x). Finally we force our FDR estimate to be non-decreasing (x<y implies that FDR(x)<FDR(y)). Note that this method produces

both an estimate of the number of true positives (i.e. measurements that are changing between two collections of conditions) and an FDR that is usually less than 100% for p=1.0. This FDR calculation was applied to protein, phosphoisoform, and normalized phosphoisoform measurements (but not motif or kinase activity predictions due to the smaller number of measurements).

7) Relevance Filter– q-value cutoff. Select an arbitrary cut-off for the FDR. Note that a q-value (FDR) is an estimate of the probability that the alternate hypothesis is incorrect, which is a different type of object from the traditional p-value. While $p<0.05$ is a traditional cutoff in much of biology (which, in principle, means that 5% of conclusions based on random noise are considered real), the cutoff for a q-value should be evaluated based on the researcher's tolerance of an incorrect answer; we have chosen to highlight changes at $q<0.1$ in this manuscript, which assumes that 10% of the changes deemed significant are wrong, which is a common cutoff used in transcriptomics (Zheng et al., 2010). However, other researches can utilize either more or less conservative q-value thresholds when utilizing our data.

Description of Proteomic Comparisons

We produced two types of comparisons: conditional and restricted. The conditional comparisons compare a subset of the conditions with the remainder of the conditions. Examples:

•BTBR: Compares BTBR mice with B6 mice. This is the strain comparison.

•BTBR_O: Compares BTBR/obese mice with all others (all B6 mice and all lean mice)

•BTBR_O_10: Compares BTBR/obese/10 week mice with all other mice. This comparison is also called Diabetes since it is the only condition where the diabetic phenotype exhibits.

We performed 8 single-condition comparisons (corresponding to the eight unique conditions), 3 two-condition comparisons (BTBR_O, BTBR_10, O_10), and 3 four-condition comparisons (BTBR, Obese, and 10 weeks), for a total 14 comparisons. For emphasis, the diabetic state is represented twice (as stated above), once as BTBR_O_10 and once as Diabetes, bringing the nominal number of comparisons to 15. We refer to single-condition comparisons as the "1v7 comparisons" (Table S2) and the rest as the "Factor comparisons" (Table S3). The rest of the comparisons, the "restricted comparisons", compare differences for a single factor (e.g. obesity) for a restricted set. Examples:

•Obesity-BTBR: Compares all obese/BTBR mice with all lean/BTBR mice

•Obesity-B6_04: Compares all B6_O_04 mice with all B6_L_04 mice

There are 3 factors to compare (Obesity (obese vs lean), Strain (BTBR vs B6), and Age (10 weeks vs 4 weeks)). For each factor, there are 4 single-factor restrictions and 4 double-factor restrictions, for a total of 24 comparisons. Thus, the total number of comparisons is 38, with 1 duplicate labeling of the same comparison (BTBR_O_10, a 1v7 comparison, is the same as Diabetes, a factor comparison). These comparisons are separated into four Microsoft Excel files (Tables S2-5, see Figure S1A for a visual key of comparisons and in which files they are found).

We also created a file referred to as Conditional Stats (Table S1). This includes mean, variance, standard deviation, and count of all measurement-conditions.

Conditional Stats is related to the 1v7 comparison but still contains unique information, as it does not compare information across the conditions (beyond the data normalization, which forces the mean of all conditions to be zero). The log2 mean presented in Conditional Stats and the log2 fold-change presented in 1v7 differ by 1/7th, since the 1v7 subtracts the mean for 7 conditions from the mean of 1 condition (which will be of opposite sign) whereas the Conditional Stats only uses the mean. The Conditional Stats file is ideal for obtaining values for graphical representation of each measurement (with standard deviations), where the comparison files (Tables S2-5) should be utilized for evaluating magnitude and statistical significance of changes between conditions. This file also includes information about sequence coverage and spectral counts for estimating absolute abundance rank, and phosphopeptide sequences used for identifying phosphorylation sites on UniProt proteins.

Kinase-Substrate Predictions

Motifs were calculated using Motif-X v1.2 (Schwartz and Gygi, 2005), using a motif width of 35, a minimum occurrence threshold of 20, and a significance threshold of 0.000001. Motif analysis was run separately for analysis of serine, threonine, and tyrosine phosphorylation. For analysis of phosphorylation motifs present in our entire dataset, all localized phosphopeptides were utilized as the input with the IPI mouse proteome as the background. For analysis of mitochondrial-specific phosphorylation motifs, only localized phosphopeptides mapping to MitoCarta proteins were utilized as the input and sequences from the mouse MitoCarta list at http://www.broadinstitute.org/ftp/distribution/metabolic/papers/Pagliarini/Mouse.MitoC

arta.fasta (Pagliarini et al., 2008) were uploaded as the background. Kinase preferences were taken from the PHOSIDA database at http://141.61.102.18/phosida/help/motifs.aspx (Gnad et al., 2011).

HMGCS2 Purification

Cells were lysed on ice in IP buffer (PBS with 0.5% NP-40) supplemented with protease (Complete, Roche) and phosphatase (PhosSTOP, Roche) inhibitor cocktail tablets added just before use. Cells were sonicated at 20% output for 15 seconds and spun at 8,000 x g to clarify the lysate. FLAG-tagged proteins were immunoprecipitated using anti-FLAG M2 beads (Sigma) overnight at 4°C and washed five times with 10mL of IP buffer. For HMGCS2 activity assays, immunoprecipitated HMGCS2-FLAG proteins were eluted with 0.25mg/mL FLAG peptide (Sigma), concentrated using a centrifugal filter unit with 10kDa pore size (Millipore) and buffer exchanged with PBS / 15% glycerol / 0.1mM DTT as described previously (Shimazu et al., 2010).

Synthesis and Extraction of Acetyl-Coenzyme A

Acetyl Coenzyme A was synthesized as previously described (Parthasarathy et al., 2011; Stadtman, 1957), with slight modifications. Acetic anhydride and 0.5 M sodium bicarbonate were cooled on ice, and the free Coenzyme A was dissolved into the sodium bicarbonate in a round-bottom flask. The reaction flask was cooled on ice, and acetonitrile was added to 10% (v/v). Acetic anhydride was then added in a 1.5:1 molar ratio to the Coenzyme A and the reaction was allowed to proceed for 15 minutes on ice. After spotting the reaction onto Whatman paper, reaction completion was monitored

by staining with nitroprusside and observing a color change after addition of methanolic sodium hydroxide. After a 15 minute reaction in a round bottom flask, the solution was acidified to a pH of ~ 2 with 6N HCl and frozen in liquid N2 before lyophilizing overnight. To isolate acetyl Coenzyme A from the reaction, C18 Sep-Pak columns (Waters) were pre-washed with methanol and equilibrated with 0.1% TFA. The acetyl Coenzyme A reaction solid was removed from the lyophilizer, placed immediately on ice, and subsequently dissolved in 0.1% TFA. The AcCoA solution was then loaded onto the Sep-Pak column and washed with 0.1% TFA. After washing, acetyl Coenzyme A was eluted using into 3 asymmetric fractions using 4 mL of 0.1% TFA/CAN (1:1). Fraction 1 contained 0.5 mL and was discarded, fraction 2 contained 2 mL and was reserved, and fraction 3 contained 1.5 mL and was also discarded. Fraction 2 was then frozen in liquid N2, lyophilized overnight, and the weight of the subsequent Acetyl-CoA was used to calculate reaction yield.

HMCSC2 Activity Assay

HMGCS2 enzymatic activity was measured as described previously (Shimazu et al., 2010; Skaff and Miziorko, 2010). Briefly, activity was measured by monitoring the formation of HMG-CoA by Ac-CoA and AcAc-CoA, as measured by DTNB detection of CoASH (Skaff and Miziorko, 2010). Ac-CoA was synthesized based on previously described methods (Parthasarathy et al., 2011; Stadtman, 1957). Assay mixtures contained 10 μM AcAc-CoA and 0-2000uM Ac-CoA. Standard assay conditions used 1 μg of FLAG-HMGCS2 protein. Absorbance at 412 nm was recorded and data reflecting linear rates was collected for all enzymes. Using non-linear regression (Prism), data

was fitted to the Michaelis-Menten equation to determine Km and Vmax for each mutant. A unit of enzyme activity is defined as the amount of enzyme required to convert 1 μmol of substrate into product in one minute.

In vitro *Kinase Assay*

Purified HMGCS2 protein (1-2 μg) was incubated with or without 5U of cAMP dependent protein kinase catalytic subunit (PKA, Promega) or 2U of Casein Kinase 2 (CK2, Promega). Incubation was performed in kinase reaction buffer (BSA, Tris, ATP) for 30min at 30°C. After incubation, enzyme activity was assayed as described above using 750 uM of Acetyl CoA as a substrate.

Ketone Body Measurements

Ketone body levels were measured following the manufacturers protocol using the Autokit Total Ketone Bodies assay (Wako). Briefly, known standards of β-hydroxybutyrate and unknown sample were loaded onto a 96-well plate (Fisher). After incubation with R1 buffer containing Thio-NAD for 5 min at RT, R2 buffer was added to the samples and the production of Thio-NADH was monitored at 405 nm for 15 min using a BioTek Synergy 2 microplate reader. The rate of the reaction at different KB concentrations was used to create a standard curve and calculate the concentration of ketone bodies in the experimental samples.

Quantitative RT-PCR

RNA was isolated from HEK293 or AML12 cells using an RNeasy kit (Qiagen)

according to manufacturer's instructions. Exon-spanning primers were designed for human HMGCS2 (accession# NM_005518) and GAPDH or murine Hmgcs2 (accession# NM_008256) and Gapdh to detect expression in 293 and AML12 cells, respectively. Primer sequences used are: human HMGCS2 (fwd: 5' TCCCTTTACCTCTCCACTCAC 3', rev: 5' CCATAAGAGAAGGCACCAATCC 3'), human GAPDH (fwd: 5' TTCGCTCTCTGCTCCTCCTGTT 3', rev: 5' GCCCAATACGACCAAATCCGTTGA 3'), mouse Hmgcs2 (fwd: 5' CATCGAGGGCATAGATACCAC 3', rev: 5' CACTCGGGTAGACTGCAATG 3'), and mouse Gapdh (fwd: 5' GCCTTCCGTGTTCCTACC 3', rev: 5' CCTCAGTGTAGCCCAAGATG 3'). RT-PCR was performed using Power SYBR Green PCR Master Mix (Invitrogen) and data was collected on an ABI-7500 Fast Real Time PCR System (Applied Biosystems). The comparative CT method was used to calculate relative Hmgcs2 or HMGCS2 expression levels.

Supplemental References

Beausoleil, S.A., Villen, J., Gerber, S.A., Rush, J., and Gygi, S.P. (2006). A probability-based approach for high-throughput protein phosphorylation analysis and site localization. Nat Biotechnol 24, 1285-1292.

Elias, J.E., and Gygi, S.P. (2007). Target-decoy search strategy for increased confidence in large-scale protein identifications by mass spectrometry. Nat Methods 4, 207-214.

Fenn, J.B., Mann, M., Meng, C.K., Wong, S.F., and Whitehouse, C.M. (1989). Electrospray ionization for mass spectrometry of large biomolecules. Science 246, 64-71.

Ficarro, S.B., Zhang, Y., Lu, Y., Moghimi, A.R., Askenazi, M., Hyatt, E., Smith, E.D., Boyer, L., Schlaeger, T.M., Luckey, C.J., et al. (2009). Improved electrospray ionization efficiency compensates for diminished chromatographic resolution and enables proteomics analysis of tyrosine signaling in embryonic stem cells. Anal Chem 81, 3440-3447.

Geer, L.Y., Markey, S.P., Kowalak, J.A., Wagner, L., Xu, M., Maynard, D.M., Yang, X., Shi, W., and Bryant, S.H. (2004). Open mass spectrometry search algorithm. J Proteome Res 3, 958-964.

Gnad, F., Gunawardena, J., and Mann, M. (2011). PHOSIDA 2011: the posttranslational modification database. Nucleic Acids Res 39, D253-260.

Good, D.M., Wenger, C.D., McAlister, G.C., Bai, D.L., Hunt, D.F., and Coon, J.J. (2009). Post-Acquisition ETD Spectral Processing for Increased Peptide Identifications. J Am Soc Mass Spectrom.

Grimsrud, P.A., den Os, D., Wenger, C.D., Swaney, D.L., Schwartz, D., Sussman, M.R., Ane, J.M., and Coon, J.J. (2010). Large-Scale Phosphoprotein Analysis in Medicago truncatula Roots Provides Insight into in Vivo Kinase Activity in Legumes. Plant Physiol 152, 19-28.

Lee, M.V., Topper, S.E., Hubler, S.L., Hose, J., Wenger, C.D., Coon, J.J., and Gasch, A.P. (2011). A dynamic model of proteome changes reveals new roles for transcript alteration in yeast. Mol Syst Biol 7, 514.

McAlister, G.C., Phanstiel, D.H., Brumbaugh, J., Westphall, M.S., and Coon, J.J. (2011). Higher-energy Collision-activated Dissociation Without a Dedicated Collision Cell. Molecular & Cellular Proteomics 10.

Pagliarini, D.J., Calvo, S.E., Chang, B., Sheth, S.A., Vafai, S.B., Ong, S.E., Walford, G.A., Sugiana, C., Boneh, A., Chen, W.K., et al. (2008). A mitochondrial protein compendium elucidates complex I disease biology. Cell 134, 112-123.

Parthasarathy, A., Pierik, A.J., Kahnt, J., Zelder, O., and Buckel, W. (2011). Substrate specificity of 2-hydroxyglutaryl-CoA dehydratase from Clostridium symbiosum: toward a bio-based production of adipic acid. Biochemistry 50, 3540-3550.

Phanstiel, D.H., Brumbaugh, J., Wenger, C.D., Tian, S., Probasco, M.D., Bailey, D.J., Swaney, D.L., Tervo, M.A., Bolin, J.M., Ruotti, V., et al. (2011). Proteomic and phosphoproteomic comparison of human ES and iPS cells. Nat Methods 8, 821-827.

Schwartz, D., and Gygi, S.P. (2005). An iterative statistical approach to the identification of protein phosphorylation motifs from large-scale data sets. Nat Biotechnol 23, 1391-1398.

Shimazu, T., Hirschey, M.D., Hua, L., Dittenhafer-Reed, K.E., Schwer, B., Lombard, D.B., Li, Y., Bunkenborg, J., Alt, F.W., Denu, J.M., et al. (2010). SIRT3 deacetylates mitochondrial 3-hydroxy-3-methylglutaryl CoA synthase 2 and regulates ketone body production. Cell metabolism 12, 654-661.

Skaff, D.A., and Miziorko, H.M. (2010). A visible wavelength spectrophotometric assay suitable for high-throughput screening of 3-hydroxy-3-methylglutaryl-CoA synthase. Anal Biochem 396, 96-102.

Stadtman, E.R. (1957). Preparation and Assay of Acyl Coenzyme A and Other Thiol Esters; Use of Hydroxylamine. Methods in Enzymology 3, 931-941.

Swaney, D.L., Wenger, C.D., Thomson, J.A., and Coon, J.J. (2009). Human embryonic stem cell phosphoproteome revealed by electron transfer dissociation tandem mass spectrometry. Proc Natl Acad Sci U S A 106, 995-1000.

Wenger, C.D., Lee, M.V., Hebert, A.S., McAlister, G.C., Phanstiel, D.H., Westphall, M.S., and Coon, J.J. (2011a). Gas-phase purification enables accurate, multiplexed proteome quantification with isobaric tagging. Nat Methods 8, 933-935.

Wenger, C.D., Phanstiel, D.H., Lee, M.V., Bailey, D.J., and Coon, J.J. (2011b). COMPASS: a suite of pre- and post-search proteomics software tools for OMSSA. Proteomics 11, 1064-1074.

Zheng, D., Kille, P., Feeney, G.P., Cunningham, P., Handy, R.D., and Hogstrand, C. (2010). Dynamic transcriptomic profiles of zebrafish gills in response to zinc supplementation. BMC Genomics 11, 553.

Supplemental Tables

Tables S1-5: All protein and phosphoisoform quantitation for the univariate and multivariate experiments

Related to Figure 1

Measured species include protein abundance, phosphoisoform abundance (both with and without normalization to protein levels), phosphorylation motif abundance (both with and without normalization of underlying phosphoisoforms to protein levels), and predicted kinase activities (both with and without normalization of underlying phosphoisoforms to protein levels). Each file contains two tabs– the first tab contains a description and the second tab contains the data (note, Table S1 contains a third tab with information on all identified phosphopeptides). See Figure S1A for a visual depiction of comparisons made in each of the following files:

Table S1: Conditional Stats

Microsoft Excel file including condition-specific statistics for each proteomic/phosphoproteomic measurement (including phosphorylation motif and kinase activity predictions), such as mean (both log2 and geometric, relative to all eight conditions), standard deviation, and the number of replicate measurements (second tab). Also includes sequence coverage for each protein, and peptide spectral counts (PSMs), localized phosphopeptide sequences, and matching kinase preferences and motifs for all phosphoisoforms (note this information is only listed in Table S1 for brevity, but applies to the corresponding phosphoisoforms in Tables S2-5 as well). Also includes information on spectral quality for every localized and non-localized

phosphopeptide identified at 1%FDR (note, only localized phosphopeptides were used for the analysis throughout this manuscript, but non-localized phosphopeptides can still provide valuable information regarding phosphorylation on proteins of interest, albeit without the assignment of the exact residue that is modified on the identified peptide at 95% probability).

Table S2: 1vs7

Microsoft Excel file including proteomic/phosphoproteomic comparisons (including phosphorylation motif and kinase activity predictions) between each physiological condition and the other seven, one at a time for all eight conditions.

Table S3: Factors

Microsoft Excel file including combinations of proteomic/phosphoproteomic comparisons (including phosphorylation motif and kinase activity predictions) between sets of physiological conditions linked by a common factor and all other conditions.

Table S4: 2vs2

Microsoft Excel file including combinations of proteomic/phosphoproteomic comparisons (including phosphorylation motif and kinase activity predictions) between a pair of two physiological conditions and another pair separated by a single variable.

Table S5: 1vs1

Microsoft Excel file including combinations of proteomic/phosphoproteomic

comparisons (including phosphorylation motif and kinase activity predictions) between one physiological condition and another separated by a single variable.

Supplemental Figures

Figure S1: Data analysis for the univariate and multivariate studies

Related to Figure 1

A) Visual key depicting all mouse sample comparisons contained in Tables S1-5. For relative fold-change comparisons made for each proteomic/phosphoproteomic measurement, the cells in the grid below the header of metabolic conditions indicate which samples were used for calculating the numerator (highlighted in black) or denominator (highlighted in white). Samples highlighted in grey were not utilized for the given comparison. The names of the Supplementary Tables (Tables S1-5) containing the statistical analysis for each comparison are indicated (red highlighting). B) Volcano plot of fold protein abundance change (obese/lean) vs. -log (p value) for each mitochondrial (red) and non-mitochondrial (grey) protein measured (univariate). C) Mitochondrial proteins rank ordered (x-axis) and graphed by fold change (y-axis). Analysis of significant changes ($q<0.1$) for mitochondrial proteins in panel B revealed modifications in the indicated mitochondrial pathways (increasing shown in red, decreasing shown in blue). D) Volcano plot of non-normalized protein phosphorylation changes, as in panel B for protein changes (univariate). E) Distribution of p-values (from 0 to 0.1) based on the number of replicate measurements comparing lean and obese 10 week-old B6 mice (multivariate), for both proteins (top) and phosphoisoforms (bottom). Lines connect the average probability densities (% of measurements falling into each bin) of p-values (100 bins of width 0.01), with the inset showing the entire range of p-values (from 0 to 1.0). The red line at a probability density of 1% indicates the distribution of theoretically random p-values. F) Abundance fold-change

(obese/lean) for all phosphoisoforms with significant obesity-dependent alterations ($q<0.1$) between 10 week-old lean and obese B6 mice in both experiments (multivariate on the x-axis and univariate on the y-axis). The percent of measurements in discordance between the two studies (light grey circles) is indicated. G) Abundance fold changes for individual glycolytic and TCA cycle proteins (see Table S2) in the univariate experiment (obese/lean in light grey) and the multivariate experiment (obese 10-week B6 relative to all other conditions in black, obese 10-week BTBR relative to all other conditions in red).

Figure S1:

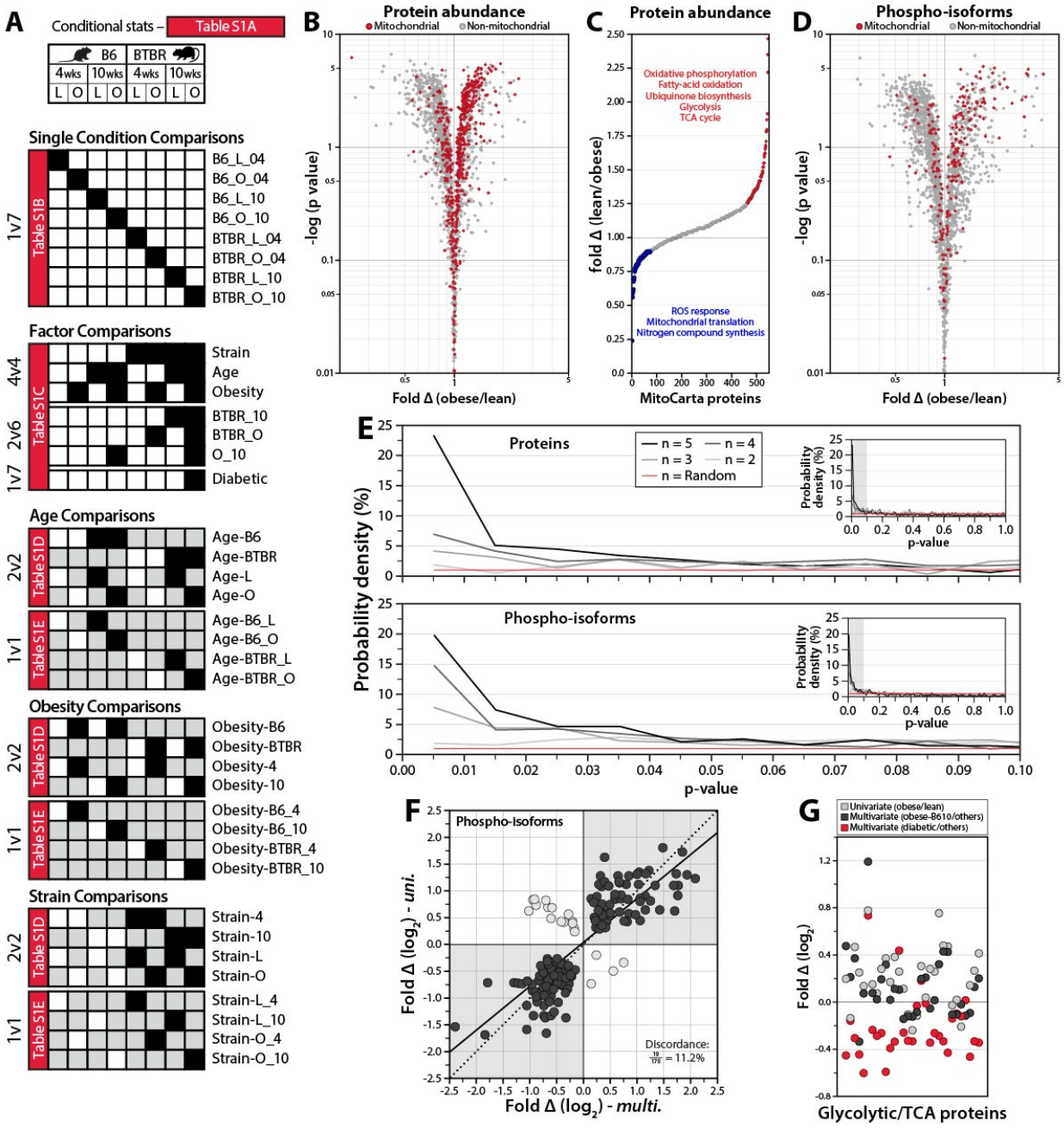
A
Conditional stats – Table S1A
B6
BTBR
4wks
10wks
4wks
10wks
L O L O L O L O
Single Condition Comparisons
1v7
Table S1B
B6_L_04
B6_O_04
B6_L_10
B6_O_10
BTBR_L_04
BTBR_O_04
BTBR_L_10
BTBR_O_10
Factor Comparisons
4v4
2v6
1v7
Table S1C
Strain
Age
Obesity
BTBR_10
BTBR_O
O_10
Diabetic
Age Comparisons
2v2
Table S1D
Age-B6
Age-BTBR
Age-L
Age-O
1v1
Table S1E
Age-B6_L
Age-B6_O
Age-BTBR_L
Age-BTBR_O
Obesity Comparisons
2v2
Table S1D
Obesity-B6
Obesity-BTBR
Obesity-4
Obesity-10
1v1
Table S1E
Obesity-B6_4
Obesity-B6_10
Obesity-BTBR_4
Obesity-BTBR_10
Strain Comparisons
2v2
Table S1D
Strain-4
Strain-10
Strain-L
Strain-O
1v1
Table S1E
Strain-L_4
Strain-L_10
Strain-O_4
Strain-O_10
B
Protein abundance
Mitochondrial
Non-mitochondrial
-log (p value)
Fold Δ (obese/lean)
C
Protein abundance
Oxidative phosphorylation
Fatty-acid oxidation
Ubiquinone biosynthesis
Glycolysis
TCA cycle
ROS response
Mitochondrial translation
Nitrogen compound synthesis
fold Δ (lean/obese)
MitoCarta proteins
D
Phospho-isoforms
Mitochondrial
Non-mitochondrial
-log (p value)
Fold Δ (obese/lean)
E
Proteins
n = 5
n = 4
n = 3
n = 2
n = Random
Probability density (%)
p-value
Phospho-isoforms
Probability density (%)
p-value
F
Phospho-Isoforms
Fold Δ (log2) - uni.
Fold Δ (log2) - multi.
Discordance:
10/170 = 11.2%
G
Univariate (obese/lean)
Multivariate (obese-B6\10/others)
Multivariate (diabetic/others)
Fold Δ (log2)
Glycolytic/TCA proteins

Figure S2: Phosphorylation of mitochondrial proteins across various expression levels

Related to Figure 2

All mitochondrial proteins (MitoCarta) are binned based on the number of phosphorylation sites detected (0, 1, 2-4, 5+). Distributions of sequence coverage, as a proxy for absolute abundance rank, are indicated by color (top). The percent distribution of sequence coverage is plotted against the number of phosphorylation sites (bottom).

Figure S2:

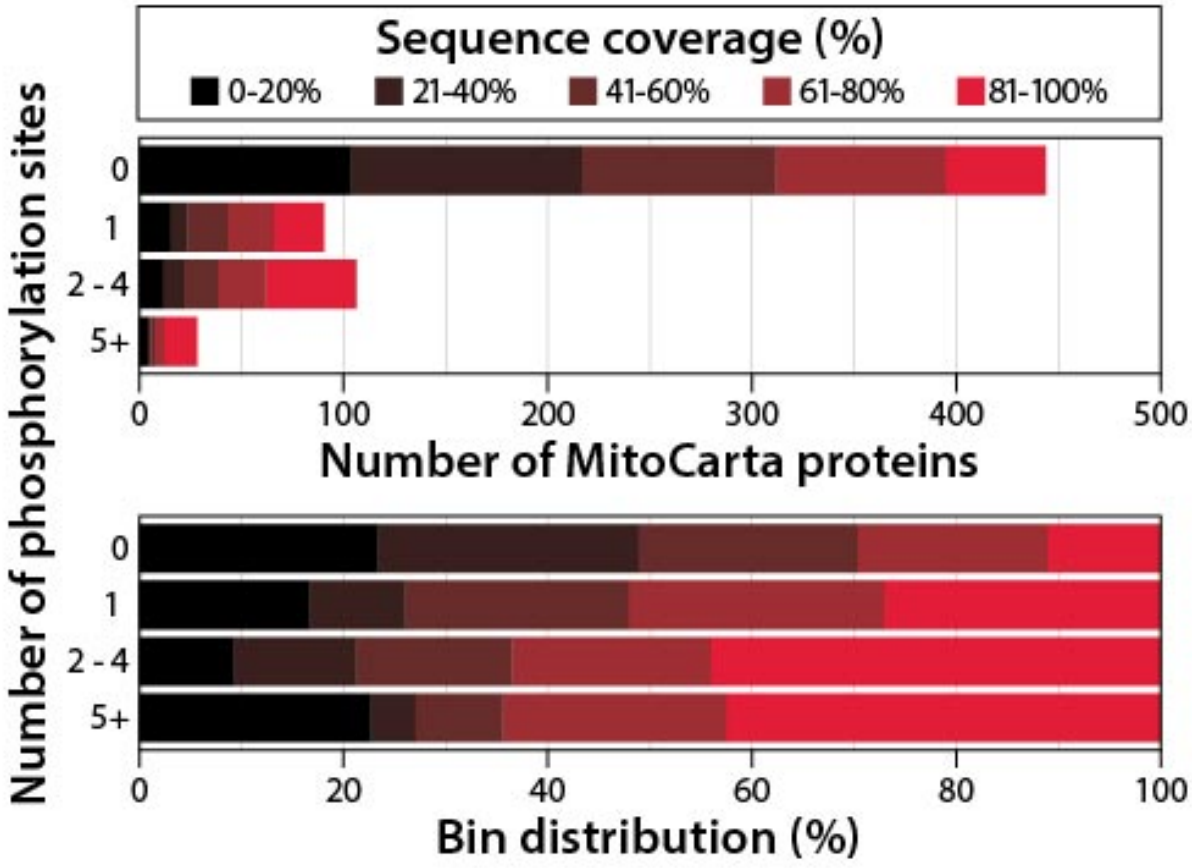
Sequence coverage (%)
0-20%
21-40%
41-60%
61-80%
81-100%
Number of phosphorylation sites
0
1
2 - 4
5+
0
100
200
300
400
500
Number of MitoCarta proteins
0
1
2 - 4
5+
0
20
40
60
80
100
Bin distribution (%)

Figure S3. Phosphorylation motif analysis

Related to Figure 5

A) All kinases and known substrate consensus sequences from the PHOSIDA database are indicated, with X indicating any amino acid and a red lower-case letter indicating the phosphorylated residue. The number of mitochondrial (MitoCarta) and total (MitoCarta and non-MitoCarta) phosphorylation sites and phosphoproteins identified by MS/MS are listed that satisfy the consensus sequence requirements for each kinase. B) All motifs identified by Motif-X analysis of our entire phosphoproteomic dataset (group by the polarity of fixed residues) and those specific to MitoCarta proteins.

Figure S3:

A

Protein Kinase	Sequence Preference	MitoCarta Phospho-sites	MitoCarta Phospho-proteins	Total Phospho-sites	Total Phospho-proteins
PKA	R-X-s/t R-R/K-X-s/t K-R-X-X-s/t	101	75	1858	1334
CK1	S-X-X-s/t S/T-X-X-X-s	184	111	3725	2038
CK2	s/t-X-X-E	93	76	1399	1069
GSK3	s-X-X-X-S	111	75	2327	1391
CDK2	s/t-P-X-K/R	20	20	710	590
CAMK2	R-X-X-s/t R-X-X-s/t-V	126	97	2880	1851
ERK/MAPK	P-X-s/t-P V-X-s/t-P P-E-s/t-P	35	34	926	745
PKB/AKT	R-R/S/T-X-s/t-X-S/T R-X-R-X-X-s/t	29	27	680	569
PKC	R-X-X-s/t-X-R	1	1	90	84
PKD	L/V/I-X-R/K-X-X-s/t	39	36	967	730
LCK	I/E/V-y-E/G-E/D/P/N-I/V/L	0	0	2	2
ABL	I/V/L-y-X-X-P/F	0	0	8	8
SRC	E/D-X-X-y-X-X-D/E/A/G/S/T	2	2	12	12
ALK	y-X-X-I/L/V/M	5	5	42	41
EGFR	D/P/S/A/E/N-X-y-V/L/D/E/I/N/P	5	5	37	35
CDK1	s/t-P-X-K/R s/t-P-K/R	34	30	1093	827
AURORA	R/K-X-s/t-I/L/V	16	15	409	376
AURORA-A	R/K/N-R-X-s/t-M/L/V/I	4	4	197	180
PLK	D/E-X-s/t-V/I/L/M-X-D/E	6	5	43	42
PLK1	E/D-X-s/t-F/L/I/Y/W/V/M	33	27	221	206
NEK6	L-X-X-s/t	43	37	594	498
CHK1/2	L-X-R-X-X-s/t	12	12	440	350
CHK1	M/I/L/V-X-R/K-X-X-s/t	45	41	1191	896
PDK1	F-X-X-F-s/t-F/Y	0	0	8	8
NIMA	F/L/M-R/K-R/K-s/t	1	1	25	25

Figure S3 Continued:

B

Basic
.....R..sP.P.....
.....P.sP.....
.....R..sP.....
.....sP...RR.....
.....GR.sP.....
.....sP.R.....
.....sP...R.....
.....RR.s.....
....K.....sP.....
.....sP....R.....
.....L.RS.s.....
.....R.R..s.....
.....K..sP.....
.....sPK.....
.....RS.s.....
.....R...sP.....
.....sP.K.....
.....L.R..s.....
.....sPR.....
.....R....sP.....
.....RT.s.....
.....R.Gs.....
.....RK.s.....
.....RQ.s.....
.....KR.s.....
.....R..s.....
.....R.s.....
.....KS.s.....
.....R..S..s.....
.....R..S.s.....
.....K.....s.....
.....R.....s.....
.....R..tP.....
.....R..t.....

Basic / Acidic
.....R.s.E.....

Acidic
.....s....E.....
.....s..D.....
.....s.E.....
.....S.s.E.....
.....s.DE.....
.....sD.D.....
.....sDEE.....
.....sE.E.....
.....sD.E.....
.....sDED.....

Nonpolar
.....sP.....
.....Gs.....
.....tSP.....
.....S.t.....
.....s.P.....
.....tPP.....
.....P.tP.....
.....tP.....

MitoCarta-specific
.....R..s.....
.....sP.....
.....s..E.....
.....tP.....

Figure S4: Additional information for screening candidate regulatory phosphosites on HMGCS2

Related to Figure 6

A) Upon sequencing the Hmgcs2 gene in B6 and BTBR mice, we confirmed that the BTBR strain harbor a coding SNP that causes a proline-to-threonine amino acid substitution at position 434 (codon change CCC to ACC). When the database used for searching the tandem MS spectra (from all mice in the multivariate study) is kept as the default UniProt sequence (left) or is manually altered to change Hmgcs2 residue 434 from P to T (right), the iTRAQ-based quantification of the non-phosphorylated peptide sequence spanning residues 433 and 434 is in agreement with strain difference in residue 434. While the different peptide sequences appear to have relatively equal abundance as estimated by spectral counts (64 vs. 62 PSMs for the non-phosphorylated sequences), the iTRAQ reporter intensity changes demonstrate how a coding SNP effects isobaric tag-based quantification of peptides spanning the effected residue. As such, although phosphorylation of serine 433 is unambiguously present in both mouse strains (21 PSMs in the context of the B6 sequence and 2 PSMs in the context of the BTBR sequence in the multivariate study), the relative abundances of this site cannot be measured using the iTRAQ system. We provide this as a cautionary reminder that such variants need to be considered in proteomic analyses seeking to compare organisms of different genetic backgrounds. B) Kinetic curve showing activity of wild type (WT), S433A, S433D, and S166A (catalytically dead) HMGCS2 at multiple concentrations of substrate. C) Enzyme activity at multiple concentrations of protein for FLAG-tagged wild type (WT), S456A, S456D, and C166A (catalytically dead) HMGCS2.

Figure S4:

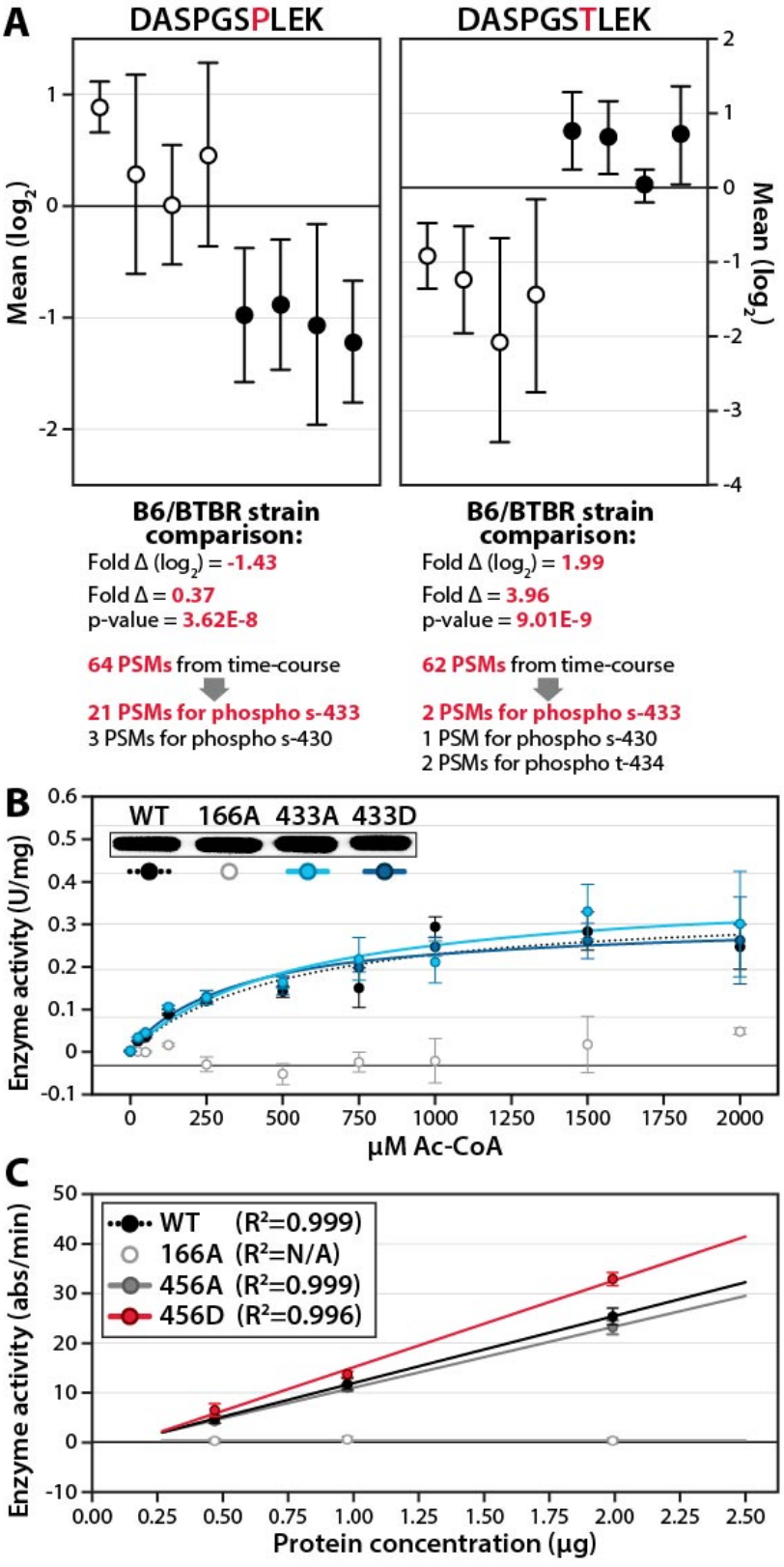
A
DASPGSPLEK
DASPGSTLEK
Mean (log2)
Mean (log2)
B6/BTBR strain comparison:
Fold Δ (log2) = -1.43
Fold Δ = 0.37
p-value = 3.62E-8
64 PSMs from time-course
21 PSMs for phospho s-433
3 PSMs for phospho s-430
B6/BTBR strain comparison:
Fold Δ (log2) = 1.99
Fold Δ = 3.96
p-value = 9.01E-9
62 PSMs from time-course
2 PSMs for phospho s-433
1 PSM for phospho s-430
2 PSMs for phospho t-434
B
WT 166A 433A 433D
Enzyme activity (U/mg)
µM Ac-CoA
C
WT (R²=0.999)
166A (R²=N/A)
456A (R²=0.999)
456D (R²=0.996)
Enzyme activity (abs/min)
Protein concentration (µg)

Figure S5: Expression of exogenous and lack of expression of endogenous HMGCS2 in HEK293 cells

Related to Figure 7

A) β-hydroxybutyrate (β-HB) levels were measured in culture medium from HEK293 cells transfected with WT or C166A HMGCS2, and subsequently cultured for 72 hours in either standard or ketogenic media. B) Immunoblot of the indicated FLAG-tagged Hmgcs2 variants (anti-FLAG antibody) and actin loading control (anti-β-actin antibody) in HEK293 cells transfected with pcDNA3.1 and cultured for 72 hours in either standard or ketogenic media (1 μg of protein from whole-cell extracted was loaded for each sample). C) RT-PCR analysis of endogenous HMGCS2 expression levels in positive control AML12 (mouse liver cell line) and HEK293 (derived from human embryonic kidney) cells used for the experiments in Figure 7. Values are expressed as mRNA levels (relative to control GAPDH) x 10,000. Error bars indicate SD and asterisks (*) indicate significance at $p<0.05$

Figure S5:

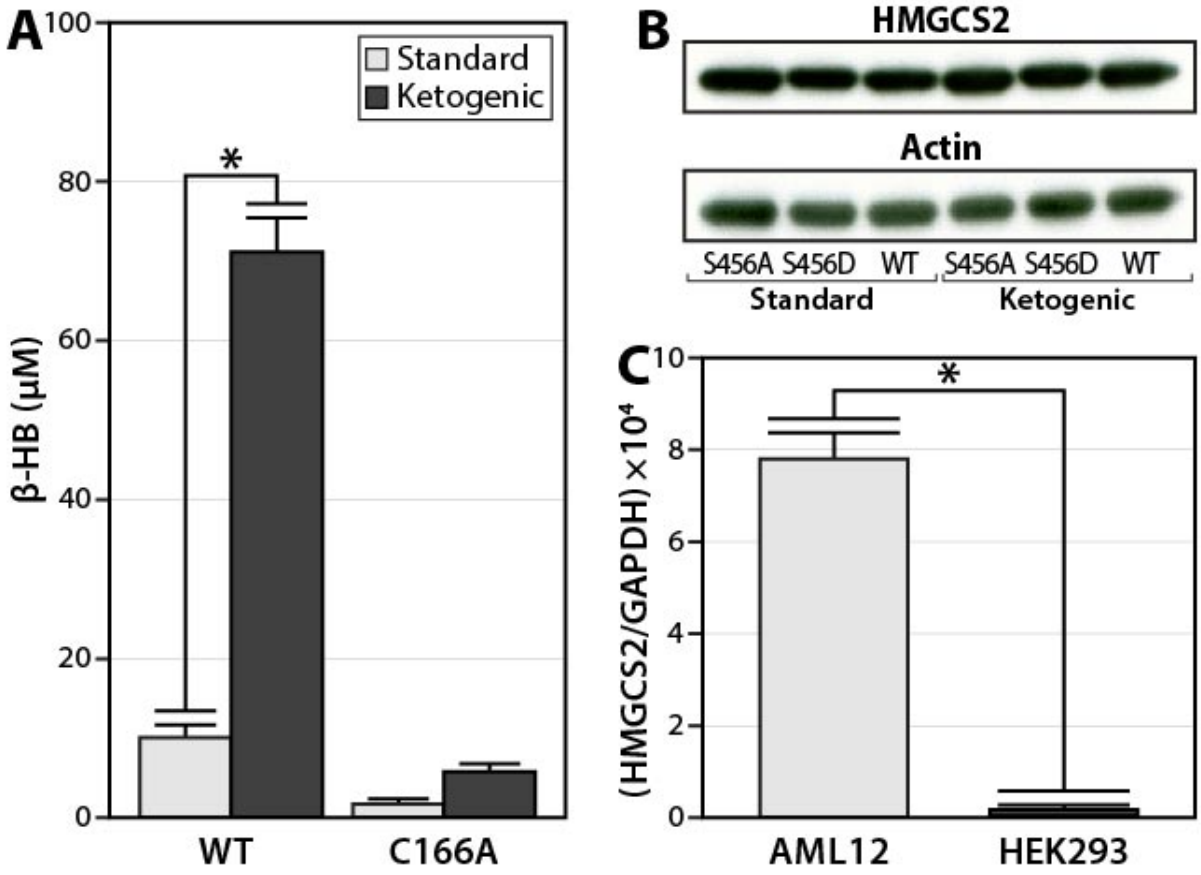
A
100
80
60
40
20
0
β-HB (μM)
Standard
Ketogenic
*
WT
C166A
B
HMGCS2
Actin
S456A S456D WT S456A S456D WT
Standard
Ketogenic
C
10
8
6
4
2
0
(HMGCS2/GAPDH) ×10⁴
*
AML12
HEK293

Graphical Abstract

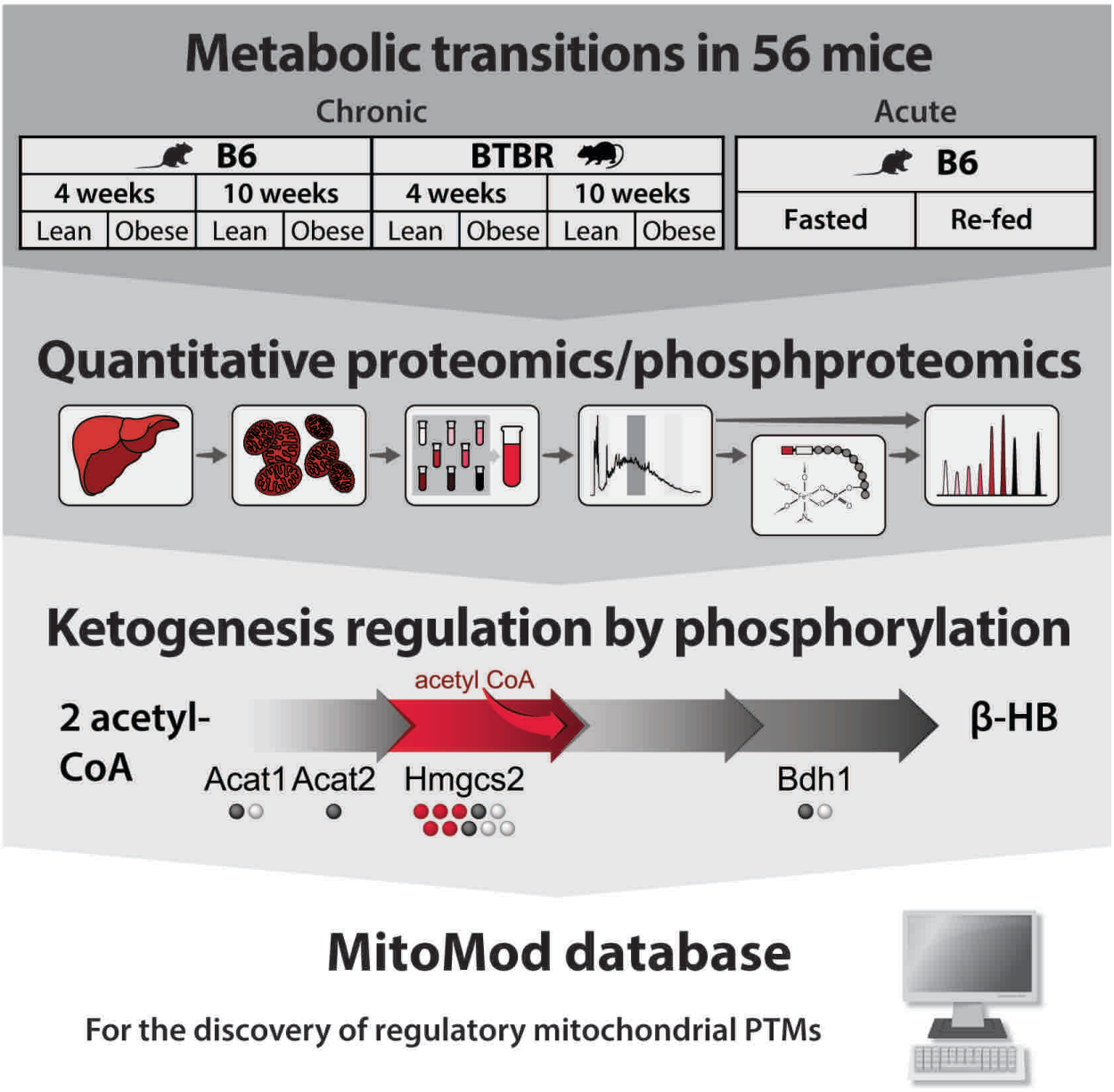

CHAPTER 3:

Identification and Characterization of Proteins Regulating Mitochondrial Phosphorylation

Contributions:

This chapter is subdivided into three parts. Part one includes identifying kinases that may reside in the mitochondria using activity based proteomics. The author carried out these experiments with assistance by Paul Grimsrud and direction by Dave Pagliarini. The second part involves identifying changing phosphorylation sites in isolated mitochondria using calcium treatment as a stimulating agent. The author carried out these experiments with direction by Dave Pagliarini. Finally, part three contains experiments identifying the targets of a mitochondrial phosphatase and characterizing the function of one phosphosite. The author carried out these experiments in conjunction with Natalie Niemi and Xiao Guo and with direction from Dave Pagliarini.

Summary

Mitochondria are dynamic organelles that need to be able to adapt to changing cellular conditions. Here, we used activity based protein profiling to identify kinases that are enriched in mitochondria, as well as kinases that are differentially enriched in the mitochondria of obese mice. We show that phosphorylation sites in isolated mitochondria can be rapidly modulated by acute (10min) treatment with calcium as a stimulus. Additionally, we report on the change in oxygen consumption rates in isolated mitochondria in response to treatment with calcium, and show that calcium uptake is also dependent on electron transport. Finally, we performed multiplexed quantitative mass spectrometry to identify the targets of the mitochondrial phosphatase PTC7. Using yeast deletion strains, we identify over 50 putative phosphorylation sites that are unique to a deletion of PTC7. Furthermore, we demonstrate that phosphorylation of a conserved serine on Hem15, the final step in heme biosynthesis, decreases enzyme activity. Collectively, this work suggests kinases that may localize to the mitochondria, and shows that phosphorylation in mitochondria is rapidly modulated and important for the response to oxidative stress.

Introduction

Mitochondria, long thought to be simply the site of energy generation in eukaryotic cells, have enjoyed a contemporary resurgence in interest as our understanding of this ancient organelle has become more complete. While the basic biochemical equations of the enzymes within mitochondria were deduced decades ago, more recent technological advances have expanded the boundaries of the field. We now know mitochondria to be a vast intracellular network that fuses, divides, and is host to a startling array of functions vital to both cellular life and death. As key centers of metabolism and signaling, mitochondrial dysfunction has become associated with a wide range of common diseases, including many inborn errors of metabolism, neurodegeneration, the aging process, cancer, and type 2 diabetes (Newgard and Sharpless, 2013; Szendroedi et al., 2011; Wallace, 2005). Although linked to mitochondria, the specific molecular basis for these diseases has not been extensively studied or, in some cases, is still entirely unknown.

Initial studies of the mitochondrial proteome revealed significant variability in mitochondria (Forner et al., 2006; Pagliarini et al., 2008), and has lead to the discovery of several gene mutations underlying specific mitochondrial disorders (Calvo and Mootha, 2010). Recent large-scale efforts have helped to define both the mitochondrial proteome as well as the myriad of post-translational modifications that decorate mitochondrial proteins (Grimsrud et al., 2012; Wang et al., 2010). Phosphorylation of mitochondrial proteins in particular has been the subject of much investigation, yet the functional relevance of mitochondrial phosphorylation has also been brought into question (Covian and Balaban, 2012).

Kinases, which comprise about 2% of the human genome, are one of the largest families of signaling proteins (Manning et al., 2002). Overall, protein kinase research is extensive and ongoing, yet mitochondrial kinases largely remain poorly studied (Pagliarini and Dixon, 2006). Nevertheless, our previous work shows widespread protein phosphorylation within the mitochondrion. To this end, we were interested in elucidating the kinases that are active in mitochondria, but there were several technical hurdles that have to be overcome. First, kinases are often proteins of low abundance that can be difficult to detect by standard shotgun proteomics (Picotti et al., 2009). Secondly, kinases can also be substrates of other signaling events and could be expressed but inactive until a signaling pathway is triggered (Shokat, 1995). The result is that, with few exceptions, we do not yet understand when, where and how mitochondrial proteins are phosphorylated. If we hope to understand the temporal variability in signaling pathways that affect mitochondria in obesity and diabetes, it is essential to also know which kinases are active at which times and not simply present in the organelle. To identify legitimate translocating kinases, a method capable of making accurate measurements of abundance and activity for a wide range of kinases across a variety of conditions is required.

By using activity-based proteomic profiling (ABPP), which only targets the active site within an enzyme, we can overcome both these hurdles in one step (Kobe and Kemp, 1999). ABPP uses reactive probes that only interact with a specific subset of active enzymes – in this case kinases – to isolate those proteins out of a complex mixture. These probes work by covalently reacting with conserved lysines that coordinate ATP in the active site of a kinase (Patricelli et al., 2007). The isolated

enzymes can then be identified by tandem MS (Fig 1A), providing higher detection sensitivity than a large-scale shotgun approach because the proteins of interest can be enriched using the probes. Since the activity of an enzyme—in this case a kinase—can be affected by a variety of conditions and modifications, using ABPP to isolate only active enzymes can provide information specific to a physiological condition that is unable to be collected from standard mRNA expression or protein abundance analysis (Cravatt et al., 2008).

Conversely, phosphatases comprise the opposite side of the phosphorylation reaction; they remove the phosphate moiety that kinases attach to a protein (Shi, 2009). While the localization of many kinases to the mitochondria remains controversial, the localization and identity of mitochondrial phosphatases has been well documented. PPTC7 is a mitochondrial phosphatase included in the MitoCarta protein compendium that belongs to the evolutionary conserved protein phosphatase family type 2C (PP2C) and is named for its homology to the yeast mitochondrial phosphatase Ptc7(Pagliarini et al., 2008). Yeast have three related mitochondrial phosphatases: Ptc5, Ptc6, and Ptc7 that are all localized to the mitochondria(Huh et al., 2003). While Ptc5 and Ptc6 have been shown to regulate the activity of the yeast pyruvate dehydrogenase complex, the endogenous substrates of Ptc7 are as yet largely undefined. (Gey et al., 2008).

Here, we performed multiplexed quantitative proteomics and phospho-proteomics as well as activity-based protein profiling in yeast and mouse mitochondria, respectively. These analysis were mainly motivated by our desire to greater understand the role of kinases and phosphatases in isolated mitochondria from mice and yeast. We also sought to further understand the role of calcium in the activation of

mitochondrial respiration rates and, potentially, kinases. To do this, we used high-resolution mass spectrometry with isobaric tagging as well as affinity probes coupled with mass spectrometry (Barglow and Cravatt, 2007; Phanstiel et al., 2011; Thompson et al., 2003).

Finally, we leveraged this data to show that phosphorylation can be rapidly modulated in isolated mitochondria by a physiological stimulus and have identified a likely target of the mitochondrial phosphatase Ptc7. Moreover, deletion of Ptc7 causes a disruption in the iron import system and the oxidative stress response in yeast and allows mutant yeast to survive iron chelation and hydrogen peroxide treatment. We have also shown that Hem15, the final step in heme biosynthesis in which iron is incorporated into the protoporphyrin ring, has increased phosphorylation in response to the deletion of Ptc7. Mutation of this site significantly decreases enzyme activity, which could explain the ability of Ptc7 mutant yeast to survive iron chelation.

Overall, we have expanded and refined the list of potential kinases that may localize to the mitochondria, and have shown how calcium may affect phosphorylation in isolated mitochondria. Additionally, we have used comparative proteomics to determine phosphorylation sites that are specific to the phosphatase Ptc7. We have also shown that Ptc7 is important for yeast iron metabolism, and that a specific phosphorylation site on Hem15 may regulate iron incorporation into protoporphyrin in the last step of heme biosynthesis.

Results and Discussion

Comparative Proteomic Analyses of Kinases Enriched in Mouse Liver Mitochondria

The goal of this proteomic analysis was to determine the localization of kinases to mitochondrial-enriched fractions of mouse liver. To do this, we performed a kinase capture technique using an activity-based protein profiling (ABPP) approach (Barglow and Cravatt, 2007). ABPP is a functional proteomic technology that uses biotin-coupled affinity probes that react with specific classes of enzymes. In this case, we chose the kinase specific probes offered by ActivX Biosciences termed KiNativ (McAllister et al., 2013; Patricelli et al., 2007). This platform uses acyl phosphates of ATP or ADP that covalently modify conserved lysine residues in the ATP-binding pocket of protein kinases, with minimal off-target effects of other ATP binding proteins (Figure 1A). However, it is important to note that this approach can generally only detect kinases in the active state where their ATP binding pockets are accessible. Therefore, we may actually be underestimating the number kinases in the mitochondria using this method.

To begin, we purified mitochondria to the extent described previously (Grimsrud et al., 2012), using the same mouse conditions as the univariate phase. We reasoned that kinases translocating to the mitochondria would be enriched in the mitochondrial fraction, and depleted in the resulting lysate (Figure 1B). In this experiment, we identified 133 total kinases and at least 21 potentially enriched in the mitochondrial fraction including the catalytic subunit of PKA, the calcium/calmodulin dependent kinase, as well as several mitogen activated kinases (Figure 1B). While there is precedent for each of these kinase classes residing in the mitochondria (Acin-Perez et

al., 2009; Galli et al., 2009; Nishio et al., 2012), this technique allows for a quantitative assessment of dozens of potential mitochondrial kinases in a single experiment.

Given the success of these analyses, we proceeded to analyze the putative kinome of mitochondria isolated from both lean and obese mouse liver (Figure 1C). This experiment enabled us to identify kinases that may be responsible for the changes in phosphorylation and metabolism seen in obesity (Buchner et al., 2009; Grimsrud et al., 2012; Holmstrom et al., 2012). Kinases identified as enriched in obese mitochondria include several MAP kinases as well as Calcium/calmodulin dependent kinases. Combined with the phosphosite consensus sequences identified from the same conditions in our previous work (Grimsrud et al., 2012), knowing which kinases are enriched in obese liver mitochondria can allow us to make hypothesis about kinase-substrate pairs.

One kinase that is of particular interest is the calcium/calmodulin-dependent kinase (CamKII). This kinase was identified in our ABPP study as having increased abundance in obese liver mitochondria compared to lean liver, it was also the second most abundant consensus sequence in our previous study with 126 MitoCarta phosphosites (Grimsrud et al., 2012). The CamKII family of kinases is known to be involved in the formation of memory, in the activation of T cells, and has more recently been shown to be involved in the heart mitochondrial stress response (Joiner et al., 2012; Lin et al., 2005; Silva et al., 1992). While the importance of calcium in the heart is perhaps of no surprise, considering its function as a continuously beating muscle, CamKII expression levels in the liver are similar to that in the heart yet it remains a relatively understudied kinase in the liver.

Treatment of Isolated Liver Mitochondria with Calcium Reveals Changing Phosphorylation Sites

Calcium is known to regulate many aspects of mitochondrial biology, including opening of the PTP, activating beta-oxidation, and increasing ATP production (Gellerich et al., 2010; Otto and Ontko, 1978; Sloan et al., 2012). Unfortunately, with a few exceptions, the mechanism of calcium action in mitochondria is largely unknown. One well-characterized action of calcium in the mitochondria is to allosterically activate pyruvate dehydrogenase phosphatase, which in turn dephosphorylates pyruvate dehydrogenase on S292, thus activating the enzyme (Denton et al., 1972; Roche et al., 2001). Because calcium is known to modulate many mitochondrial pathways, we were first interested in establishing how calcium treatment effects the respiration rate in isolated mitochondria, with the intention of later investigating phosphorylation changes in isolated mitochondria.

When isolated mitochondria were first subjected to treatment with either water or EDTA, they responded to a stress test in the typical manner (Figure 2A). Respiration rates increased with the addition of ADP (state4), rates decreased with the addition of Oligomycin (state3o) and then increased with the addition of FCCP (state4u). This result was consistent when either succinate or glutamate/malate were used as the substrates for OXPHOS. When isolated mitochondria were first treated with calcium (5uM, red dots), the results were significantly different. In rotenone and succinate, the OCR increased dramatically upon the addition of calcium, and before the addition of any other compound. Then, after the addition of ADP, the respiration rate decreased

and was unable to be modified by any other compound. In glutamate and malate (Figure 2B), there was no change in the respiration rate after the addition of calcium, yet these mitochondria were unable to respond as expected to the addition of any other compound. Therefore, the dramatic increase in OCR that is observed is dependent on Complex I being inhibited and Complex II being the entry point for electrons in the respiratory chain.

While there is some evidence for calcium regulating respiration rates in isolated mitochondria, most previous studies have been performed in porcine heart using glutamate and malate as substrates (Hopper et al., 2006). Our results appear to be a liver specific effect, as calcium does not affect mitochondria isolated from murine heart in the same manner in our hands (data not shown). Furthermore, our results are a direct result of the respiratory chain, as administration of Antimycin A, a Complex III inhibitor, blocks the calcium effect of increased oxygen consumption (Figure 2C). Overall, it appears that the increase in respiration that we see is independent of Complex V (OCR increase before addition of ADP) yet dependent on Complex II being engaged (OCR increase only in the presence of succinate and rotenone).

To further characterize the effect of calcium treatment on isolated mitochondria, we measured the rate of calcium uptake into isolated mitochondria using Calcium Green 5N (Molecular Probes). This cell-impermeable probe exhibits an increase in fluorescence emission upon binding with Ca2+. The probe is included in the buffer, and when isolated mitochondria are exposed to a burst of calcium, the probe will briefly fluoresce, and then decrease in fluorescence as the mitochondria take up the calcium (Figure 2D-G). As a control, the calcium uptake inhibitor, Ru360, can be used

to block calcium influx into the isolated mitochondria, and the Calcium Green 5N signal increases with each addition of calcium (Figure 2D).

We were first interested in investigating whether there was a difference in calcium uptake between mitochondria from diverse mouse strains, and indeed, liver mitochondria from the CAST strain took up calcium about 60% more quickly than mitochondria from standard B6 mice (Figure 2E, injection 3). Independent of strain differences, this calcium uptake effect is dependent on oxidative respiration, as treatment with Antimycin A blocks calcium uptake (Figure 2F, red). Furthermore, treatment with rotenone, a Complex I inhibitor, has no effect on the rate of calcium uptake in isolated mitochondria (Figure 2F, blue). Collectively, this data shows that Complex I is likely not involved in the mitochondrial calcium response in liver, yet flux through the respiratory chain is still necessary for both calcium import as well as the increase in oxygen consumption. Finally, to determine the potential influence of phosphatases in this process, we pretreated mitochondria with a phosphatase inhibitor (PhosSTOP, Roche) before treatment and observed a marked increase (30sec) in calcium uptake (Figure 2G, and inset).

Our analysis above provides a more thorough understanding of how calcium import and mitochondrial respiration are closely linked. Given this link, and our discovery of calcium responsive kinases in mitochondrial fractions, we were interested in knowing if calcium treatment alone was sufficient to change the phosphorylation state of proteins in isolated mitochondria. To do this, we treated isolated mitochondria with calcium for 10min, then subjected the isolated mitochondria to the same phosphoproteomics workflow described previously (Grimsrud et al., 2012). As can be

seen in Figure 2H, of the 49 phosphosites identified, 13 of them were mitochondrial, including sites on the enzymatic proteins: Cps1, Acly, and Hmgcs2, as well as proteins involved in signal transduction (Akap1) and microtubule dynamics (Fam82a2). Taken together, these data show that mitochondrial phosphorylation can be rapidly modulated by a physiologically relevant stimulus, and combined with our activity based protein profiling, suggests that specific kinases may reside in the mitochondria.

Proteomic Analysis of Mitochondrial Phosphatases in S. cerevisiae

While our ABPP approach suggested kinases that are active and may reside in the mitochondria, our treatment of isolated mitochondria with calcium indicated that phosphatases might also be an important regulator of mitochondrial phosphorylation events. We were interested in learning more about mitochondrial phosphatases, specifically the phosphatase PPTC7.

PPTC7 is a type 2C protein phosphatase that is conserved from mammals to yeast, and has been shown to be an active phosphatase against a generic phosphatase substrate pNPP (Figure 3A). PPTC7, and its yeast homolog, Ptc7, have both been shown to localize to the mitochondria in their respective species. In yeast, Ptc7 belongs to a family of mitochondrial Type 2C phosphatases, which include Ptc5 and Ptc6 (Zhao et al., 2012). While Ptc5 and Ptc6 have proposed substrates, the specific substrates of Ptc7 are still largely unknown (Gey et al., 2008). Ptc7 is a relatively unique protein in yeast in that it undergoes an alternative splicing event, with the unspliced protein localizing to the nuclear envelope and the spliced isoform localizing to the mitochondria (Juneau et al., 2009). While the submitochondrial

localization of yeast Ptc7 has yet to be definitively identified, a predicted homolog in *Arabidopsis* (PBCP) has been shown to dephosphorylate photosystem II proteins, implying that Ptc7 is likely localized to the matrix (Samol et al., 2012). Furthermore, the mammalian homologue of Ptc7, PPTC7, has been identified in the mitochondrial matrix in a high-throughput, proteomic mapping technique using spatially restricted enzymatic tagging (Rhee et al., 2013).

Using the existence of the homologues of Ptc7—Ptc5 and Ptc6—we were able to design a proteomics experiment to identify the endogenous targets of the mitochondrial phosphatase. Because signaling by phosphorylation is a complex process, and deletion of a phosphatase could trigger off-target phosphorylation events, we tested deletion of all three related mitochondrial phosphatases in an attempt to discover *bona fide* Ptc7 targets. We grew yeast through the diauxic shift, a natural metabolic cycle that yeast undergo when grown in liquid culture. As yeast cells exhaust their fermentable carbon supply, they enter what is known as the diauxic shift, the portion of yeast growth categorized by a switch from fermentative to oxidative metabolism (DeRisi et al., 1997; Zaman et al., 2008). During this shift, mitochondrial biogenesis is initiated, and Ptc7 splicing switches from the nuclear envelope-bound isoform to the mitochondrial isoform (Figure 3C, D).

Here, we used isobaric tagging and quantitative phosphoproteomics to identify phosphorylation sites that were changing between wild type (WT) yeast and deletion strains of Ptc5, Ptc6, and Ptc7 (Figure 3E). Samples were taken 17 hours after the dilution of yeast into media containing 2% glucose, to ensure maximal induction of mitochondrial biogenesis as well as Ptc7 splicing (Figure 3C,D). Using this

methodology, we identified 2562 phosphorylation sites on 1116 proteins, including 145 mitochondrial proteins and 297 mitochondrial phosphorylation sites. When changes occurring due to Ptc5 deletion are plotted against changes due to Ptc7 deletion, a relatively strong correlation is seen (R^2=0.73, Figure 3E). This could indicate an overlap in the phosphorylation sites that are shared or redundant between these two phosphatases. When Ptc7 deletion is compared to Ptc6 deletion (Figure 3F), no correlation is seen, supporting the idea that these phosphatases have entirely different substrate preferences. Using this correlation pattern, we were able to examine a group of phosphorylation sites that were significantly increasing in a Ptc7Δ, but saw no change when Ptc5 was deleted, indicating that these sites may be specific for Ptc7 (Figure 3G, inset highlighted in Figure 3E). A few of the potential Ptc7 targets included: Aco1, the yeast mitochondrial aconitase, Hsp60, a chaperone required for complex assembly, and Yml6, a member of the large subunit of the mitochondrial ribosome.

In parallel, we also performed quantitative proteomics and phosphoproteomics on multiple replicates of only WT and Ptc7Δ yeast strains. This was because our previous work had highlighted the importance of using replicates and statistical analysis in the comparison of phosphorylation events (Grimsrud et al., 2012). From this data combined with our previous analysis, we identified 70 phosphorylation events on 56 unique proteins that are statically significant ($P<0.01$), highly upregulated (fold change >1.5), and on proteins localized to the mitochondria (Figure 4A). These phosphosites constitute our primary candidate Ptc7 substrates.

Iron Metabolism Dysruption and Oxidative Stress in ptc7Δ yeast

Our list of potential Ptc7 substrates was large, so in an attempt to prioritize candidate phosphosubstrates from the list we generated, we examined the global protein profile of this strain compared to WT yeast to determine if any cellular processes or pathways were altered. Analysis of the ptc7Δ yeast proteome showed very interesting changes in total protein expression relative to wild type yeast - of the top 15 most downregulated proteins, four are involved in intracellular iron transport (Figure 4B). When the 15 previously mentioned proteins were subjected to GO term enrichment analysis, iron transport was highlighted as highly significant in this subset of proteins (Figure 4C, top). Furthermore, the most upregulated proteins in PTC7Δ yeast include a variety of proteins involved in the response to oxidative stress, such as catalase (Ctt1, Figure 4B), resulting in a proteomic signature enriched in oxidative stress functions via GO analysis (Figure 4C, bottom). These data led us to hypothesize that Ptc7-null yeast would have altered sensitivity to iron chelation and oxidative stressing agents. To test this, we plated yeast in 10-fold serial dilutions onto media containing the iron chelator, dipyridine, and the oxidant, H_2O_2. Interestingly, PTC7Δ yeast are resistant to iron chelation (Figure 4D) as well as H_2O_2-induced oxidative stress (Figure 4E), indicating a dysregulation in the pathways required for these processes in wild type cells. Importantly, of the phosphosites we identified, 7 are on proteins that have been previously linked to oxidative stress responses, while 3 proteins are linked to maintenance of iron homeostasis (Figure 4F). Collectively, these data suggest that the inactivation of Ptc7 leads to dysfunctional iron and oxidative

stress responses, which could be mediated through the phosphorylation of these ten phosphosites.

To determine whether these phenotypes were specific to Ptc7Δ yeast, we tested deletion strains for the two other mitochondrial phosphatases, Ptc5 and Ptc6, for sensitivity to iron chelation and oxidative stress. To do this, we grew cultures of yeast in a 96-well plate and monitored their growth overnight using OD600 in an automated plate reader (Biotek). Surprisingly, we found that the Ptc5Δ yeast have a nearly identical response to dipyridine (DP, Figure 4G) and hydrogen peroxide (H_2O_2, Figure 4H) as Ptc7Δ yeast. By contrast, Ptc6Δ yeast were susceptible to both stimuli. This is particularly interesting, as both Ptc5 and Ptc6 have been previously identified as semi-redundant regulators of the pyruvate dehydrogenase (PDH) complex as mentioned earlier (Gey et al., 2008; Krause-Buchholz et al., 2006). Our phenotypic data combined with our previous phosphoproteomic data suggest that Ptc5 and Ptc7 together may regulate similar mitochondrial processes, while Ptc6 likely has a separate and distinct role in mitochondrial functioning. Nevertheless, while Ptc7 and Ptc5 may have some phenotypical redundancies, our analysis of the phosphoproteome of these strains allows us to determine phosphorylation sites that are likely to be distinct to Ptc7.

Phosphorylation of S102 on Hem15 Disrupts Protein Function

The combination of our quantitative proteomics data along with treatment of yeast with an iron chelator allowed us to predict which phosphorylation events linked to the phosphatase Ptc7 might regulate specific mitochondrial proteins. One of the phosphorylation sites that had the most specificity to Ptc7 compared to the other

phosphatases was Hem15 (Figure 5C). Hem15 also had one of the most significantly changing phosphorylation sites when multiple replicates of Ptc7Δ yeast were analyzed. (Figure 5D). This enzyme catalyzes the final step in heme biosynthesis, where ferrous iron is inserted into protoporphyrin IX to form protoheme IX. In humans, deficiency in the Hem15 homologue, ferrochelatase (FECH), causes protoporphyria, a disease characterized by liver cirrhosis and hepatic failure (Bonkowsky et al., 1975; Brenner et al., 1992). While having little total conservation at the primary sequence level (<10%), Hem15 remains highly conserved in a loop region between alpha helix 3 and 4, an area that contains S102 (Wu et al., 2001). As highlighted in Figure 5A, S102 on Hem15 also falls within a proline directed phosphorylation motif (xxsP), a motif we have previously shown to be overrepresented on mitochondrial phosphoproteins (Grimsrud et al., 2012). Finally, we hypothesize that phosphorylation of this serine will decrease enzyme activity, as this serine is involved in coordinating the protoporphyrin ring (Figure 5B, (Karlberg et al., 2002; Medlock et al., 2007), and the addition of a large, negatively charged phosphate moiety would likely disrupt binding.

To evaluate the effects of this phosphorylation site on Hem15 enzymatic activity, we performed biochemical activity assays on modified Hem15 protein. Using site-directed mutagenesis, we mutated the phosphorylated residue to an acidic residue (glutamic acid) to mimic phosphorylation. We immunoprecipitated this mutant, along with wild-type and catalytically inactive (H236A) Hem15 from yeast and tested the activity of each variant in an *in vitro* enzymatic assay (Taketani, 2001). As seen in Figure 5 E and F, the phosphomimetic for S102 resulted in an approximately 70% decrease in enzyme activity while still retaining increased catalytic activity compared to the

enzymatically dead variant. Taken together, these data suggest that Hem15 is a target of the mitochondrial phosphatase Ptc7, and phosphorylation of Hem15 can affect enzyme activity and, by extension, iron content and heme biosynthesis in yeast.

Conclusions

Here, we have established a quantitative proteomic survey of the enzymes that modulate mitochondrial phosphorylation – kinases and phosphatases. Our measurements enable the examination of phosphorylation events that may be linked to specific kinases and phosphatases that are important to mitochondrial homeostasis and modification. Beginning with an activity based protein-profiling methodology; we were able to identify kinases that are enriched in the mitochondrial fraction of mouse liver. While the existence of a kinase-based phosphorylation system inside the mitochondria has been debated (Covian and Balaban, 2012), this analysis provides support for the hypothesis that kinases at least transiently migrate to the mitochondria. Our large-scale approach also generated a detailed enrichment profile of approximately 130 kinases both between the mitochondria and the rest of the cell, and between mitochondria from lean and obese mice.

While our ABPP investigation provides an important first step in understanding the localization of kinases to mitochondria in both lean and obese states, much work still needs to be accomplished. Moving forward, it will be interesting to apply this methodology to the multiple conditions for which we have previously measured phosphorylation patterns. As kinases are widely considered ‘druggable’ targets, it may be possible to inactivate a kinase only at certain timepoints or in certain metabolic states in order to achieve a desired clinical outcome (Tarrant and Cole, 2009). Using an ABPP based method to understand kinases that are more enriched (or more active) in the mitochondria during specific metabolic states will allow us to generate hypothesis about what kinases could be inactivated therapeutically.

In addition, we have used the results of our ABPP method and our previous knowledge of the importance of calcium to mitochondrial function in both the heart and skeletal muscle allowed us to make new observations about calcium in the liver. Consistent with other reports (Balaban, 2009; Gellerich et al., 2010), our data show that the oxidative phosphorylation cascade in the liver is also modulated by calcium levels, and that respiration is necessary for calcium uptake into the mitochondria. While the mechanism of this modulation has yet to be determined, it is likely not the direct binding of calcium to respiratory chain components, and others have suggested that post-translational modifications may be the cause (Bender and Kadenbach, 2000; Glancy et al., 2013; Panov and Scaduto, 1995). By treating isolated mitochondria with calcium, we have shown that there are several phosphorylation events that seem to respond to calcium concentrations. This will be important to investigate more rigorously, as our initial experiment utilized only crude mitochondrial extracts and the proteomic coverage was low. Future experiments should utilize Percoll gradients in order to achieve maximally pure mitochondria, and Ru360 would be an ideal control, as calcium import into the mitochondria would be entirely blocked. Finally, there have been some recent advances in small molecules that can modulate mitochondrial function and in understanding of the calcium induced opening of the permeability transition pore (Gohil et al., 2010; Roy et al., 2009). If it were possible to increase the amount of calcium that could be imported into the mitochondria before the opening of the permeability transition pore, then it may be possible to find phosphorylation sites with maximal occupancy.

While the existence and localization of mitochondrial phosphatases is not in

question, the specific targets of the phosphatase Ptc7 had not been discovered. Although Ptc7 has been suggested to be involved in Coenzyme Q biosynthesis (Martin-Montalvo et al., 2013), its complete role in the regulation of mitochondrial phosphorylation has yet to be elucidated. Our work has shown that Ptc7 is involved in both maintaining iron homeostasis and in the response to oxidative stress. Furthermore, our use of a comparative proteomics strategy to differentiate between the three mitochondrial phosphatases in yeast has allowed us to identify phosphorylation sites that are likely direct substrates of Ptc7. We have also been able to determine that in contrast to previously published reports; Ptc6 is likely the sole pyruvate dehydrogenase phosphatase in yeast, while Ptc5, although still retaining distinct targets, is conceivably regulating similar mitochondrial processes to Ptc7.

Moving forward, it will also be interesting to see the acute effects of the loss of Ptc7 on mitochondrial metabolism in yeast. Our work on mouse liver has shown acute and chronic effects can both be important when considering phosphorylation networks, and because phosphorylation is generally considered a rapid response it may be important to investigate acute inactivation of Ptc7. One caveat of our yeast experiments is that the yeast deletion library from which our strains were obtained is a permanent knock-out of Ptc7 (Winzeler et al., 1999). This could obscure the direct targets of Ptc7 and only reveal adaptive phosphorylation events rather than direct ones. It would be interesting to repeat a portion of this analysis with a method that allows for rapid and inducible inactivation of a gene such as a Cre-Lox system or a temperature sensitive mutant (Cheng et al., 2000; Li et al., 2011).

Finally, while this resource provides valuable information on the phosphorylation

of serine and threonine targets, other phosphorylation sites remain difficult to detect, such as those containing labile histidine phosphorylation (Grimsrud et al., 2010b). Fortunately, recent advancements have been made in this area (Kee and Muir, 2012; Kee et al., 2013; McAlister et al., 2012), and it will be important to understand if histidine phosphorylation has a similar dynamic phosphorylation pattern. Overall, we have begun to elucidate the signaling networks that control mitochondrial function, and this resource continues to refine the signaling molecules that could be targeted therapeutically to treat mitochondrial dysfunction.

Experimental Procedures

Animal Models

Breeding, sacrificing, and tissue harvesting of mice from our in-house colonies at the University of Wisconsin Biochemistry Department was described previously (Grimsrud et al., 2012). Briefly, all mice were male, bred and housed in an environmentally controlled facility on a 12-h light/dark cycle (6 am–6 pm, respectively). Mice were provided free access to water at all times and to a standard rodent chow (Purina no. 5008) ad libitum after which they were sacrificed by CO2 asphyxiation followed by cervical dislocation. Liver tissue was dissected, flash frozen with liquid N2, and stored at -80°C until use, except for respiratory rate measurements and calcium uptake measurements, for which fresh liver was used. The University of Wisconsin Animal Care and Use Committee approved all procedures.

Respiratory Rate Measurements

Mitochondria were isolated using differential centrifugation in MSHE buffer with 1% BSA. After isolation, mitochondria were quantified by wet weight using an analytical scale and resuspended to 100ug/uL in assay buffer (MAS). Mitochondria were then diluted to 2ug/uL in MAS buffer supplemented with either glutamate/malate or rotenone/succinate, and 40ug of mitochondria were added to each well of a XF96 assay plate (Seahorse Biosciences). After a 20min spin at 4°C to adhere mitochondria to the bottom of each well, MAS buffer with substrate (G/M, R/S) was added to bring the volume in each well to 120uL. Respiration rates were measured on an XF96, with a 3 min read contributing to each individual respiration rate (1-10). Four injections were

administered over the course of the experiment, the first injection contained either Calcium (red) EDTA (gray) or Water (black), followed by injections of ADP, Oligomycin and FCCP.

Calcium Uptake

Mitochondria were isolated from mouse liver using differential centrifugation as described above. After isolation, mitochondria were resuspended in calcium assay buffer: 140mM KCl, 10mM HEPES pH 7.4, 2.5mM MgCl2, 3mM KH2PO4, 5mM Succinate, 5mM Glutamate, 5mM Malate, 50uM EGTA, 100nM Calcium Green 5N (Molecular Probes). Using a plate reader equipped with injector ports (BioTek) mitochondria were resuspended to 1mg/mL in calcium assay buffer in a 96 well plate. Samples were treated with a variety of compounds for different measurements: Ru360, which blocks calcium uptake, and Antimycin A, which blocks electron transfer from Complex III. 50uM CaCl2 was injected every 2 minutes and in between injections, intensity was detected with an excitation/emission of 480/540.

Activity Based Protein Profiling

Following sample preparation, the KiNativ probe is added to the lysate (at 5 μM) and the reaction is allowed to proceed for10 minutes. Samples are then subjected to a typical proteomics workup including denaturation, reduction, alkylation and trypsin digestion, followed by enrichment of biotinylated peptides with streptavidin resin. The eluted probe-modified peptides are then analyzed using customized time-segmented LC-MS/MS protocols on a linear ion trap mass spectrometer. The MS protocols are

designed based on known m/z and elution time parameters for probe-kinase peptide pairs using standardized LC gradients. Data is analyzed using customized software based on a “reference spectrum” concept whereby experimental fragment spectra are compared to archived high quality reference spectra (from historical data) and where a spectral match is found, signals are extracted based on fragment (MS/MS) ions showing clean chromatographic peaks. Control sample coefficient of variation (CV) values with these methods are typically ~15% averaged across all kinases.

Proteomics Sample Preparation

Proteins from yeast were extracted using previous methods also with the use of LysC and trypsin to digest all samples (Grimsrud et al., 2010a). Peptides for each preparation were labeled with a unique 6-plex TMT label (Thermo). . Peptides were separated by strong cation exchange chromatography (SCX), and after aliquots were removed for unmodified peptide quantitation, immobilized metal affinity chromatography (IMAC) was performed on each fraction to enrich for phosphopeptides as described (Phanstiel et al., 2011).

Tandem MS Data Collection and Analysis

Phosphorylated and unmodified peptides were analyzed by nano reverse phase liquid chromatography coupled to an Orbitrap Elite (Thermo). A survey MS^1 scan was performed by Orbitrap at 30,000 resolving power and followed by data-dependent top 10 MS^2 analyses. Samples were also fragmented using the HCD method (Olsen et al., 2007) for all analyses. Tandem MS data was searched with OMSAA (Geer et al.,

2004)against a concatenated target-decoy UniProt database consisting of yeast proteins (Elias and Gygi, 2007). Our custom software COMPASS (Wenger et al., 2011) was then utilized to filter the resulting peptide identifications to 1% FDR, normalize iTRAQ reporter ion intensities for all peptide spectral matches (PSMs) across each replicate separately, group peptides from all replicates to common parsimonious protein groups at 1% FDR, localize phosphorylation sites to specific residues at 95% probability, and sum the reporter ion intensities of all PSMs for all unique proteins and protein phosphorylation sites identified in individual replicates.

Proteomics Statistical Analysis

Microsoft Excel were utilized for statistical analysis of protein and site-specific phosphorylation measurements. We evaluated the significance of a given protein, phosphoisoform, or normalized phosphoisoform change by computing p-values, and assuming a log-normal distribution for measurement error.

Yeast Growth Curves

Yeast were grown overnight in YEP media supplemented with 2% glucose on a rotating incubator drum. The next day yeast were diluted to 1x10E5 cells per 100uL and transferred to a 96-well plate. Yeast were assessed for growth via OD600 over a 16hr time period in YEP media with .5% glucose and 3% glycerol to determine the ability of the yeast to grow through the diauxic shift.

Biochemical Assessment of Hem15 Regulation

Yeast BY4741 cells were transfected with plasmids containing HEM15 tagged with the HA epitope tag using the Funk yeast expression system (Mumberg et al., 1995). Site-directed mutagenesis to create Hem15 variants was performed using standard PCR-based cloning techniques and all constructs were verified by DNA sequencing. Tagged Hem15 was purified and its activity asses as described previously (Taketani, 1993; 2001). Briefly, when a zinc ion is used as a metal substrate, the enzyme reaction can be detected using a substitute metal acceptor, mesoporphyrin, which fluoresces only when zinc is assembled into the ring with an excitation/emission spectra of 410/580. Zinc acetate is injected into a solution containing purified enzyme and mesoporphyrin, the reaction is allowed to proceed for 15min while detection takes place on a plate reader equipped with the proper fluorescence detection (BioTek). The rate of reaction is calculated using a standard curve of purchased zinc-mesoporphyrin.

References

Acin-Perez, R., Salazar, E., Kamenetsky, M., Buck, J., Levin, L.R., and Manfredi, G. (2009). Cyclic AMP Produced inside Mitochondria Regulates Oxidative Phosphorylation. Cell Metabolism *9*, 265–276.

Balaban, R.S. (2009). The role of Ca2+ signaling in the coordination of mitochondrial ATP production with cardiac work. BBA - Bioenergetics *1787*, 1334–1341.

Barglow, K.T., and Cravatt, B.F. (2007). Activity-based protein profiling for the functional annotation of enzymes. Nat Meth *4*, 822–827.

Bender, E., and Kadenbach, B. (2000). The allosteric ATP-inhibition of cytochrome c oxidase activity is reversibly switched on by cAMP-dependent phosphorylation. FEBS Letters *466*, 130–134.

Bonkowsky, H.L., Bloomer, J.R., Ebert, P.S., and Mahoney, M.J. (1975). Heme synthetase deficiency in human protoporphyria. Demonstration of the defect in liver and cultured skin fibroblasts. J. Clin. Invest. *56*, 1139–1148.

Brenner, D.A., Didier, J.M., Frasier, F., Christensen, S.R., Evans, G.A., and Dailey, H.A. (1992). A molecular defect in human protoporphyria. Am. J. Hum. Genet. *50*, 1203–1210.

Buchner, D.A., Yazbek, S.N., Solinas, P., Burrage, L.C., Morgan, M.G., Hoppel, C.L., and Nadeau, J.H. (2009). Increased Mitochondrial Oxidative Phosphorylation in the Liver Is Associated With Obesity and Insulin Resistance. Nature *19*, 917–924.

Calvo, S.E., and Mootha, V.K. (2010). The mitochondrial proteome and human disease. Annu Rev Genomics Hum Genet *11*, 25–44.

Cheng, T.H., Chang, C.R., Joy, P., Yablok, S., and Gartenberg, M.R. (2000). Controlling gene expression in yeast by inducible site-specific recombination. Nucleic Acids Research *28*, E108.

Covian, R., and Balaban, R.S. (2012). Cardiac mitochondrial matrix and respiratory complex protein phosphorylation. AJP: Heart and Circulatory Physiology *303*, H940–H966.

Cravatt, B.F., Wright, A.T., and Kozarich, J.W. (2008). Activity-Based Protein Profiling: From Enzyme Chemistry to Proteomic Chemistry. Annu. Rev. Biochem. *77*, 383–414.

Denton, R.M., Randle, P.J., and Martin, B.R. (1972). Stimulation by calcium ions of pyruvate dehydrogenase phosphate phosphatase. Biochem. J. *128*, 161–163.

DeRisi, J.L., Iyer, V.R., and Brown, P.O. (1997). Exploring the metabolic and genetic control of gene expression on a genomic scale. Science *278*, 680–686.

Elias, J.E., and Gygi, S.P. (2007). Target-decoy search strategy for increased confidence in large-scale protein identifications by mass spectrometry. Nat Meth *4*, 207–214.

Forner, F., Foster, L.J., Campanaro, S., Valle, G., and Mann, M. (2006). Quantitative proteomic comparison of rat mitochondria from muscle, heart, and liver. Mol. Cell Proteomics *5*, 608–619.

Galli, S., Jahn, O., Hitt, R., Hesse, D., Opitz, L., Plessmann, U., Urlaub, H., Poderoso, J.J., Jares-Erijman, E.A., and Jovin, T.M. (2009). A New Paradigm for MAPK: Structural Interactions of hERK1 with Mitochondria in HeLa Cells. PLoS ONE *4*, e7541.

Geer, L.Y., Markey, S.P., Kowalak, J.A., Wagner, L., Xu, M., Maynard, D.M., Yang, X., Shi, W., and Bryant, S.H. (2004). Open mass spectrometry search algorithm. J. Proteome Res. *3*, 958–964.

Gellerich, F.N., Gizatullina, Z., Trumbeckaite, S., Nguyen, H.P., Pallas, T., Arandarcikaite, O., Vielhaber, S., Seppet, E., and Striggow, F. (2010). The regulation of OXPHOS by extramitochondrial calcium. Biochim. Biophys. Acta *1797*, 1018–1027.

Gey, U., Czupalla, C., Hoflack, B., Rödel, G., and Krause-Buchholz, U. (2008). Yeast pyruvate dehydrogenase complex is regulated by a concerted activity of two kinases and two phosphatases. The Journal of Biological Chemistry *283*, 9759–9767.

Glancy, B., Willis, W.T., Chess, D.J., and Balaban, R.S. (2013). Effect of Calcium on the Oxidative Phosphorylation Cascade in Skeletal Muscle Mitochondria. Biochemistry *52*, 2793–2809.

Gohil, V.M., Sheth, S.A., Nilsson, R., Wojtovich, A.P., Lee, J.H., Perocchi, F., Chen, W., Clish, C.B., Ayata, C., Brookes, P.S., et al. (2010). Nutrient-sensitized screening for drugs that shift energy metabolism from mitochondrial respiration to glycolysis. Nature Biotechnology *28*, 249–255.

Grimsrud, P.A., Os, den, D., Wenger, C.D., Swaney, D.L., Schwartz, D., Sussman, M.R., Ane, J.M., and Coon, J.J. (2010a). Large-Scale Phosphoprotein Analysis in Medicago truncatula Roots Provides Insight into in Vivo Kinase Activity in Legumes. Plant Physiol. *152*, 19–28.

Grimsrud, P.A., Carson, J.J., Hebert, A.S., Hubler, S.L., Niemi, N.M., Bailey, D.J., Jochem, A., Stapleton, D.S., Keller, M.P., Westphall, M.S., et al. (2012). A quantitative map of the liver mitochondrial phosphoproteome reveals posttranslational control of ketogenesis. Cell Metabolism *16*, 672–683.

Grimsrud, P.A., Swaney, D.L., Wenger, C.D., Beauchene, N.A., and Coon, J.J. (2010b). Phosphoproteomics for the Masses. ACS Chem. Biol. *5*, 105–119.

Holmstrom, M.H., Iglesias-Gutierrez, E., Zierath, J.R., and Garcia-Roves, P.M. (2012). Tissue-specific control of mitochondrial respiration in obesity-related insulin resistance and diabetes. AJP: Endocrinology and Metabolism *302*, E731–E739.

Hopper, R.K., Carroll, S., Aponte, A.M., Johnson, D.T., French, S., Shen, R.-F., Witzmann, F.A., Harris, R.A., and Balaban, R.S. (2006). Mitochondrial Matrix Phosphoproteome: Effect of Extra Mitochondrial Calcium †. Biochemistry *45*, 2524–2536.

Huh, W.-K., Falvo, J.V., Gerke, L.C., Carroll, A.S., Howson, R.W., Weissman, J.S., and O'Shea, E.K. (2003). Global analysis of protein localization in budding yeast. Nature *425*, 686–691.

Joiner, M.-L.A., Koval, O.M., Li, J., He, B.J., Allamargot, C., Gao, Z., Luczak, E.D., Hall, D.D., Fink, B.D., Chen, B., et al. (2012). CaMKII determines mitochondrial stress responses in heart. Nature *491*, 269–273.

Juneau, K., Nislow, C., and Davis, R.W. (2009). Alternative Splicing of PTC7 in Saccharomyces cerevisiae Determines Protein Localization. Genetics *183*, 185–194.

Karlberg, T., Lecerof, D., Góra, M., Silvegren, G., Labbe-Bois, R., Hansson, M., and Al-Karadaghi, S. (2002). Metal binding to Saccharomyces cerevisiae ferrochelatase. Biochemistry *41*, 13499–13506.

Kee, J.-M., and Muir, T.W. (2012). Chasing Phosphohistidine, an Elusive Sibling in the Phosphoamino Acid Family. ACS Chem. Biol. *7*, 44–51.

Kee, J.-M., Oslund, R.C., Perlman, D.H., and Muir, T.W. (2013). a pan-specific antibody for direct detection of protein histidine phosphorylation. Nature Chemical Biology *9*, 416–421.

Kobe, B., and Kemp, B.E. (1999). Active site-directed protein regulation. Nature *402*, 373–376.

Krause-Buchholz, U., Gey, U., Wünschmann, J., Becker, S., and Rödel, G. (2006). YIL042c and YOR090c encode the kinase and phosphatase of the Saccharomyces cerevisiae pyruvate dehydrogenase complex. FEBS Letters *580*, 2553–2560.

Li, Z., Vizeacoumar, F.J., Bahr, S., Li, J., Warringer, J., Vizeacoumar, F.S., Min, R., VanderSluis, B., Bellay, J., DeVit, M., et al. (2011). Systematic exploration of essential yeast gene function with temperature-sensitive mutants. Nature Biotechnology *29*, 361–367.

Lin, M.Y., Zal, T., Ch'en, I.L., Gascoigne, N.R.J., and Hedrick, S.M. (2005). A pivotal role for the multifunctional calcium/calmodulin-dependent protein kinase II in T cells: from activation to unresponsiveness. J. Immunol. *174*, 5583–5592.

Manning, G., Whyte, D.B., Martinez, R., Hunter, T., and Sudarsanam, S. (2002). The protein kinase complement of the human genome. Science *298*, 1912–1934.

Martin-Montalvo, A., Gonzalez-Mariscal, I., Pomares-Viciana, T., Padilla-Lopez, S., Ballesteros, M., Vazquez-Fonseca, L., Gandolfo, P., Brautigan, D.L., Navas, P., and Santos-Ocana, C. (2013). The Phosphatase Ptc7 Induces Coenzyme Q Biosynthesis by Activating the Hydroxylase Coq7 in Yeast. Journal of Biological Chemistry *288*, 28126–28137.

McAlister, G.C., Russell, J.D., Rumachik, N.G., Hebert, A.S., Syka, J.E., Geer, L.Y., Westphall, M.S., Pagliarini, D.J., and Coon, J.J. (2012). Analysis of the acidic proteome with negative electron-transfer dissociation mass spectrometry. Anal. Chem. *84*, 2875–2882.

McAllister, F.E., Niepel, M., Haas, W., Huttlin, E., Sorger, P.K., and Gygi, S.P. (2013). Mass Spectrometry Based Method to Increase Throughput for Kinome Analyses Using ATP Probes. Anal. Chem. *85*, 4666–4674.

Medlock, A., Swartz, L., Dailey, T.A., Dailey, H.A., and Lanzilotta, W.N. (2007). Substrate interactions with human ferrochelatase. Proc. Natl. Acad. Sci. U.S.a. *104*, 1789–1793.

Mumberg, D., Müller, R., and Funk, M. (1995). Yeast vectors for the controlled expression of heterologous proteins in different genetic backgrounds. Gene *156*, 119–122.

Newgard, C.B., and Sharpless, N.E. (2013). Coming of age: molecular drivers of aging and therapeutic opportunities. J. Clin. Invest. *123*, 946–950.

Nishio, S., Teshima, Y., Takahashi, N., Thuc, L.C., Saito, S., Fukui, A., Kume, O., Fukunaga, N., Hara, M., Nakagawa, M., et al. (2012). Activation of CaMKII as a key regulator of reactive oxygen species production in diabetic rat heart. Journal of Molecular and Cellular Cardiology *52*, 1103–1111.

Olsen, J.V., Macek, B., Lange, O., Makarov, A., Horning, S., and Mann, M. (2007). Higher-energy C-trap dissociation for peptide modification analysis. Nat Meth *4*, 709–712.

Otto, D.A., and Ontko, J.A. (1978). Activation of mitochondrial fatty acid oxidation by calcium. Conversion to the energized state. The Journal of Biological Chemistry *253*, 789–799.

Pagliarini, D.J., and Dixon, J.E. (2006). Mitochondrial modulation: reversible phosphorylation takes center stage? Trends in Biochemical Sciences *31*, 26–34.

Pagliarini, D.J., Calvo, S.E., Chang, B., Sheth, S.A., Vafai, S.B., Ong, S.-E., Walford, G.A., Sugiana, C., Boneh, A., and Chen, W.K. (2008). A Mitochondrial Protein Compendium Elucidates Complex I Disease Biology. *134*, 112–123.

Panov, A.V., and Scaduto, R.C. (1995). Influence of calcium on NADH and succinate oxidation by rat heart submitochondrial particles. Archives of Biochemistry and Biophysics *316*, 815–820.

Patricelli, M.P., Szardenings, A.K., Liyanage, M., Nomanbhoy, T.K., Wu, M., Weissig, H., Aban, A., Chun, D., Tanner, S., and Kozarich, J.W. (2007). Functional Interrogation of the Kinome Using Nucleotide Acyl Phosphates. Biochemistry *46*, 350–358.

Phanstiel, D.H., Brumbaugh, J., Wenger, C.D., Tian, S., Probasco, M.D., Bailey, D.J., Swaney, D.L., Tervo, M.A., Bolin, J.M., Ruotti, V., et al. (2011). Proteomic and phosphoproteomic comparison of human ES and iPS cells. Nat Meth 1–10.

Picotti, P., Bodenmiller, B., Mueller, L.N., Domon, B., and Aebersold, R. (2009). Full dynamic range proteome analysis of S. cerevisiae by targeted proteomics. Cell *138*, 795–806.

Rhee, H.-W., Zou, P., Udeshi, N.D., Martell, J.D., Mootha, V.K., Carr, S.A., and Ting, A.Y. (2013). Proteomic mapping of mitochondria in living cells via spatially restricted enzymatic tagging. Science *339*, 1328–1331.

Roche, T.E., Baker, J.C., Yan, X., Hiromasa, Y., Gong, X., Peng, T., Dong, J., Turkan, A., and Kasten, S.A. (2001). Distinct regulatory properties of pyruvate dehydrogenase kinase and phosphatase isoforms. Prog. Nucleic Acid Res. Mol. Biol. *70*, 33–75.

Roy, S.S., Madesh, M., Davies, E., Antonsson, B., Danial, N., and Hajnóczky, G. (2009). Bad Targets the Permeability Transition Pore Independent of Bax or Bak to Switch between Ca2+-Dependent Cell Survival and Death. Mol. Cell *33*, 377–388.

Samol, I., Shapiguzov, A., Ingelsson, B., Fucile, G., Crevecoeur, M., Vener, A.V., Rochaix, J.D., and Goldschmidt-Clermont, M. (2012). Identification of a Photosystem II Phosphatase Involved in Light Acclimation in Arabidopsis. The Plant Cell *24*, 2596–2609.

Shi, Y. (2009). Serine/threonine phosphatases: mechanism through structure. Cell *139*, 468–484.

Shokat, K.M. (1995). Tyrosine kinases: modular signaling enzymes with tunable specificities. Chemistry & Biology *2*, 509–514.

Silva, A.J., Stevens, C.F., Tonegawa, S., and Wang, Y. (1992). Deficient hippocampal long-term potentiation in alpha-calcium-calmodulin kinase II mutant mice. Science *257*, 201–206.

Sloan, R.C., Moukdar, F., Frasier, C.R., Patel, H.D., Bostian, P.A., Lust, R.M., and Brown, D.A. (2012). Mitochondrial permeability transition in the diabetic heart: Contributions of thiol redox state and mitochondrial calcium to augmented reperfusion injury. Journal of Molecular and Cellular Cardiology *52*, 1009–1018.

Szendroedi, J., Phielix, E., and Roden, M. (2011). The role of mitochondria in insulin resistance and type 2 diabetes mellitus. Nature Reviews Endocrinology.

Taketani, S. (1993). Molecular and genetic characterization of ferrochelatase. Tohoku J. Exp. Med. *171*, 1–20.

Taketani, S. (2001). Measurement of ferrochelatase activity. Curr Protoc Toxicol *Chapter 8*, Unit8.7.

Tarrant, M.K., and Cole, P.A. (2009). The Chemical Biology of Protein Phosphorylation. Annu. Rev. Biochem. *78*, 797–825.

Thompson, A., Schäfer, J., Kuhn, K., Kienle, S., Schwarz, J., Schmidt, G., Neumann, T., Johnstone, R., Mohammed, A.K.A., and Hamon, C. (2003). Tandem Mass Tags: A Novel Quantification Strategy for Comparative Analysis of Complex Protein Mixtures by MS/MS. Anal. Chem. *75*, 1895–1904.

Wallace, D.C. (2005). A mitochondrial paradigm of metabolic and degenerative diseases, aging, and cancer: a dawn for evolutionary medicine. Annu. Rev. Genet. *39*, 359–407.

Wang, Q., Zhang, Y., Yang, C., Xiong, H., Lin, Y., Yao, J., Li, H., Xie, L., Zhao, W., Yao, Y., et al. (2010). Acetylation of Metabolic Enzymes Coordinates Carbon Source Utilization and Metabolic Flux. Science *327*, 1004–1007.

Wenger, C.D., Phanstiel, D.H., Lee, M.V., Bailey, D.J., and Coon, J.J. (2011). COMPASS: a suite of pre- and post-search proteomics software tools for OMSSA. Proteomics *11*, 1064–1074.

Winzeler, E.A., Shoemaker, D.D., Astromoff, A., Liang, H., Anderson, K., Andre, B., Bangham, R., Benito, R., Boeke, J.D., Bussey, H., et al. (1999). Functional characterization of the S. cerevisiae genome by gene deletion and parallel analysis. Science *285*, 901–906.

Wu, C.K., Dailey, H.A., Rose, J.P., Burden, A., Sellers, V.M., and Wang, B.C. (2001). The 2.0 A structure of human ferrochelatase, the terminal enzyme of heme biosynthesis. Nat. Struct. Biol. *8*, 156–160.

Zaman, S., Lippman, S.I., Zhao, X., and Broach, J.R. (2008). How Saccharomyces responds to nutrients. Annu. Rev. Genet. *42*, 27–81.

Zhao, Y., Feng, J., Li, J., and Jiang, L. (2012). Mitochondrial type 2C protein phosphatases CaPtc5p, CaPtc6p, and CaPtc7p play vital roles in cellular responses to antifungal drugs and cadmium in Candida albicans. FEMS Yeast Research *12*, 897–906.

Tables and Figures

Figure 1: Activity-based protein profiling allows for large-scale identification of active mitochondrial kinases

A) Experimental Design: Mitochondria were extracted and lysed from the livers corresponding to the highlighted conditions from our previous phosphoproteomics study. Kinases, illustrated by red circles, are extracted from each sample using activity-based probes and identified/quantified by tandem MS. B-C) Data from study showing kinases enriched in mitochondrial fractions compared to mitochondria-depleted livers (B) and kinases enriched in mitochondria from obese mice compared to lean mice (C).

Figure 1:

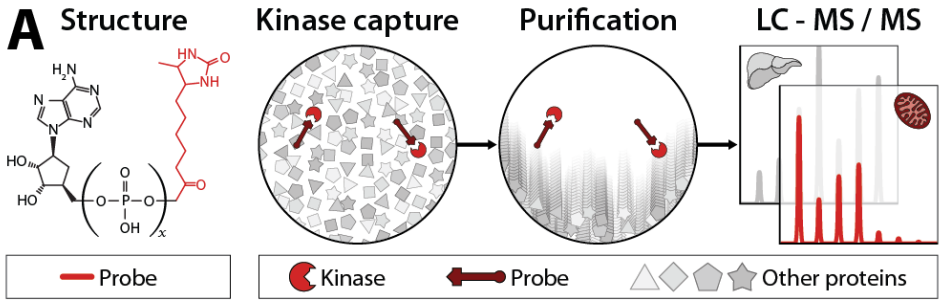

B6				BTBR			
4 weeks		10 weeks		4 weeks		10 weeks	
lean	obese	lean	obese	lean	obese	lean	obese

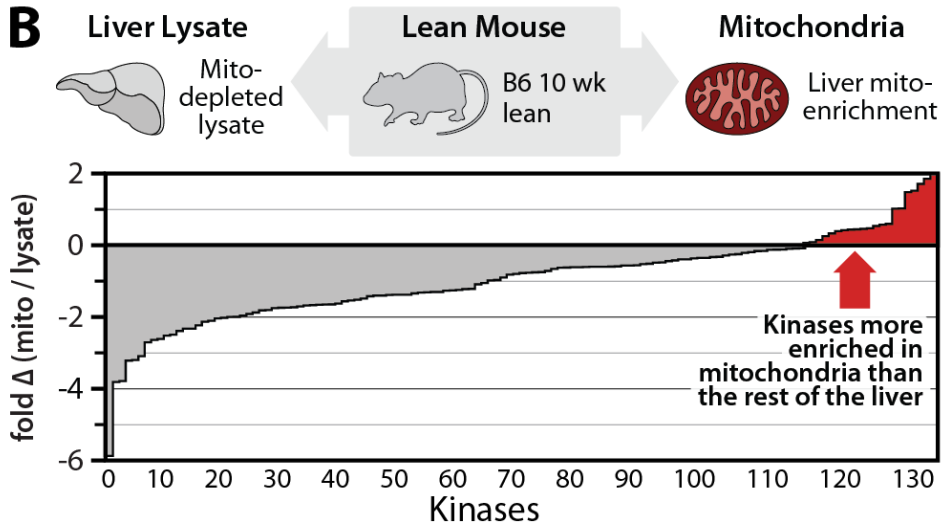

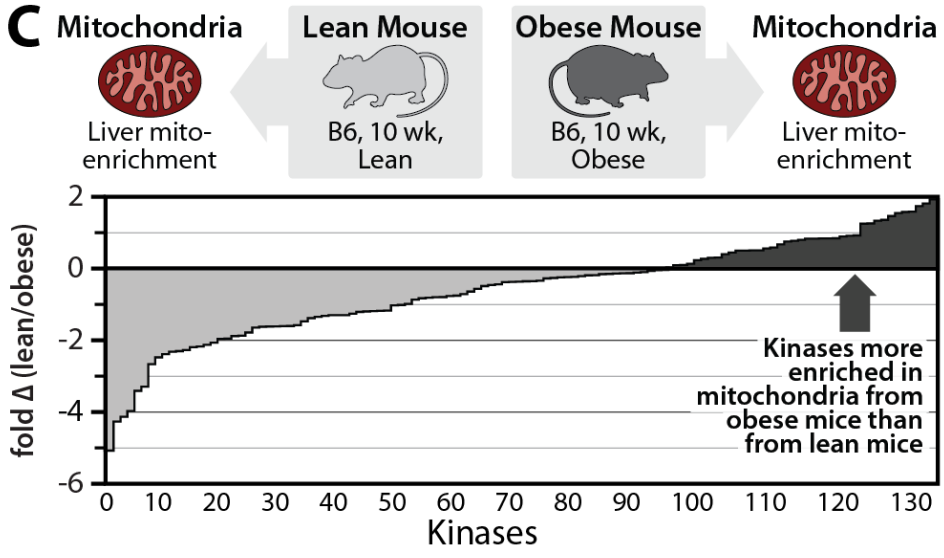

Figure 2: Biophysical and proteomic response of mitochondria to treatment with extramitochondrial calcium

A,B) Oxygen consumption rates (OCR), in isolated mitochondria given either succinate (A) or glutamate and malate (B) as substrates for oxidative phosphorylation. Four injections were administered over the course of the experiment, the first injection 'A' contained either calcium (red) EDTA (gray) or water (black), followed by injections of ADP (CV substrate), Oligomycin (CV inhibitor) and FCCP (uncoupler). C) Oxygen consumption rates (OCR), in isolated mitochondria given Antimycin A (red) or water (black) in the first injection, followed by calcium. D-G) Calcium uptake in isolated mitochondria using Calcium Green 5N (Molecular Probes) as an indicator of free calcium. All error bars represent SD. A mitochondrial calcium uptake inhibitor (Ru360, D (red)) can be used as a control for selectivity of the assay. Calcium uptake differed in response to mouse strain (E), various OXPHOS inhibitors (F) and phosphatase inhibitors (G). H) Rank order (x axis) by fold change compared to wild type (WT) of the quantitation of all phosphoisoforms discovered in the ptc7Δ yeast strain. Mitochondrial phosphorylation sites are indicated by red dots.

Figure 2:

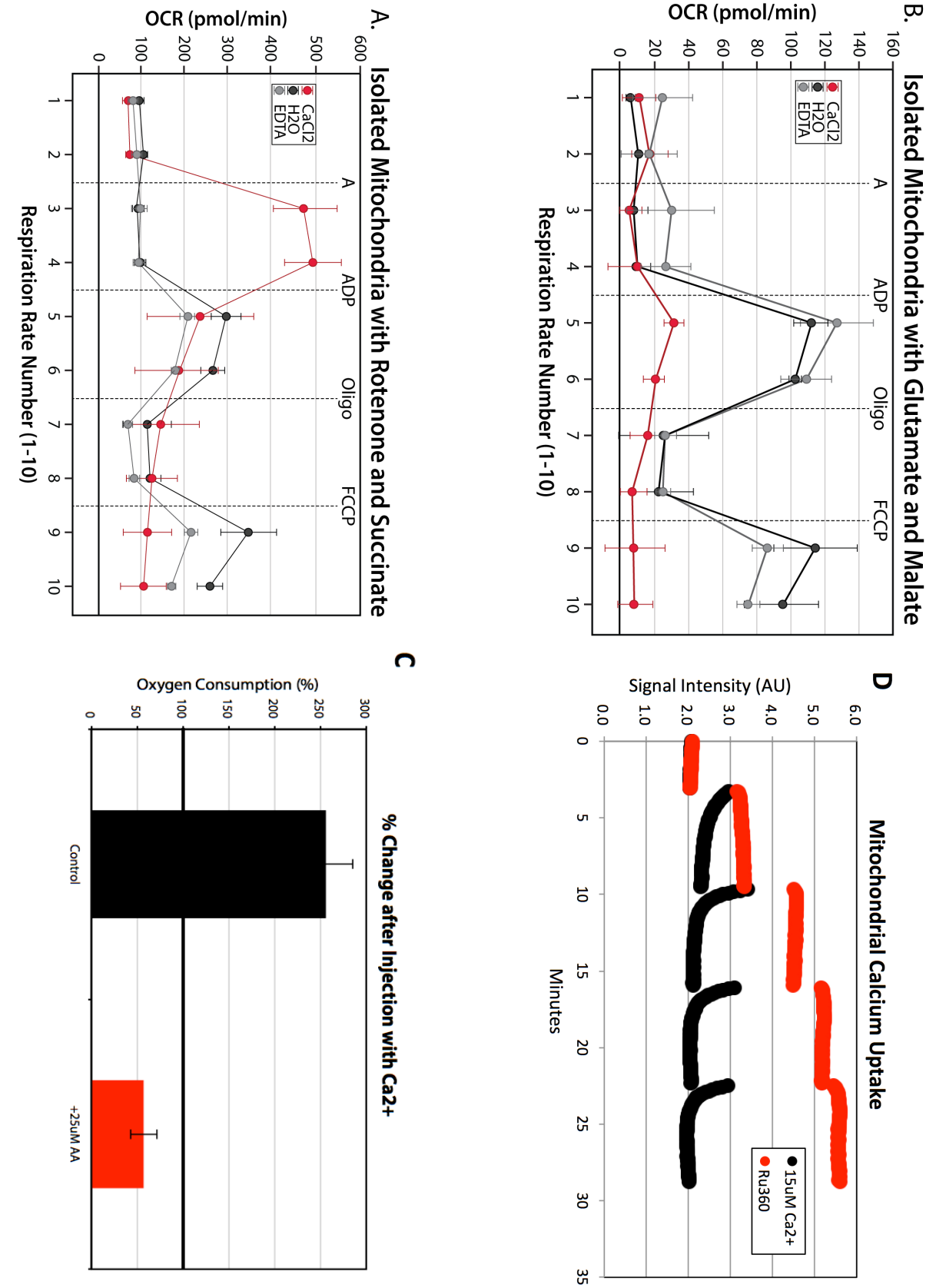
A.
Isolated Mitochondria with Rotenone and Succinate
OCR (pmol/min)
CaCl2
H2O
EDTA
A
ADP
Oligo
FCCP
Respiration Rate Number (1-10)
B.
Isolated Mitochondria with Glutamate and Malate
OCR (pmol/min)
CaCl2
H2O
EDTA
A
ADP
Oligo
FCCP
Respiration Rate Number (1-10)
C
% Change after Injection with Ca2+
Oxygen Consumption (%)
Control
+25uM AA
D
Mitochondrial Calcium Uptake
Signal Intensity (AU)
15uM Ca2+
Ru360
Minutes

Figure 2 Continued

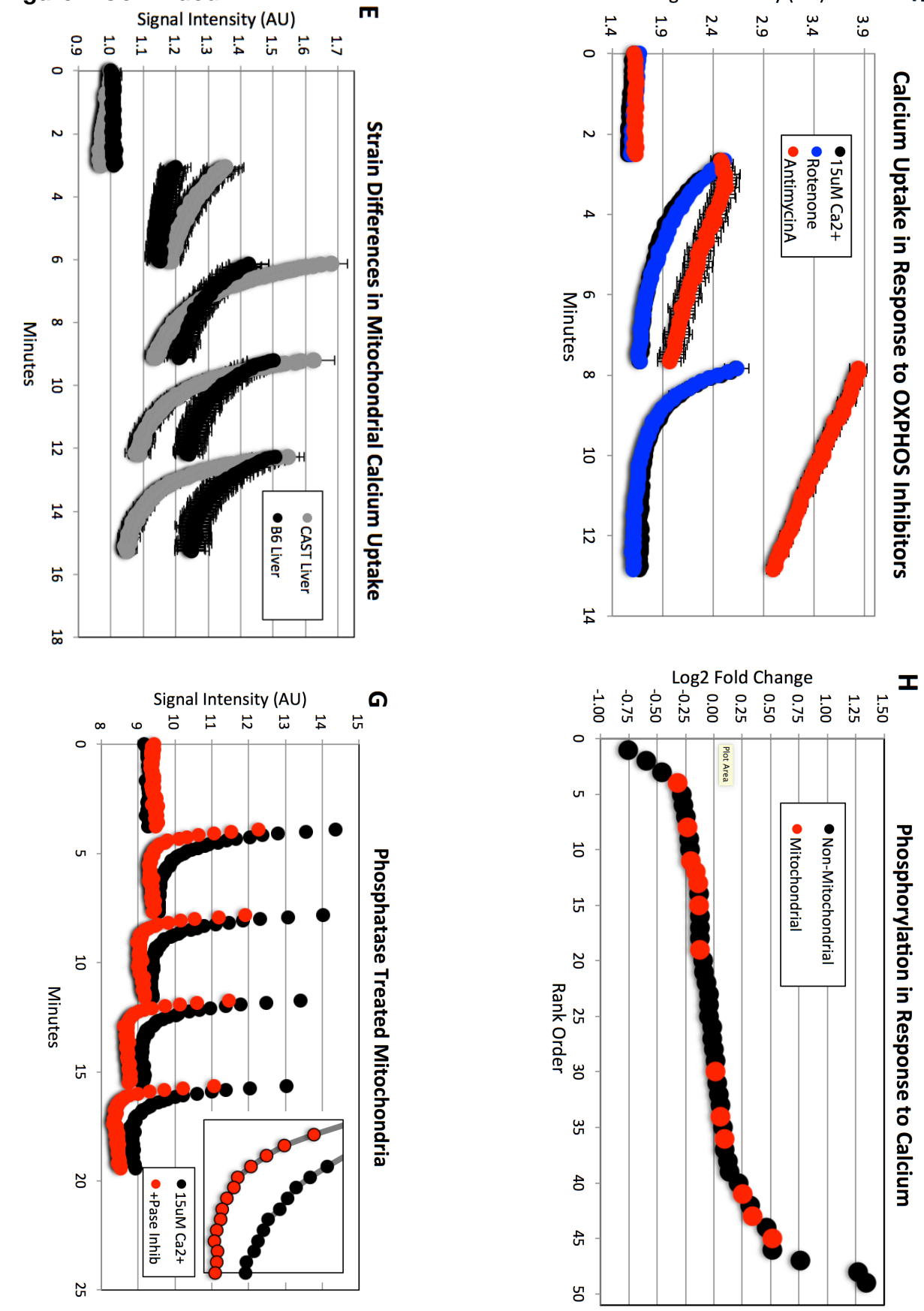

Figure 3: Muliplexed proteomic and phosphoproteomic analysis of yeast phosphatase knock-out strains

A) Activity of recombinant PPTC7 with pNPP as a substrate, and with different divalent cations used for catalysis. Error bars represent SE. B) Phylogenetic tree showing the evolutionary relationships between the seven different Type 2C yeast phosphatases. C) Timecourse of HA-tagged Ptc7 yeast as the strain is grown through the diauxic shift, an arrow is shown indicating the spliced (mitochondrial) isoform, Pdi1 is shown as a loading control. D,E) Schematic of our proteomic workflow. We performed our analysis by enriching mitochondria from four different yeast strains (WT, ptc5Δ, ptc6Δ, and ptcΔ) that were collected four hours after the diauxic shift, represented in D. We then performed high-resolution quantitative proteomic and phosphoproteomics analysis using TMT tags (E). F,G) Abundance fold change compared to wild type (WT) for ptc7Δ strain compared to both ptc5Δ (F) and ptc6Δ (G). H) Inset from (F) showing identified phosphorylation sites that are elevated in ptc7Δ/wt but not in ptc5Δ/wt.

Figure 3:

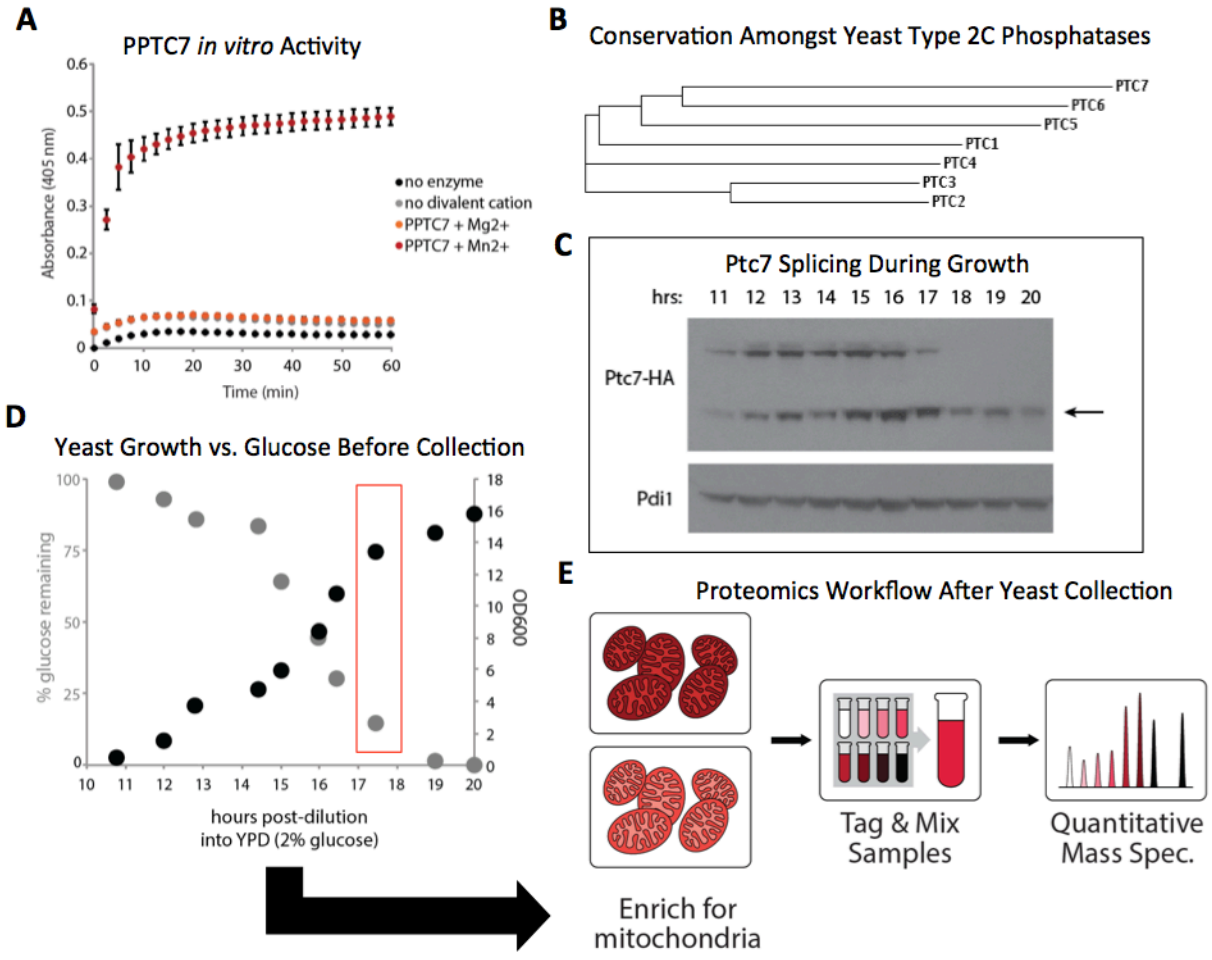
A
PPTC7 *in vitro* Activity
Absorbance (405 nm)
Time (min)
no enzyme
no divalent cation
PPTC7 + Mg2+
PPTC7 + Mn2+
B
Conservation Amongst Yeast Type 2C Phosphatases
PTC7
PTC6
PTC5
PTC1
PTC4
PTC3
PTC2
C
Ptc7 Splicing During Growth
hrs: 11 12 13 14 15 16 17 18 19 20
Ptc7-HA
Pdi1
D
Yeast Growth vs. Glucose Before Collection
% glucose remaining
OD600
hours post-dilution into YPD (2% glucose)
E
Proteomics Workflow After Yeast Collection
Enrich for mitochondria
Tag & Mix Samples
Quantitative Mass Spec.

Figure 3 Continued

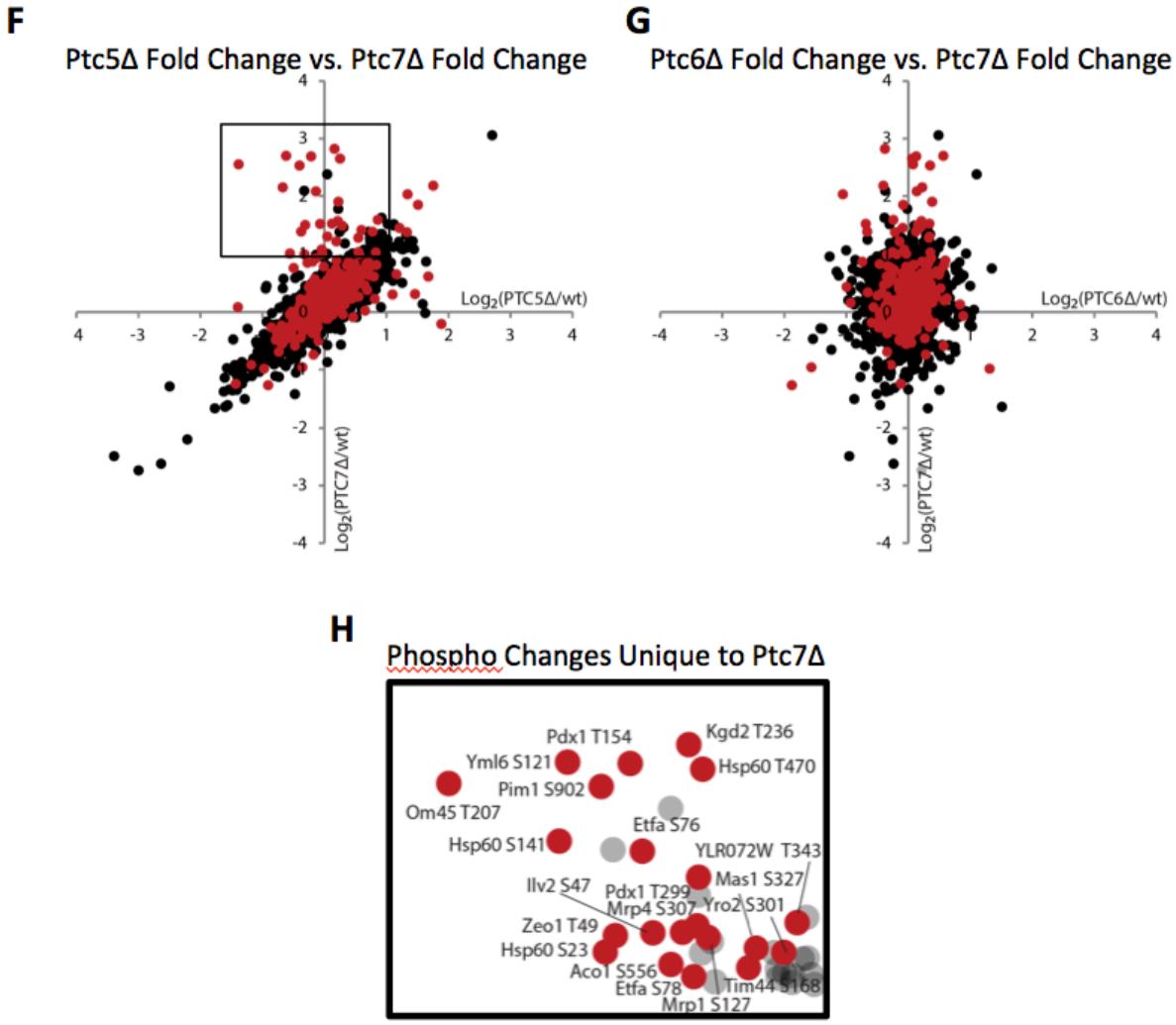

Figure 4: Ptc7Δ yeast have altered iron metabolism and increased resistance to oxidative stress

A) Our phosphoproteomics analysis identified 70 candidate phosphorylation sites on mitochondrial proteins that are increased in Ptc7Δ strains relative to wild type. B) Total proteome analysis of Ptc7Δ yeast reveals a downregulation of iron transporters (blue) and an increase in proteins involved in oxidative stress (red). Ptc7 itself is highlighted for comparison. C) GO term analysis of the proteins with the biggest decreases in expression show an enrichment in iron transport (top, blue) and analysis of proteins with the biggest increases in expression show an enrichment in oxidative stress pathways. D,E) Serial dilution of WT (BY4741) and Ptc7Δ yeast treated with either the iron chelator dipyridine (D) or the oxidant H2O2 (E) reveals that knockout confers resistance to these stressors. F) Of our 70 candidate proteins, 10 phosphosites on 8 unique proteins are upregulated in Ptc7Δ yeast; 3 are linked to iron homeostasis, and 7 are linked to the oxidative stress response. G) Yeast growth curve for wild-type (WT), Ptc5Δ, Ptc6Δ and Ptc7Δ strains grown in 50uM dipyridine (DP). Error bars indicate SD. H) Yeast growth curve for wild-type (WT), Ptc5Δ, Ptc6Δ and Ptc7Δ strains grown in 1mM hydrogen peroxide (H2O2). Error bars indicate SD.

Figure 4:

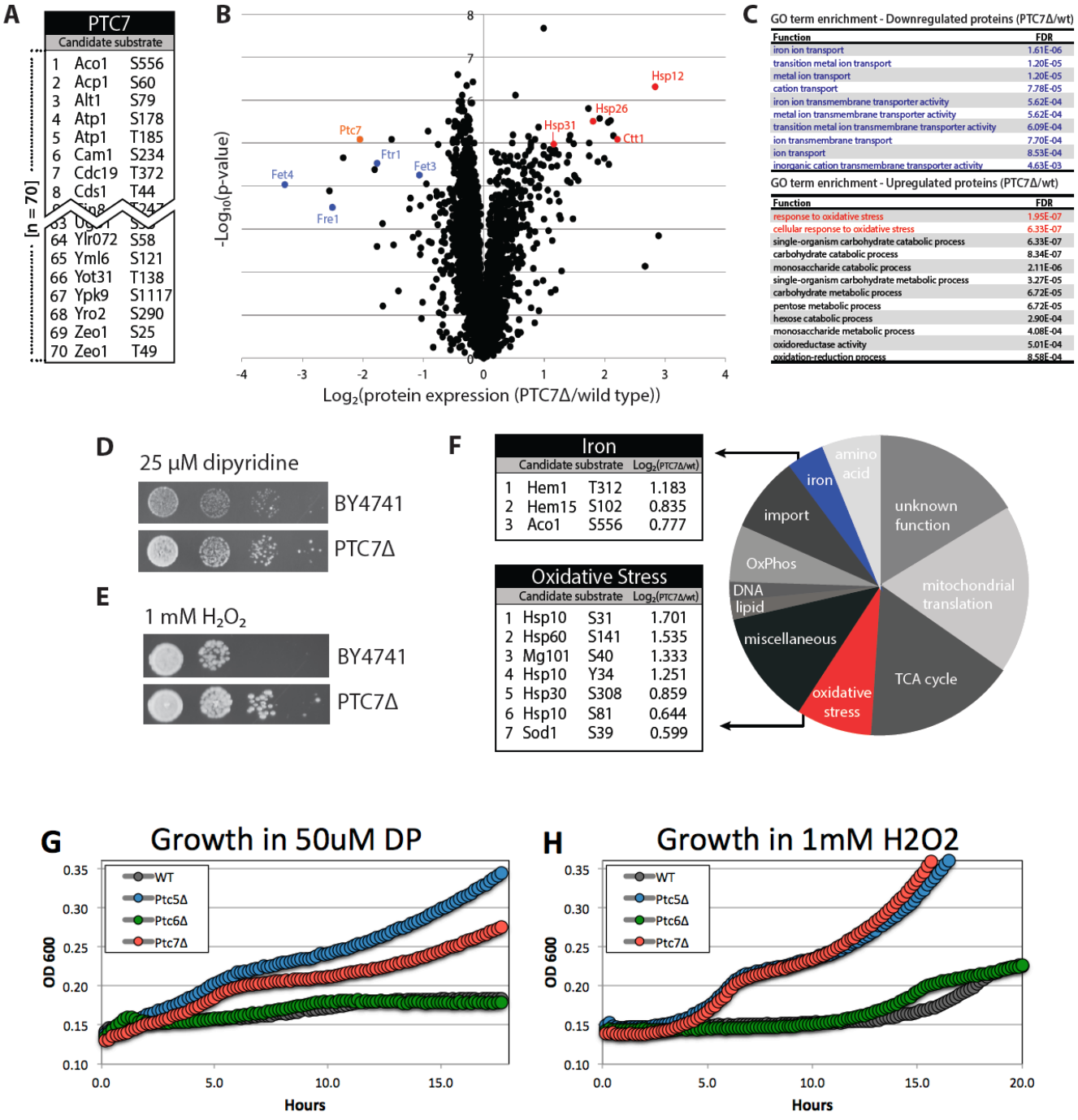
A
PTC7
Candidate substrate
[n = 70]
1 Aco1 S556
2 Acp1 S60
3 Alt1 S79
4 Atp1 S178
5 Atp1 T185
6 Cam1 S234
7 Cdc19 T372
8 Cds1 T44
64 Ylr072 S58
65 Yml6 S121
66 Yot31 T138
67 Ypk9 S1117
68 Yro2 S290
69 Zeo1 S25
70 Zeo1 T49
B
-Log10(p-value)
Log2(protein expression (PTC7Δ/wild type))
Hsp12
Hsp26
Hsp31
Ctt1
Ptc7
Ftr1
Fet3
Fet4
Fre1
C
GO term enrichment - Downregulated proteins (PTC7Δ/wt)
Function FDR
iron ion transport 1.61E-06
transition metal ion transport 1.20E-05
metal ion transport 1.20E-05
cation transport 7.78E-05
iron ion transmembrane transporter activity 5.62E-04
metal ion transmembrane transporter activity 5.62E-04
transition metal ion transmembrane transporter activity 6.09E-04
ion transmembrane transport 7.70E-04
ion transport 8.53E-04
inorganic cation transmembrane transporter activity 4.63E-03
GO term enrichment - Upregulated proteins (PTC7Δ/wt)
Function FDR
response to oxidative stress 1.95E-07
cellular response to oxidative stress 6.33E-07
single-organism carbohydrate catabolic process 6.33E-07
carbohydrate catabolic process 8.34E-07
monosaccharide catabolic process 2.11E-06
single-organism carbohydrate metabolic process 3.27E-05
carbohydrate metabolic process 6.72E-05
pentose metabolic process 6.72E-05
hexose catabolic process 2.90E-04
monosaccharide metabolic process 4.08E-04
oxidoreductase activity 5.01E-04
oxidation-reduction process 8.58E-04
D
25 μM dipyridine
BY4741
PTC7Δ
E
1 mM H2O2
BY4741
PTC7Δ
F
Iron
Candidate substrate Log2(PTC7Δ/wt)
1 Hem1 T312 1.183
2 Hem15 S102 0.835
3 Aco1 S556 0.777
Oxidative Stress
Candidate substrate Log2(PTC7Δ/wt)
1 Hsp10 S31 1.701
2 Hsp60 S141 1.535
3 Mg101 S40 1.333
4 Hsp10 Y34 1.251
5 Hsp30 S308 0.859
6 Hsp10 S81 0.644
7 Sod1 S39 0.599
amino acid
iron
import
unknown function
OxPhos
mitochondrial translation
DNA lipid
miscellaneous
TCA cycle
oxidative stress
G
Growth in 50uM DP
OD 600
Hours
WT
Ptc5Δ
Ptc6Δ
Ptc7Δ
H
Growth in 1mM H2O2
OD 600
Hours
WT
Ptc5Δ
Ptc6Δ
Ptc7Δ

Figure 5: Phosphorylation of serine 102 on Hem15 decreases enzyme activity

A) Schematic of overrepresented phosphorylation motif found in our previous work (top) and Hem15 primary sequence, highlighting identified phosphorylation residues at site S102. B) Using structure coordinates from the human (left) and yeast ferrochealatase (right), PDB 2HRE and 1LBQ respectively, S102 is shown interacting with the protoporphyrin ring and facing into the active site. C) Phosphosite occupancy (Log2) compared to a WT strain was calculated for each phosphatase mutant. D) Volcano plot of fold phosphorylation changes versus –log (p value) for all of the phosphorylation sites identified in the Ptc7Δ strain. Phosphorylation sites on Hem1, Hem15 and Pda1 are highlighted in red. E) F)

Figure 5:

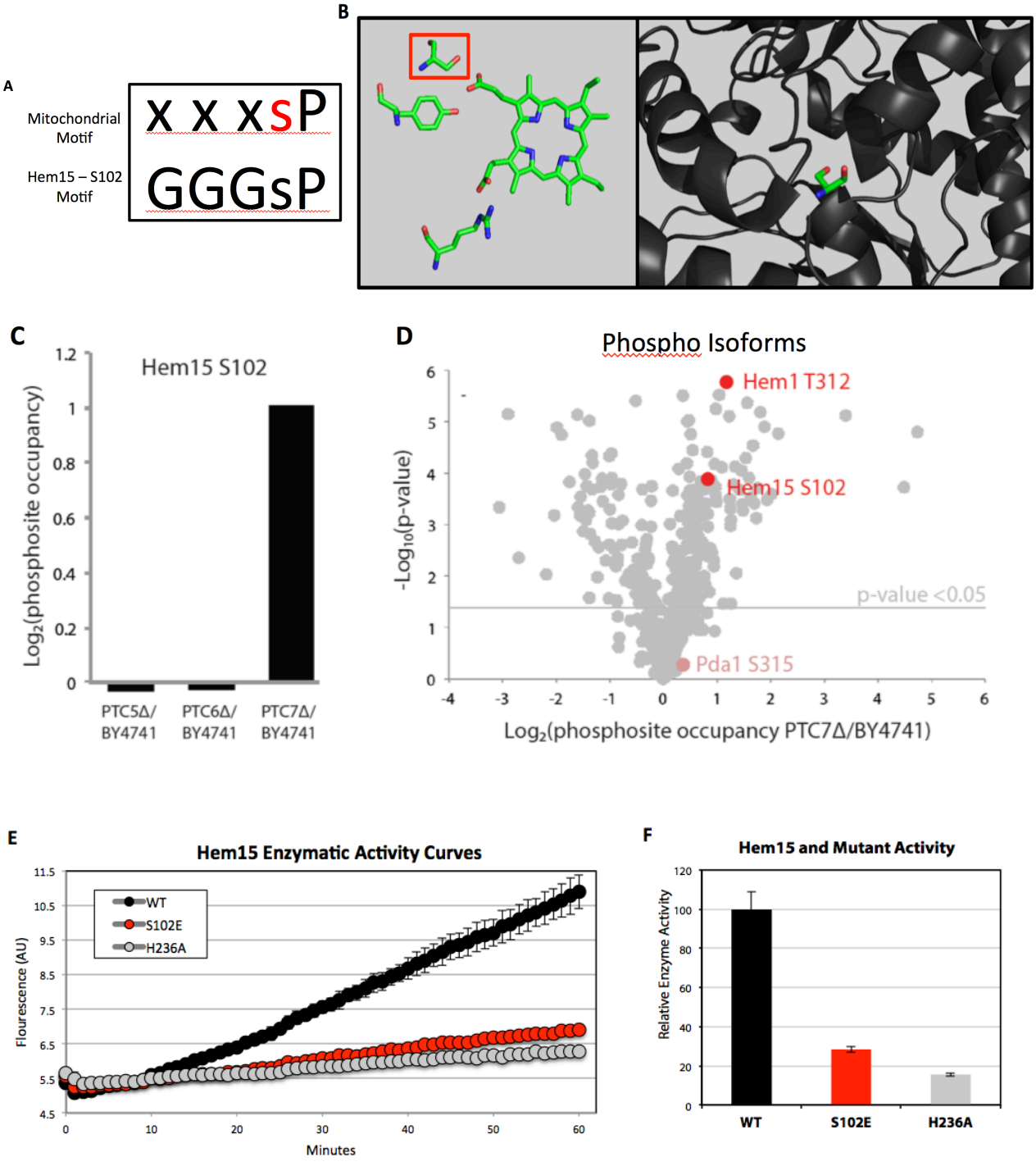
A
Mitochondrial Motif
x x xsP
Hem15 – S102 Motif
GGGsP
B
C
Hem15 S102
Log2(phosphosite occupancy)
PTC5Δ/ BY4741
PTC6Δ/ BY4741
PTC7Δ/ BY4741
D
Phospho Isoforms
Hem1 T312
Hem15 S102
Pda1 S315
p-value <0.05
-Log10(p-value)
Log2(phosphosite occupancy PTC7Δ/BY4741)
E
Hem15 Enzymatic Activity Curves
WT
S102E
H236A
Flourescence (AU)
Minutes
F
Hem15 and Mutant Activity
Relative Enzyme Activity
WT
S102E
H236A

CHAPTER 4: Conclusions, Future Directions, and Impact

Conclusions

Throughout the work on this thesis, I have increased our understanding of the role phosphorylation plays in the mitochondria. My research has quantified the proteome and phosphoproteome of mice in multiple physiological states, and has shown that phosphorylation is a key regulator of ketogenesis. In addition, I have extended this work through an investigation of kinases and phosphatases, the enzymes that control phosphorylation dynamics. I utilized activity-based proteomics to identify kinases that may be localizing to the mitochondria differentially in lean and obese states. I have shown that calcium may be playing a unique role in the liver, and that phosphorylation in liver mitochondria is dynamic in response to treatment with calcium. Finally, I used a yeast deletion approach to identify phosphorylation sites that are likely targets of an understudied mitochondrial phosphatase, PTC7. We have shown that PTC7 is involved in cellular iron homeostasis, and that a putative PTC7 phosphorylation site on Hem15 can affect enzyme activity. Taken together, my work has shown that phosphorylation is a prevalent and dynamic modification in mitochondria, that kinases are likely part of this dynamic response, and we have begun to identify the specific substrates of a mitochondrial phosphatase.

All of this work was made possible by the rapid advancements that have been made in the last decade in mass spectrometry (Coon, 2009; Grimsrud et al., 2010). The advent of isobaric tags and the increase in MS speed and sensitivity has vastly improved the power of shotgun proteomics and quantitative MS (Merrill and Coon, 2013). It is now possible to identify thousands of phosphorylation sites in one experiment, and when coupled with enrichment methods for other PTMs, a single

mouse model can provide a rich source for information on the regulation of proteins (Grimsrud et al., 2012; Keller et al., 2008; Still et al., 2013).

Moving forward it will be increasingly important to compare biological conditions and multiple tissues when evaluating the importance of phosphorylation and PTMs in the mitochondria. We and others have shown that mitochondria are highly dynamic organelles in both normal fasting and refeeding states as well as in diabetes, obesity and caloric restriction (Grimsrud et al., 2012; Hebert et al., 2013; Still et al., 2013). Mitochondria are also extremely divergent within an organism, as different tissues contain vastly different mitochondrial protein content (Mootha et al., 2003; Pagliarini et al., 2008). Future studies will need to evaluate not only changes in PTMs in one tissue, but also how the same protein in various tissues may respond differently to a change in nutritional status.

Future Directions

Phosphorylation Stoichiometry

With the recent resurgence of mitochondria as a center of signaling in human health and disease, it has become increasingly important to understand the role that phosphorylation plays in regulating mitochondrial proteins and pathways (Lane, 2006; Pagliarini and Rutter, 2013; Wallace, 2013). We have shown that phosphorylation can be altered in response to changing metabolic states (Grimsrud et al., 2012), but a relative two-fold change in quantitation cannot distinguish between 1-2% or 50-100%. It is possible that a small percentage change in occupancy could have a significant physiological affect if a phosphorylation site is activating, as in the case of HMGCS2. On the other hand, if a phosphorylation site is inactivating, such as Hem15, it is unlikely to have a significant physiological affect unless a significant portion of the enzyme is inactivated.

Methods, such as AQUA, do exist for determining absolute stoichiometry (Gerber et al., 2003). Unfortunately, this method requires synthesis of individual isotopically labeled peptides, which is costly and low-throughput. Fortunately, techniques that begin to solve some of these problems are becoming more widely researched and used (Wu et al., 2011). Moving forward it will be important to investigate phosphorylation occupancy when considering not only the role of specific phosphorylation sites on the activity of a protein, but on the overall role that phosphorylation may be playing in the regulation of mitochondria.

Other PTMs

While this work has focused on the role of phosphorylation in the mitochondria it is important to consider the affect that other PTMs may be having on mitochondrial function. Acetylation is another prevalent PTM in the mitochondria, which has seen a dramatic increase in interest in recent years. Large-scale studies have discovered over 2000 acetylation sites in mitochondria, predominantly located on metabolic enzymes (Hebert et al., 2013; Wang et al., 2010). Furthermore, similarly to phosphorylation, acetylation has been shown to regulate many different mitochondrial pathways (Hirschey et al., 2010; Jiang et al., 2011; Shimazu et al., 2010). One way that acetylation differs from phosphorylation in the mitochondria is the current lack of a known deacetylase. While a few studies have hinted at the identity of a mitochondrial deacetylase (Scott et al., 2014), the likelihood that mitochondrial acetylation is an entirely non-enzymatic modification is still possible as mitochondria contain a suitable environment for chemical acylation (Wagner and Payne, 2013). Fortunately, the problem of stoichiometry in acetylation is not as prevalent as in phosphorylation, as the large-scale measurement of acetylation occupancy in an entire proteome is now possible (Baeza et al., 2014).

Combinatorial PTMs on a Single Protein

With the ability to use MS to look at a wide variety of PTMs within the mitochondria, it is becoming increasingly important that the interactions between different modifications be considered. Large-scale studies have shown that in addition to phosphorylation and acetylation, succinlyation and malonoylation are also prevalent

modifications in mitochondria (Du et al., 2011; Park et al., 2013). Indeed, while our work has shown that phosphorylation is capable of regulating HMGCS2 activity (Grimsrud et al., 2012), others have shown that HMGCS2 can also be regulated by acetylation, succinylation and palmitoylation (Kostiuk et al., 2010; Quant et al., 1990; Shimazu et al., 2010). It will be intriguing to see what, if any, the interplay between these modifications can have on the control of ketogenesis. Others have reported the role that phosphorylation and acetylation in concert can have on the activity of the PDC (Fan et al., 2014), and it will be important to investigate if this is true for other enzyme complexes as well.

One hurdle to the investigation of multiple PTMs on a single protein is the standard shotgun proteomics technique. In bottom-up proteomics, a protein is first digested into easily ionizable peptides, then sequenced using tandem MS, and finally reconstructed using protein databases. While this method is ideal for large-scale analysis and quantitation of individual PTMs, when different PTMs appear on different peptides, it is impossible to know if they came from the same protein at the same time. For example, it would be impossible to know if all of a protein was 50% acetylated and 50% phosphorylated, or if half of a protein was 100% acetylated and the other half was 100% phosphorylated. One way to overcome this method is using top-down proteomics (Kelleher et al., 2014). In the top down method, entire proteins are ionized, and it may be possible to look at the different proportion of modifications. This technology is still in its infancy though, and only recently have advances been made that allow analysis of large molecular weight proteins and quantitation between different biological samples (Han et al., 2006; Rhoads et al., 2014).

Mitochondrial Kinases and Phosphatases

Through the work of our group and others, we have shown that phosphorylation in mitochondria is prevalent and is dynamic in response to changing physiological states (Deng et al., 2011; Grimsrud et al., 2012; Zhao et al., 2010). Furthermore, phosphorylation has recently been shown to be important for regulating key mitochondrial pathways such as protein import and proteolytic processing (Bin Lu et al., 2012; Schmidt et al., 2011)To continue this work, it will be important to know more about the enzymes that are involved in the addition and removal of this modification. While several classic studies have shown that phosphorylation regulates the activities of the PDC and the BCKDC (Pagliarini and Dixon, 2006), the majority of the known phosphorylation events in the mitochondria have no kinase or phosphatase associated with them.

Our ABPP approach has begun to identify kinases that are enriched in mitochondrial fractions and kinases that are differentially identifiable in lean and obese liver mitochondria. To continue this work, several technical conditions must be met. It seems possible, even likely, that if kinases are transiently translocating to the mitochondria, it will be important to profile as many different conditions as possible. Furthermore, we have shown that using biological replicates for statistical power is important for identifying regulatory phosphorylation sites, and it will likely be similarly important for identifying kinases. Finally, while crude mitochondrial preps were desirable for our earlier studies, moving forward it will be important to utilize density

gradients to obtain pure mitochondrial preps if we hope to definitively identify *bona fide* mitochondrial kinases.

Calcium has also been known to be important to mitochondrial function for decades (Otto and Ontko, 1978), yet in many cases the mechanism for calcium action in the mitochondria is unknown (Balaban, 2009). Interestingly, there are calcium responsive kinases and phosphatases in the cytosol, and it is tempting to speculate that calcium import into the mitochondria could be affecting as-yet-unidentified mitochondrial kinases or phosphatases. Recently, the molecular identity of the calcium uniporter has been discovered (Baughman et al., 2011), and its role in rapid calcium uptake has been shown in a mouse knockout model (Pan et al., 2013). It would be especially illuminating to profile the phosphoproteome in mice lacking the calcium uniporter. Finally, we and others have shown that calcium can increase both mitochondrial respiration rates and ATP concentration (Graier et al., 2007). Moreover, a recent report by the Pozzan group has shown that mitochondrial calcium can induce cAMP generation in the matrix (Di Benedetto et al., 2013), and the Manfredi group has provided evidence for a complete adenylyl cyclase and phosphodiesterase system in the mitochondrial matrix (Acin-Perez et al., 2011; 2009). Taken together, this evidence seems to point toward a cAMP dependent kinase that is localized to the mitochondria and proposes a mechanism though which calcium can regulate ATP generation.

While the identities of mitochondrial phosphatases are well characterized, the specific targets of most of these phosphatases are still unknown. It may even be true that the kinase/phosphatase system in the mitochondria mirrors that of the acetylation system in which the addition of the modification may be non-enzymatic while the

removal of the modification is the key to regulation. It has been proposed that phosphorylation may be a non-enzymatic side effect of the OXPHOS system and high ATP concentrations in the matrix (Covian and Balaban, 2012). It will also be important in the future to investigate non-canonical phosphorylation sites, such as histidine, arginine, and aspartate. The bacterial lineage of the mitochondria, and several recent studies, have suggested that these unappreciated phosphorylation sites may be important for mitochondrial function (Kee and Muir, 2012; Klumpp and Krieglstein, 2009).

Future Studies on PTC7 and Mitochondrial Adaptation

Our recent work has begun to identify the substrates of a mitochondrial phosphatase, PTC7. Using phosphoproteomics and a yeast deletion system, we have identified 70 phosphorylation sites that are likely targets of PTC7. While this is a strong beginning, more work remains to fully understand the role of this phosphatase. In the future, it will be important to rescue by overexpression the phenotypes that are seen regarding iron chelation and resistance to oxidative stress. It is possible that deletion of PTC7 causes a mild stress response (shown by upregulated HSPs and catalase), which in turn allows the Ptc7Δ strain to better overcome future stress. This phenomenon has been seen in other contexts and is termed ‘mitohormesis’ (Yun and Finkel, 2014). Indeed, even the reactive oxygen species produced by CIII have also been shown to have protective effects and be important for cellular function (Sena and Chandel, 2012). It will be important to test if Ptc7Δ yeast have greater levels of ROS than their WT counterparts.

Identifying *bona fide* targets of PTC7, as opposed to stochastic, downstream or adaptive sites is a challenge. This challenge stems partly from the timing of our proteomic experiments. Even if yeast are grown through the diauxic shift to achieve maximal mitochondrial utilization and PTC7 expression (in WT), this process takes hours and there could still be a long term adaptation to a removal of a gene. We are working on developing a rapid, inducible PTC7 knockout system in yeast based on the classic Cre-Lox gene editing technique (Cheng et al., 2000). Once this is in place, we will be able to rapidly delete the gene and, depending on protein turnover, be able to investigate rapid changes in phosphorylation during the transition to oxidative respiration (Kanshin et al., 2015).

Further work also remains in the characterization of the effect of phosphorylation on the activity of Hem15. Total iron and heme content of Ptc7Δ yeast will need to be measured. More investigation of the catalytic rates of Hem15 will be needed to determine if phosphorylation is affecting the V_{max} or K_d of the protein. Also, the mechanism of inhibition will need to be examined; binding experiments should be conducted to determine if S102 phosphorylation is blocking the ability of the enzyme to bind the protoporphyrin ring. Finally, while the efficiency remains low, it will soon be possible to use orthogonal translation systems in bacteria to crease site-specific phosphoserine incorporation (Lajoie et al., 2013). This will overcome the difficulty of using phosphomimetic mutations to approximate phosphorylation. Overall, these future experiments will allow us to fully understand the role the phosphorylation is playing in the activity of Hem15 and in iron homeostasis in yeast.

Impact

Throughout the course of my dissertation research I have endeavored to expand our knowledge of the role that phosphorylation plays in the regulation of mitochondrial biochemical pathways. I believe that the future of this field is bright and that there are many interesting and complex questions yet to be answered. Our increased understanding of the role that mitochondria play in the progression of many human diseases begs for more work to be undertaken. Here, I have shown that phosphorylation is a dynamic mitochondrial PTM, and that kinases and phosphatases are likely regulators of this modification from within the organelle. More work still needs to be undertaken to understand the functions and regulation of the hundreds of phosphorylation sites now known on mitochondrial proteins.

References

Acin-Perez, R., Russwurm, M., Günnewig, K., Gertz, M., Zoidl, G., Ramos, L., Buck, J., Levin, L.R., Rassow, J., Manfredi, G., et al. (2011). A phosphodiesterase 2A isoform localized to mitochondria regulates respiration. Journal of Biological Chemistry *286*, 30423–30432.

Acin-Perez, R., Salazar, E., Kamenetsky, M., Buck, J., Levin, L.R., and Manfredi, G. (2009). Cyclic AMP Produced inside Mitochondria Regulates Oxidative Phosphorylation. Cell Metabolism *9*, 265–276.

Baeza, J., Dowell, J.A., Smallegan, M.J., Fan, J., Amador-Noguez, D., Khan, Z., and Denu, J.M. (2014). Stoichiometry of Site-specific Lysine Acetylation in an Entire Proteome. Journal of Biological Chemistry *289*, 21326–21338.

Balaban, R.S. (2009). The role of Ca2+ signaling in the coordination of mitochondrial ATP production with cardiac work. BBA - Bioenergetics *1787*, 1334–1341.

Baughman, J.M., Perocchi, F., Girgis, H.S., Plovanich, M., Belcher-Timme, C.A., Sancak, Y., Bao, X.R., Strittmatter, L., Goldberger, O., Bogorad, R.L., et al. (2011). Integrative genomics identifies MCU as an essential component of the mitochondrial calcium uniporter. Nature *476*, 341–345.

Bin Lu, Lee, J., Nie, X., Li, M., Morozov, Y.I., Venkatesh, S., Bogenhagen, D.F., Temiakov, D., and Suzuki, C.K. (2012). Phosphorylation of Human TFAM in Mitochondria Impairs DNA Binding and Promotes Degradation by the AAA+ Lon Protease. Mol. Cell 1–12.

Cheng, T.H., Chang, C.R., Joy, P., Yablok, S., and Gartenberg, M.R. (2000). Controlling gene expression in yeast by inducible site-specific recombination. Nucleic Acids Research *28*, E108.

Coon, J.J. (2009). Collisions or electrons? Protein sequence analysis in the 21st century. Anal. Chem. *81*, 3208–3215.

Covian, R., and Balaban, R.S. (2012). Cardiac mitochondrial matrix and respiratory complex protein phosphorylation. AJP: Heart and Circulatory Physiology *303*, H940–H966.

Deng, N., Zhang, J., Zong, C., Wang, Y., Lu, H., Yang, P., Wang, W., Young, G.W., Wang, Y., Korge, P., et al. (2011). Phosphoproteome analysis reveals regulatory sites in major pathways of cardiac mitochondria. Molecular & Cellular Proteomics *10*, M110.000117–M110.000117.

Di Benedetto, G., Scalzotto, E., Mongillo, M., and Pozzan, T. (2013). Mitochondrial Ca. Cell Metabolism *17*, 965–975.

Du, J., Zhou, Y., Su, X., Yu, J.J., Khan, S., Jiang, H., Kim, J., Woo, J., Kim, J.H., Choi, B.H., et al. (2011). Sirt5 is a NAD-dependent protein lysine demalonylase and desuccinylase. Science *334*, 806–809.

Fan, J., Shan, C., Kang, H.-B., Elf, S., Xie, J., Tucker, M., Gu, T.-L., Aguiar, M., Lonning, S., Chen, H., et al. (2014). Tyr Phosphorylation of PDP1 Toggles Recruitment between ACAT1 and SIRT3to Regulate the Pyruvate Dehydrogenase Complex. Mol. Cell 1–15.

Gerber, S.A., Rush, J., Stemman, O., Kirschner, M.W., and Gygi, S.P. (2003). Absolute quantification of proteins and phosphoproteins from cell lysates by tandem MS. Proc. Natl. Acad. Sci. U.S.a. *100*, 6940–6945.

Graier, W.F., Frieden, M., and Malli, R. (2007). Mitochondria and Ca2+ signaling: old guests, new functions. Pflugers Arch. *455*, 375–396.

Grimsrud, P.A., Carson, J.J., Hebert, A.S., Hubler, S.L., Niemi, N.M., Bailey, D.J., Jochem, A., Stapleton, D.S., Keller, M.P., Westphall, M.S., et al. (2012). A quantitative map of the liver mitochondrial phosphoproteome reveals posttranslational control of ketogenesis. Cell Metabolism *16*, 672–683.

Grimsrud, P.A., Swaney, D.L., Wenger, C.D., Beauchene, N.A., and Coon, J.J. (2010). Phosphoproteomics for the Masses. ACS Chem. Biol. *5*, 105–119.

Han, X., Jin, M., Breuker, K., and McLafferty, F.W. (2006). Extending top-down mass spectrometry to proteins with masses greater than 200 kilodaltons. Science *314*, 109–112.

Hebert, A.S., Dittenhafer-Reed, K.E., Yu, W., Bailey, D.J., Selen, E.S., Boersma, M.D., Carson, J.J., Tonelli, M., Balloon, A.J., Higbee, A.J., et al. (2013). Calorie Restriction and SIRT3 Trigger Global Reprogramming of the Mitochondrial Protein Acetylome. Mol. Cell *49*, 186–199.

Hirschey, M.D., Shimazu, T., Goetzman, E., Jing, E., Schwer, B., Lombard, D.B., Grueter, C.A., Harris, C., Biddinger, S., Ilkayeva, O.R., et al. (2010). SIRT3 regulates mitochondrial fatty-acid oxidation by reversible enzyme deacetylation. Nature *464*, 121–125.

Jiang, W., Wang, S., Xiao, M., Lin, Y., Zhou, L., Lei, Q., Xiong, Y., Guan, K.-L., and Zhao, S. (2011). Acetylation regulates gluconeogenesis by promoting PEPCK1 degradation via recruiting the UBR5 ubiquitin ligase. Mol. Cell *43*, 33–44.

Kanshin, E., Bergeron-Sandoval, L.-P., Isik, S.S., Thibault, P., and Michnick, S.W. (2015). A Cell-Signaling Network Temporally Resolves Specific versus Promiscuous Phosphorylation. CellReports *10*, 1202–1214.

Kee, J.-M., and Muir, T.W. (2012). Chasing Phosphohistidine, an Elusive Sibling in the Phosphoamino Acid Family. ACS Chem. Biol. *7*, 44–51.

Kelleher, N.L., Thomas, P.M., Ntai, I., Compton, P.D., and LeDuc, R.D. (2014). Deep and quantitative top-down proteomics in clinical and translational research. Expert Review of Proteomics *11*, 649–651.

Keller, M.P., Choi, Y., Wang, P., Belt Davis, D., Rabaglia, M.E., Oler, A.T., Stapleton, D.S., Argmann, C., Schueler, K.L., Edwards, S., et al. (2008). A gene expression network model of type 2 diabetes links cell cycle regulation in islets with diabetes susceptibility. Genome Research *18*, 706–716.

Klumpp, S., and Krieglstein, J. (2009). Reversible phosphorylation of histidine residues in proteins from vertebrates. Sci Signal *2*, pe13–pe13.

Kostiuk, M.A., Keller, B.O., and Berthiaume, L.G. (2010). Palmitoylation of ketogenic enzyme HMGCS2 enhances its interaction with PPAR and transcription at the Hmgcs2 PPRE. The FASEB Journal *24*, 1914–1924.

Lajoie, M.J., Rovner, A.J., Goodman, D.B., Aerni, H.-R., Haimovich, A.D., Kuznetsov, G., Mercer, J.A., Wang, H.H., Carr, P.A., Mosberg, J.A., et al. (2013). Genomically recoded organisms expand biological functions. Science *342*, 357–360.

Lane, N. (2006). Mitochondrial disease: powerhouse of disease. Nature *440*, 600–602.

Merrill, A.E., and Coon, J.J. (2013). Quantifying proteomes and their post-translational modifications by stable isotope label-based mass spectrometry. Curr Opin Chem Biol *17*, 779–786.

Mootha, V.K., Bunkenborg, J., Olsen, J.V., Hjerrild, M., Wisniewski, J.R., Stahl, E., Bolouri, M.S., Ray, H.N., Sihag, S., Kamal, M., et al. (2003). Integrated analysis of protein composition, tissue diversity, and gene regulation in mouse mitochondria. Cell *115*, 629–640.

Otto, D.A., and Ontko, J.A. (1978). Activation of mitochondrial fatty acid oxidation by calcium. Conversion to the energized state. The Journal of Biological Chemistry *253*, 789–799.

Pagliarini, D.J., and Dixon, J.E. (2006). Mitochondrial modulation: reversible phosphorylation takes center stage? Trends in Biochemical Sciences *31*, 26–34.

Pagliarini, D.J., and Rutter, J. (2013). Hallmarks of a new era in mitochondrial biochemistry. Genes & Development *27*, 2615–2627.

Pagliarini, D.J., Calvo, S.E., Chang, B., Sheth, S.A., Vafai, S.B., Ong, S.-E., Walford, G.A., Sugiana, C., Boneh, A., and Chen, W.K. (2008). A Mitochondrial Protein Compendium Elucidates Complex I Disease Biology. *134*, 112–123.

Pan, X., Liu, J., Nguyen, T., Liu, C., Sun, J., Teng, Y., Fergusson, M.M., Rovira, I.I., Allen, M., Springer, D.A., et al. (2013). The physiological role of mitochondrial calcium revealed by mice lacking the mitochondrial calcium uniporter. Nature Cell Biology.

Park, J., Chen, Y., Tishkoff, D.X., Peng, C., Tan, M., Dai, L., Xie, Z., Zhang, Y., Zwaans, B.M.M., Skinner, M.E., et al. (2013). SIRT5-Mediated Lysine Desuccinylation Impacts Diverse Metabolic Pathways. Mol. Cell *50*, 919–930.

Quant, P.A., Tubbs, P.K., and Brand, M.D. (1990). Glucagon activates mitochondrial 3-hydroxy-3-methylglutaryl-CoA synthase in vivo by decreasing the extent of succinylation of the enzyme. Eur. J. Biochem. *187*, 169–174.

Rhoads, T.W., Rose, C.M., Bailey, D.J., Riley, N.M., Molden, R.C., Nestler, A.J., Merrill, A.E., Smith, L.M., Hebert, A.S., Westphall, M.S., et al. (2014). Neutron-encoded mass signatures for quantitative top-down proteomics. Anal. Chem. *86*, 2314–2319.

Schmidt, O., Harbauer, A.B., Rao, S., Eyrich, B., Zahedi, R.P., Stojanovski, D., Schönfisch, B., Guiard, B., Sickmann, A., Pfanner, N., et al. (2011). Regulation of Mitochondrial Protein Import by Cytosolic Kinases. Cell *144*, 227–239.

Scott, I., Webster, B.R., Chan, C.K., Okonkwo, J.U., Han, K., and Sack, M.N. (2014). GCN5-like Protein 1 (GCN5L1) Controls Mitochondrial Content through Coordinated Regulation of Mitochondrial Biogenesis and Mitophagy. Journal of Biological Chemistry *289*, 2864–2872.

Sena, L.A., and Chandel, N.S. (2012). Physiological Roles of Mitochondrial Reactive Oxygen Species. Mol. Cell *48*, 158–167.

Shimazu, T., Hirschey, M.D., Hua, L., Dittenhafer-Reed, K.E., Schwer, B., Lombard, D.B., Li, Y., Bunkenborg, J., Alt, F.W., Denu, J.M., et al. (2010). SIRT3 Deacetylates Mitochondrial 3-Hydroxy-3-Methylglutaryl CoA Synthase 2 and Regulates Ketone Body Production. Cell Metabolism *12*, 654–661.

Still, A.J., Floyd, B., Hebert, A.S., Bingman, C.A., Carson, J.J., Gunderson, D.R., Dolan, B., Grimsrud, P.A., Dittenhafer-Reed, K.E., Stapleton, D.S., et al. (2013). Quantification of mitochondrial acetylation dynamics highlights prominent sites of metabolic regulation. Journal of Biological Chemistry.

Wagner, G.R., and Payne, R.M. (2013). Widespread and Enzyme-independent N -Acetylation and N -Succinylation of Proteins in the Chemical Conditions of the Mitochondrial Matrix. Journal of Biological Chemistry *288*, 29036–29045.

Wallace, D.C. (2013). A mitochondrial bioenergetic etiology of disease. J. Clin. Invest. *123*, 1405–1412.

Wang, Q., Zhang, Y., Yang, C., Xiong, H., Lin, Y., Yao, J., Li, H., Xie, L., Zhao, W., Yao, Y., et al. (2010). Acetylation of Metabolic Enzymes Coordinates Carbon Source Utilization and Metabolic Flux. Science *327*, 1004–1007.

Wu, R., Haas, W., Dephoure, N., Huttlin, E.L., Zhai, B., Sowa, M.E., and Gygi, S.P. (2011). A large-scale method to measure absolute protein phosphorylation stoichiometries. Nat Meth.

Yun, J., and Finkel, T. (2014). Mitohormesis. Cell Metabolism *19*, 757–766.

Zhao, X., León, I.R., Bak, S., Mogensen, M., Wrzesinski, K., Højlund, K., and Jensen, O.N. (2010). Phosphoproteome analysis of functional mitochondria isolated from resting human muscle reveals extensive phosphorylation of inner membrane protein complexes and enzymes. Molecular & Cellular Proteomics *10*, M110.000299–M110.000299.